博士論文

Quantitative Evaluation of Microbial Contamination of Meat with Fluorescence Spectroscopy

(蛍光分光分析による食肉加工プロセスにおける清浄度評価)

白井宏明

Contents

1. Introduction

World meat consumption continues to increase (FAO, 2014). Animals are slaughtered, and the meat is cut into parts and shipped to secondary processing facilities, finally reaching the consumers. At meat processing plants, the prevention of microbial contamination is critical to food safety. Primary contamination is the direct contamination of meat by microbial pathogens present in the intestinal tract of the animal. Secondary, or "cross-contamination," is the transfer of pathogens from meat-processing apparatus to the meat. The main sources of contamination at meat processing plants are feces, blood, and the animal intestinal tracts, which contains microbial pathogens such as *campylobacter* and *salmonella.* Recent outbreaks of foodborne illness in Japan include the following: (i) 9523 people were sickened and three died after consuming elementary school lunch service food contaminated with *Escherichia coli* O:157 in July 1996, (ii) five people died and 24 became seriously ill after consuming yuk-hoe (Korean-style steak tartare) contaminated with hemorrhagic *Escherichia coli O:*11 in April 2011. The top five United States meat product recalls are as follows: (i) 18 million kg of hot dogs/packaged meats potentially contaminated with *Listeria monocytogenes*, on December 22, 1988; (ii) 18 million kg of various ready-to-eat poultry products potentially contaminated with *Listeria monocytogenes* on January 22, 1999; (iii) 14 million kg of fresh and frozen ready-to eat poultry products potentially contaminated with *Listeria monocytogenes* on October 12, 2002; (iv) 13 million kg of ground beef potentially contaminated with *Escherichia coli*

O157:H7 on August 12, 1977; and (v) 9.5 million kg of beef trimmings and ground beef potentially contaminated with *Escherichia coli* O157:H7 on July 19, 2002. Thus, food safety at meat processing plant is critically important.

For the inspection of meat for bacteriological safety, one method used to determine the degree of contamination is the swabbing technique. By swabbing the meat surface, followed by incubation at 35°C for 48 h; the resulting aerobic plate count is used as a measure of hygiene quality. The measure of ATP content has recently attracted attention as an alternative tool for evaluating meat contamination. . Because all organisms contain ATP as energy currency, its presence is a sign of life and can be used as an indicator of microbial contamination. Food residue, a potential source of microbial contamination, also can be detected by ATP assessment. The advantage of the bioluminescence/ATP swabbing is that it gives rapid results. The microbial ATP bioluminescence assay can be used to rapidly detect fecal contamination of red meat carcasses and to gauge decontamination effectiveness; thus, this method is useful for monitoring the critical control points designated in a processing-plant

Hazard Analysis and Critical Control Point (HACCP) plan (Siragusa & Cutter, 1995).

Sanitation standards in Japan define the target aerobic plate count for the chicken carcass surface as 1.0×10^3 CFU cm^2 (The Ministry of Heath, Labor and Welfare, 1993). The hygiene of chicken processing plants in Japan was investigated by Shimidzu et al. (1998) (82 broiler processing plants and 31 adult chicken processing plants), determining the hygiene of the carcass, preliminary washing water, and main washing water. Specimens just after final processing and 120 minutes after processing were used to measure the aerobic plate count (APC), and the number of *salmonella* and *campylobacter*. The mean concentration of aerobic plate count just after processing was 1.7×10^4 CFU cm^{-2} and 6.9 x 10^4 CFU cm^2 for broiler and adult chicken carcasses, respectively. For the main cooling water just after processing, the APC was 4.9×10^3 CFU ml^{-1} and 1.7×10^5 CFU ml^{-1} and for the main cooling water, the APC was 4.9×10^3 CFU ml^{-1} and 1.7×10^5 CFU ml^{-1} (Figure 1, revised from Shimidzu et al., 1998). Therefore, the mean APC of broiler and adult chickens at the meat processing plants was above the targeted concentration of 1.0×10^3 CFU cm^2; thus, chickens with bacterial counts above this value had been shipped.

Tokoro et al. (1995) also investigated the sanitation of a broiler processing plant. The mean APC of the skinned broiler and the surface of the carcasses after washing was 1.5×10^3–1.3×10^4 CFU cm^{-2}, which was above the target concentration of 1.0×10^3 CFU cm^{-2}. The APC of the skinned broiler and the surface of the carcasses after cooling was 3.5×10^2–2.5×10^3 CFU cm^{-2}, which was close to the targeted concentration. A study of the

sanitary condition of slaughterhouses in Japan that were certified by ISO22000 or certified by the Japanese government as slaughterhouses for exporting meat to the US reported that the geometrical mean of the APC was 23.9 CFU cm^{-2} in summer and 16.2 CFU cm^{-2} in winter (Morita et al., 2010). While APCs vary between meat processing plants, the observation that APCs are above the Japanese government target concentration of 1.0 x 10^3 CFU cm^{-2} strongly suggests that improving sanitation monitoring at meat processing plants is critical to food safety in Japan.

For the European countries, the EU has introduced Decision 2001/471/EC, which mandates the use of all seven HACCP principles and sets forth microbiological performance criteria for the measurement of beef carcass hygiene (Anonymous, 2001). McEvoy et al. (2004) examined beef carcass microbial contamination for all major processing operations during dressing, washing, chilling, and boning at a commercial beef processing facility. Although not explicitly stated in the decision, it has been proposed that microbiological performance criteria for samples taken by swabbing be set at 20% of the values set for excised samples. Accordingly, the log mean aerobic plate count in carcass swab samples taken before chilling were determined to be acceptable at <2.8 log_{10} CFU cm^2, marginal at 2.8–4.30 log_{10} CFU cm^{-2}, and unacceptable at >4.3 log_{10} CFU cm^{-2}. By these criteria, the total viable count (TVC) on carcasses in the study of McEvoy's group was in the marginal range. However, it should be noted that the TVCs of beef carcasses

after boning (the final stage of processing) was 4.04–4.35 $\log_{10}$ CFU cm^{-2}; boning led to an increase in the number of all groups of bacteria examined. This increase is likely the result of cross-contamination from the surfaces and equipment within the boning hall and from personnel (Sheridan & Lynch, 1992; Gill et al., 1999). The meat is thus more susceptible to microbial spoilage and possibly threatens food safety. Therefore, determining the hygiene condition of meat after boning (before shipping) is important. In European countries, the TVCs of some beef carcasses were reported to be above 4.3 $\log_{10}$ CFU cm^{-2} (McEvoy et al., 2004). Thus, it is also important to monitor beef carcass hygiene to prevent further spread of microbial contamination.

In the United States, the USDA Pathogen Reduction Act requires meat and poultry processors to develop HACCP plans and sanitation programs for their establishments (USDA, 1996). Eisel et al. (1997) investigated the APC, coliform bacteria, and *Escherichia Coli* in beef products, on food contact surfaces, environmental surfaces, and in the air. APCs of fresh meat samples for beef carcass brisket, skirt steak, round steak, and boxed beef were 6.9, 6.7, 4.3, 4.1, and 6.6 $\log_{10}$ CFU g^{-1}. The APC of processing equipment was 3.9, 2.2, and 2.6 $\log_{10}$ CFU cm^{-2} for the fabrication line, ground beef line, and retail packing line, respectively. The authors concluded that microbial reduction strategies for slaughtering operations should include greater efforts to reduce microbial contamination on highly-contaminated regions of carcasses such as the brisket and skirt. In addition, they

determined that environmental sources of potential contamination, such as contact surfaces, floors, walls, and air, are probably not a significant source of overall microbial contamination.

As described above, the APC of carcass surfaces surpasses the target value set by the government or union in meat processing plants around the world. Therefore, reducing microbial contamination at meat processing plants and monitoring the hygiene of carcasses before shipping are critically important for food safety. These activities require quantitative evaluation of carcass microbial contamination. However, the presently used swabbing technique is time-consuming and laborious. APCs are typically used to assess hygiene; however, this procedure requires 48 hours for cultivation. In actual practice, the contaminated samples are often shipped to the secondary processing before the results are known. In addition, the swabbing technique only assesses bacterial contamination at the tested sites; the condition of the whole samples is unknown. At meat processing plants, a large volume of water is used to wash the processing apparatus to prevent microbial contamination. Thus, a non-destructive and rapid evaluation technique for assessing microbial spoilage is desired.

Several methods for detecting microbial spoilage have been developed, including the Fourier transform infrared (FT-IR), near-infrared (NIR), mid-infrared (MIR), ultraviolet or

visible (UV/Vis), raman, and hyperspectral imaging techniques. Ellis et al. (2002) demonstrated that Fourier transform infrared (FT-IR) spectroscopy, a rapid, noninvasive technique, can be directly used on the surface of food to produce a biochemically interpretable "fingerprint." Quantitative interpretation of FT-IR spectra was possible using partial least-squares regression (PLSR), which allowed accurate estimation of bacterial loads on the meat surface in 60 s. Ellis et al. (2004) demonstrated that rapid detection of microbial spoilage of beef is possible using FT-IR and machine learning. Sahar and Dufour (2014) explored the potential of mid-infrared (MIR) spectroscopy to detect spoilage microorganisms on the surface of chicken breast filets that were kept under aerobic conditions at 5°C for 0, 1, 2, 3, 5, and 8 days and at 15°C for 0, 0.5, 1, 2, 3, and 5 days. The results showed that MIR spectroscopy (range, 4000–1000 cm^{-1} range) coupled with an attenuated total reflectance (ATR) accessory can be used directly on the surface of meat samples to produce microbial fingerprints.

Recent applications of spectroscopic and hyperspectral imaging techniques with chemometric analysis for rapid inspection of microbial spoilage in muscle foods have been well documented by Cheng and Sun (2015).

Fluorescence spectroscopy, which has high sensitivity and selectivity, is used in this study. Fluorescence is emitted when the energy state of a substance transits from the first

excited state to the ground state. Compared with other spectroscopic methods such as UV/Vis and NIR, fluorescence spectroscopy has a two or three orders of magnitude higher sensitivity. This difference is because the background light effect in fluorescence spectroscopy is almost zero, while reflectance spectroscopy quantifies absorbance (or reflectance) relative to a reference value. Particular attention has been focused on excitation-emission matrix (EEM) fluorescence spectroscopy. EEMs are obtained by scanning both excitation and emission wavelengths, yielding three-dimensional data that provides more information than the previous technique that scanned the emission spectra against only one excitation wavelength. The application of EEM to food technology is throughly described in Christensen et al. (2007) and Sugiyama & Tsuta (2013).

The monitoring of meat hygiene is usually conducted on the meat surface; however, bacteria penetrate into meat (Gill & Penney, Gill et al., 1984, Thomas et al., 1987). Bacterial penetration into tissue has significant implications for the effectiveness of decontamination methods, because these unexposed cells are difficult to remove and are protected from the effects of sanitizing chemicals (Frank, 2001). Additionally, bacterial penetration leads to microbial spoilage of meat. Therefore, mechanistic understanding of bacterial penetration into meat might assist in developing methods to alleviate the microbial spoilage of meat.

Based on the needs indicated by the background information, this study has two objectives: one to quantitatively evaluate microbial contamination of meat with greater accuracy using fluorescence spectroscopy, and 2) to use mathematical modeling to elucidate the mechanism of penetrate ion of aerobic bacteria into meat for mechanistic understanding. The prediction models using fluorescence spectroscopy have been developed which reflected changes in tryptophan and NAD(P)H (Oto et al., 2013). However, fluorescence from ATP has not been detected because ATP fluorescence is masked by tryptophan's strong fluorescence peak. Detection of ATP fluorescence allows for higher prediction accuracy since microorganisms contain ATP, there should be a higher correlation between ATP fluorescence signal and aerobic plate count is expected. To separate the overlapping peaks of ATP and tryptophan, a derivative procedure was used. Derivative procedure has an advantage of separating overlapping peaks (Kitamura, 2005). For EEM, which is three-dimensional data, a two-dimensional derivative procedure can be applied. For example, a new method of preprocessing of EEMs via two-dimensional Savitzky–Golay second-order differentiation has been proposed, extending the Savitzky–Golay derivatives technique to yield three-dimensional EEM data.

Bacteria penetrate into meat within the gaps between the muscle fibers and endomysium (Gill et al., 1984). These gaps are filled with sarcoplasmic protein (Offer & Cousins, 1992), and bacteria are thought to penetrate into meat by degrading sarcoplasmic protein by proteolysis. via extracellular proteases. However, the role of proteolysis in this process is

unclear, with conflicting reports of proteolysis being required (Gill & Penney, 1977), not required (Sikes and Maxcy, 1982), and making a significant difference in bacterial penetration since sarcoplasmic protein offers little resistance to bacterial penetration because it has low viscosity. Thus, the mechanistic understanding of bacterial penetration is missing. This study uses mathematical modeling to investigate this question. We focused on *Pseudomonas fluorescens*, which is highly aerobic.

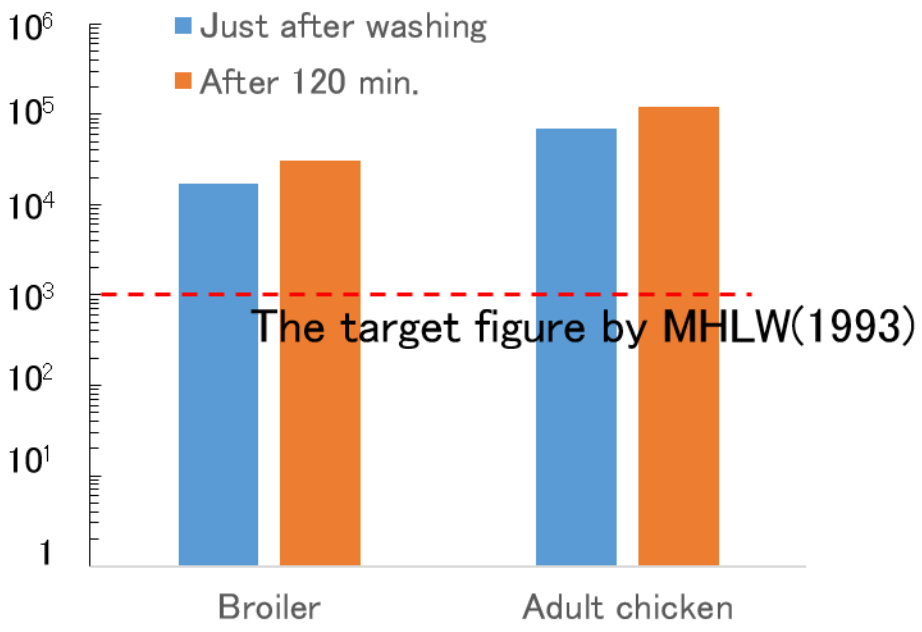

Figure 1. The aerobic plate count of broiler and adult chicken at meat processing plants (revised from the Table by Shimidzu et al., 2007).

2. Quantitative Evaluation of Microbial Contamination of Meat Surface with EEMs

2.1 Background

Hygiene monitoring at meat processing plants is critical for food safety. Cross contamination frequently occurs between meat and processing apparatus; therefore, contamination of meat is a serious problem. In the inspection of meat hygiene, swabbing is a widely used, standard technique. By swabbing each spot, aerobic plate count of meat surface is measured by incubating 35°C for 48 h. Recently, ATP content assessment has been used for the rapid monitoring of meat hygiene. Because all microorganisms contain ATP, the ATP content can be used as an indicator of microbial contamination of poultry carcasses (Siragura et al., 1996). A high correlation was observed between aerobic plate count and relative light unit (RLU) (correlation coefficient of 0.82), the measure of ATP content. The presence of ATP can also indicate food residue, which potentially lead to microbial contamination. Therefore, the ATP swabbing technique has also been used for hygiene monitoring of the surfaces of processing equipment. However, the swabbing technique, used for determining both aerobic plate count and ATP content, is time-consuming and laborious. Because of the 48 h incubation period required for APC determination, contaminated meat might be shipped for secondary processing before the results are available. If contaminated meat is shipped, it is very difficult to prevent contamination from spreading. In addition, the swabbing technique is a spot check that

does not monitor all of the processed meat blocks. Therefore, quantitative evaluation of the hygiene condition of meat using spectroscopy has been focused for rapid and non-destructive hygiene monitoring. Quantitative evaluation of microbial spoilage of meat using spectroscopy will facilitate the monitoring of all meat blocks. Furthermore, the hygiene condition of meat is determined directly using spectroscopy, yielding rapid results. Therefore, it is desirable to establish a non-destructive and rapid hygiene monitoring system that employs spectroscopy.

Fluorescence spectroscopy, which has high sensitivity and selectivity, is used in this study. Fluorescence is emitted when the energy state of a substance transits from the first excited state to the ground state. Fluorescence spectroscopy scans the emission spectra resulting from excitation of a sample at a certain wavelength. This technique has recently become a popular tool in biological sciences related to food technology (Karoui & Blecker, 2011). The application of fluorescence spectroscopy to food systems is well-described in reviews of multivariate autofluorescence of intact food systems (Christensen et al., 2006). For example, the use of front-face fluorescence spectroscopy (FFFS) for discriminating between milks from different geographical regions was also evaluated by Karoui et al. (2005). Wold et al. (2002) demonstrated the potential of solid sample fluorescence spectroscopy for non-destructive assessment of light-induced oxidation of Swiss cheese, cream cheese, and sour cream. Front-face fluorescence spectroscopy has been used to

monitor the freshness of 4 different species of fish. Emission spectra of aromatic amino acids and nucleic acids (AAA + NA), tryptophan, and NADH were scanned after excitation at 250, 290, and 336 nm, respectively. The authors concluded that AAA + NA fluorescence spectra were fingerprints that might allow discrimination between fresh and aged fish filets (Dufour et al., 2003).

Swatland, a pioneer in the field of meat, focused on measuring collagen and elastin fluorescence in connective tissue. With excitation at 365 nm, the peak of the fluorescence spectrum was observed at 510 nm, with a secondary plateau at 430–450 nm (Swatland, 1987). Wold et al. (1999) measured autofluorescence spectra to determine the content of collagenous connective tissue (hydroxyproline) and fat in ground beef. The excitation wavelength of 332 nm may be feasible for simultaneous determination of fat and connective tissue. The authors concluded that autofluorescence spectroscopy might be well suited for rapid on-line determination of collagen content in ground beef. Swatland & Barbut (1995) assessed raw turkey breast, using the structural range normally used in meat processing, using an optical probe for fluorescence of connective tissues. The frequency of fluorescence peaks in raw samples correlated with the maximum force required for penetration of the cooked product ($r = 0.74$) and with Young's modulus ($r = -0.71$). In another study, dissected, raw, heated (70°C) perimysial sheets from bovine masseter were subjected to fluorescence spectroscopy and tensile testing (Egelandsdal et

al., 1996). They applied the bilinear methods principle component analysis (PCA) and PLSR to evaluate the autofluorescence emission spectra of meat.

Ait-Kaddour et al. (2011) developed a portable spectrofluorometer for measuring the microbial spoilage of minced food. They demonstrated that it is possible to quantify the load of different bacteria in minced meat using a portable spectrofluorometer with excitation wavelengths of 280, 320, and 380 nm. Sahar et al. (2011) investigated the potential of synchronous front-face fluorescence spectroscopy along with chemometric methods for the determination of microbial load in chicken breast filets stored aerobically at 5°C and 15°C. Pu et al. (2013) measured the native fluorescence spectra of muscle foods (meat) stored at 4°C (refrigerated) and 25°C (room temperature) at a selected excitation wavelength of 340 nm as a function of storage time to determine meat spoilage status. The change in reduced NADH content was determined from the fluorescence spectra and Multivariate Curve Resolution with Alternating Least-Squares (MCR-ALS) analysis, which reflects the microbial spoilage of muscle foods involved in metabolic processes. For the availability of porphyrins fluorescence as an indicator of meat quality, Schneider et al. (2008) investigated the applicability of fluorescence spectroscopy using protoporphyrins as indicators of meat aging. The authors concluded that increased zinc protoporphyrin fluorescence caused by temperature-related changes in the physiological properties of meat can serve as a quality indicator. Durek et al. (2012) evaluated the

potential of fluorescence as an indicator of pork quality by determining the effects of various conditions on fluorescence signatures (excitation at 420 nm, emission at 550–750 nm), concluding that porphyrin fluorescence analysis is a potential means to indicate pork quality changes and remaining shelf life. Durek et al. (2016) developed a non-destructive mobile system for meat quality monitoring and investigated its possible application along the entire fresh meat production chain. The fluorescence of NADH and several porphyrins correlated with the growth of diverse bacteria and thus could be used for contamination monitoring. The authors noted that for the purpose of monitoring meat contamination, the detection of fluorescing porphyrins is more appropriate than that of NADH because the increase in NADH fluorescence was slow and the relative increase was low at 5°C. They concluded that porphyrins would be more suitable for contamination monitoring during meat production because they directly correlated with the total viable bacterial content and the beginning of the increase was distinct. However, there was a lag in the increase in porphyrin fluorescence. Moreover, a big variation in porphyrin fluorescence intensity even at the same stage of microbial spoilage was observed. A different technique for the evaluation of microbial contamination of meat is needed.

Chemometrics, a technique for the multivariate analysis of data, has been widely used in combination with spectroscopy. In the past, quantitative evaluation of quality or safety was carried out primarily using multilinear regression (MLR). However, for the analysis of

spectroscopic data, a problem of multicollinearity occurs in constructing a prediction model because spectroscopic data usually has strong multicollinearity, that is, the adjacent data in spectra are usually very close. Chemometrics can be used to solve this problem. Specifically, PCA and PLSR have been widely used in spectroscopic analysis. Principle component analysis decomposes the spectroscopic data into score (T) and loading (P^T) and is described in mathematics as singular value decomposition, expressed as $X = TP^T$, where T is score, P^T is loading, and X is the spectroscopic data in the matrix (wavelength in column and sample number in row). This decomposition is conducted to extract the maximum information possible from spectroscopic data. Principle component analysis is useful for extracting information from spectroscopic analysis. PCA is widely used for the analysis of spectroscopic data, particularly for understanding trends in spectral data. PLSR is one of the most commonly used regression techniques for multivariate data. PCA and PLSR are widely used in food analysis. Nicoial et al. (2007) reviewed the NIR spectroscopic measurement of vegetables and fruits using chemometric analysis. Chemometric analysis in combination with fluorescence spectroscopy related to food is well reviewed in Sádecká and Tóthová (2007).

Recent studies report the use of excitation–emission matrix (EEM) obtained by scanning excitation and emission wavelengths in fluorescence spectroscopic analysis. EEM provides huge three-dimensional data sets and can contribute to the discrimination of a target

ingredient in intact food (Sugiyama & Tsuta, 2013). Yoshimura et al. (2014) demonstrated that fluorescence fingerprint (FF) spectroscopy coupled with PLS regression was able to correlate FF with the aerobic plate count of beef with a bacterial contamination load ranging from 1.7 to 7.8 log CFU cm^{-2} (prediction error of RMSEP, 0.752 log CFU cm^{-2}). Fluorescence from tryptophan, NAD(P)H, and vitamin A and autofluorescence from porphyrins and flavins in bacteria can be monitored in the FF of beef. Nishino et al. (2013) optimized an excitation–emission bandpass filter for visualizing viable bacteria on the surface of pork meat based on the degradation of tryptophan. Oto et al. (2013) used fluorescence spectroscopy to evaluate meat hygiene and obtained EEMs of pork meat surfaces. By applying PLSR analysis, the ATP content and plate count were predicted with reasonably good coefficients of determination (R^2_{val}, 0.88; RMSEP, 0.97 log CFU cm^{-2} for aerobic plate count). These models reflected the changes in fluorescence intensity of tryptophan and NADPH. Previous studies such as Oto et al. (2013) and Yoshimura et al. (2014) have presented prediction models for aerobic plate count and ATP content of pork surface; however, the model accuracy was not sufficient for practical use. The prediction error of RMSEP of approximately 1.0 $\log_{10}$ (CFU cm^{-2}) indicates that the predicted values have a variation of 1.0 $\log_{10}$ (CFU cm^{-2}). For example, for a predicted value of 10^5 CFU cm^{-2} with RMSEP of 1.0, the actual value will be in the range of 10^4–10^6 CFU cm^{-2}. Oto et al. (2013) reported RMSEP prediction accuracies of 0.97 log CFU cm^{-2} and a correlation coefficient of prediction of 0.94. The microbial contamination level required for detection at meat processing plants is 3.0 $\log_{10}$ (CFU cm^{-2}) (MHLW, 1993). However, the prediction

error in this aerobic plate count range was especially large (Figure 5b in Oto et al. (2013)). Therefore, a method for the quantitative evaluation of microbial spoilage of meat with higher accuracy is required.

With the aim of achieving higher prediction accuracies, this study used the detection of ATP fluorescence. This method likely has higher prediction accuracy because ATP is present in microorganisms, but probably not in the meat. Durek et al. (2016) noted that ATP and NAD(P) are naturally occurring in fresh meat, but the ATP in drops to almost zero at 48 h post-mortem (Hamm, 1977). ATP fluorescence is normally masked by the strong fluorescence peak from tryptophan. In the EEM of pork surface (Figure 2), the largest peak at Ex 290 nm and Em 340 nm is assigned to tryptophan (**a** in Fig. 2.1). The ATP fluorescence peak is located at Ex 284 nm and Em 388 nm or 412 nm (red dashed circle, **b**, in Fig. 1), but the ATP fluorescent peak is apparently masked the large tryptophan peak. Thus, in this study, detect ATP fluorescence is aimed by separating these overlapping peaks using derivative procedures widely used for peak separation (Kitamura, 2007). Advantages of using a derivative procedure are as follows: i) overlapping peaks can be separated; ii) the relationship between concentration and absorbance (of fluorescence intensity) remains; (iii) the spectral strength can be intensified with a derivative procedure, as expressed by $(D_1/D_2) = (W_2/W_1)^n$, where D_i is the spectral strength and W_i is the half-value width (Kitamura, 2007). A two-dimensional derivative procedure can be

applied to the three-dimensional data of EEMs. For preprocessing of EEMs, we applied two-dimensional Saviztky–Golay second-order differentiation, which is an extended Savitzky–Golay derivative procedure for three-dimensional data. This procedure allowed for the detection of ATP fluorescence. Prediction models for aerobic plate count and ATP content were then developed based on fluorescent changes in ATP as well as tryptophan and NAD(P)H.

The aim of this study is to quantitatively evaluate the aerobic plate count and ATP content of pork surface using fluorescence spectroscopy. To detect ATP fluorescence, two-dimensional Savitzky–Golay second-order differentiation was usedto separate the overlapping peaks of tryptophan and ATP. Our goal was to develop prediction models for aerobic plate count and ATP content of pork surface with higher prediction accuracies than those of present methods. We show that the models we developed reflect changes in ATP as well as tryptophan and NAD(P)H.

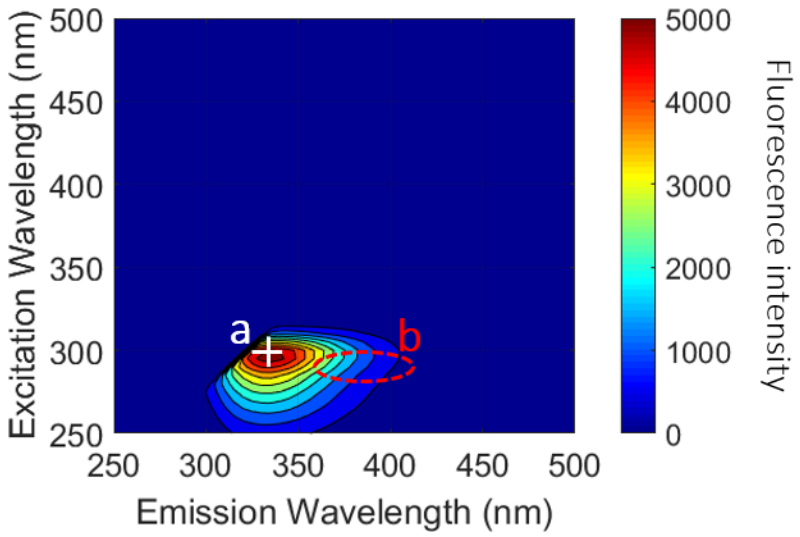

Figure 2.1. Example of EEM of pork surface. The fluorescent peak shown at (a) is that of tryptophan. The ATP peak is located in the red-dashed circle area but is masked by the tryptophan peak.

2.2 Development of two-dimensional Savitzky–Golay second-order differentiation to facilitate ATP fluorescence detection

2.2.1 Materials and Methods

2.2.1.1 Measurement of ATP standard EEMs

Sample preparations

EEM of an ATP standard solution was obtained to confirm the location of the ATP fluorescence peak. Two forms of ATP solution were prepared: ATP 2-sodium hydrate (Sigma Aldrich, Japan) and ATP standard solution (10^{-7} mol l^{-1}) (LL-101-1, Toyo-B-Net Co., Japan). The ATP 2-sodium hydrate solution (10^{-3} mol l^{-1}) was prepared by diluting the reagent into distilled water.

Measurement of fluorescence intensities

The fluorescence intensities of ATP standard solution prepared above were measured in quartz cuvettes using a fluorescence spectrophotometer (F7000, Hitachi, Japan), and EEMs were obtained. For the ATP 2-sodium hydrate solution, the slit widths of excitation and emission light were 5 nm and 10 nm, respectively. The photomultiplier tube (PMT) voltage was 700 V. The excitation wavelength range was 250–400 nm, and the emission wavelength range of 250–450 nm. A sampling resolution of 2 nm was used for both wavelengths, and the scanning speed was at 12 000 nm min^{-1}. For the ATP standard

solution of 110^{-7} mol l^{-1}, a slit width of 10 nm for both excitation and emission wavelength was used. The photomultiplier voltage was set to 800 V. The sampling resolution was 5 nm, and the scanning speed was 60 000 nm min^{-1}.

2.2.1.2 Measurement of EEMs of *Pseudomonas fluorescens* culture

Culture preparation

Bacterial cultures of *Pseudomonas fluorescence Migula* (ATCC 13525) were prepared as following. A glass ampule containing *Pseudomonas fluorescens Migula* (ATCC 13525) was broken carefully and added to 0.2 mL LB liquid medium (LB Daigo, Nihon Pharmaceutical Co. Ltd., Japan). The strain suspension was obtained by shaking the ampule, followed by inoculation onto LB agar medium (LB Daigo) at 30 °C for one day. The grown *Pseudomonas fluorescence* culture was then inoculated into LB liquid medium and was incubated with shaking at approximately 160 rpm (Shaker-VR, TAITEC, Japan) at 30°C overnight. The resulting culture was washed with 1% physiological saline solution to prevent any effects of the LB liquid medium on fluorescence intensities. The bacterial concentration of washed culture was measured using Petrifilm (AC plate, Sumitomo 3 M Ltd., Japan), which was incubated at 35°C for 48 h.

Measurement of fluorescence intensities

Fluorescence intensities were measured in the same manner as described in Sec. 2.2.1.2. The wavelength range for excitation and emission was 250–400 nm and 250–430 nm, respectively, with 2 nm sampling resolution. The photomultiplier tube voltage was 550 V, and the slit widths were set at 10 nm for both excitation and emission wavelengths. The scanning speed was at 12 000 nm min^{-1}.

2.2.1.3 Two-dimensional Savitzky–Golay second-order differentiation (EEM preprocessing)

Two-dimensional Savitzky–Golay second-order differentiation was proposed and applied to the pork surface EEMs to separate overlapping peaks of tryptophan and ATP. The schematic of calculation of two-dimensional Savitzky–Golay second-order differentiation is shown in Fig. 2.2. The fluorescence intensities of an area of (2 m + 1) x (2 m + 1) (m = 1, 2, 3) points (i.e., 4 m [nm] x 4 m [nm]) were extracted from each EEM. The fluorescence intensities were then fitted using the following quadratic expression (Eqn. 1):

$$f(x, y) = a_0 + a_1 x + a_2 y + a_3 x^2 + a_4 xy + a_5 y^2 \quad (1)$$

where a_0 to a_5 are the coefficients of quadratic surface, x and y are the locations of data in the axis of excitation and emission wavelengths, respectively (therefore, x = −2, −1, 0, 1, 2; y = −2, −1, 0, 1, 2). Explained variable f(x, y) is the fluorescence intensity of the corresponding pair of excitation and emission wavelengths. The coefficients a_0 to a_5 were usually calculated using the least squares method. Then, the second-order total

differentiation was calculated at the center point of the extracted window, where (x, y) = (0, 0) for each EEM by Eqn. 2:

$$d^2 f = \frac{\partial^2 f}{\partial x^2} dx^2 + 2\frac{\partial^2 f}{\partial x \partial y} dxdy + \frac{\partial^2 f}{\partial y^2} dy^2 \quad (2)$$

Therefore, the second-order total differential can be calculated using Eqn. 3, which is derived by substituting Eqn. (1) into Eqn. (2) at (x, y) = (0, 0):

$$d^2 f = 2a_3 + 2a_4 + 2a_5 \quad (3)$$

An advantage of the Savitzky–Golay method is that it is not necessary to repeat the least squares calculation to determine a_0 to a_5 in Eqn. (1); instead, we just multiplied the coefficient **C** as expressed in Eqn. (4):

$$\mathbf{a} = \mathbf{fC} \quad (4)$$

where **a** is the vector consisting of a_0 to a_5, **f** is the fluorescence intensity for each location, and **C** is the weight coefficient for the two-dimensional Savitzky-Golay technique. The determination of **C** followed the method reported by Krumm (2001). The second-order total differentiation then can be calculated using Eqn. (3) and Eqn. (4). The second-derivative EEM was obtained by repeating this procedure for all areas of the excitation and emission wavelengths. The fourth-derivative EEMs also can be obtained by repeating this processing twice on raw EEMs.

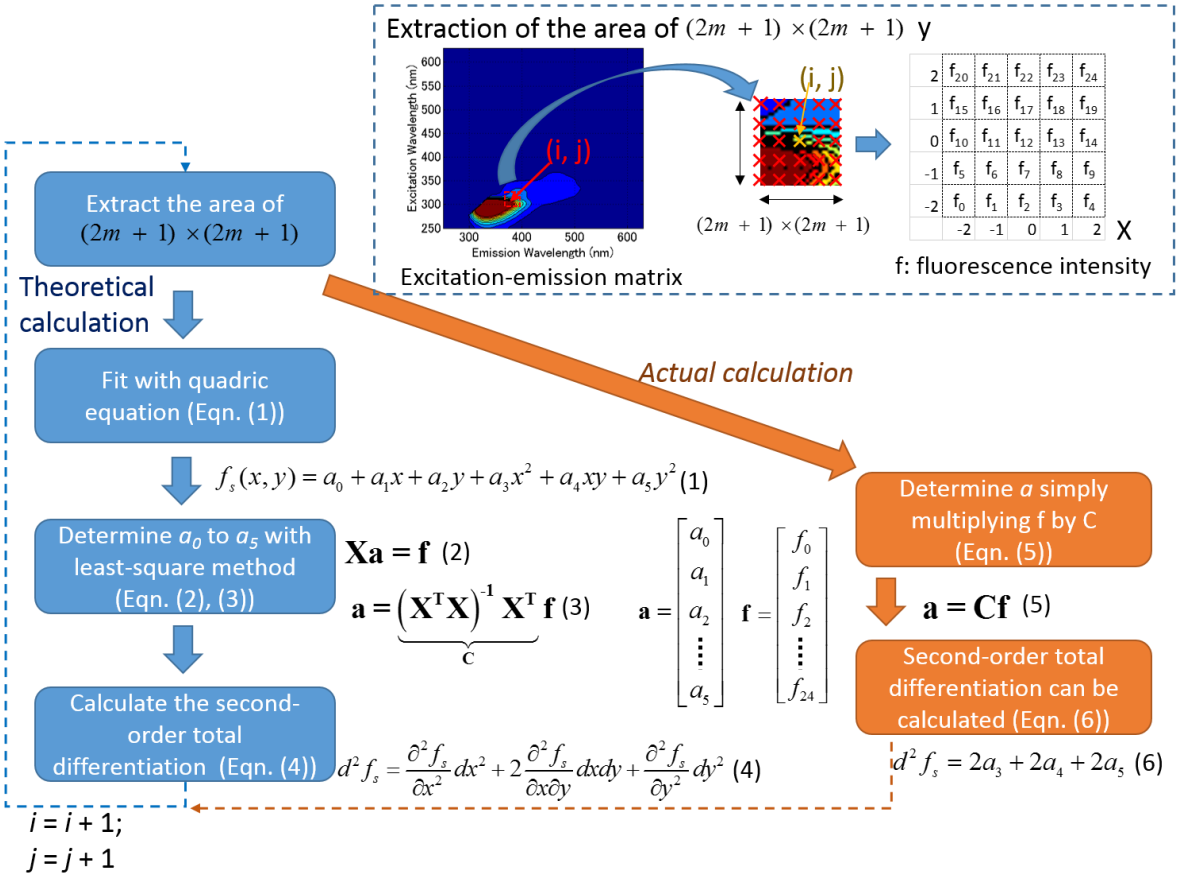

Figure 2.2. A schematic for calculating the two-dimensional Savitzky–Golay second-order differentiation for preprocessing of EEMs. The small window consisting of fluorescence intensity was extracted from each EEM, and fluorescence intensities of the extracted window were fitted using the quadratic equation (Eqn. 2). The coefficients of the quadratic equation of a_0 to a_5 can be calculated by simply multiplying the matrix consisting of the fluorescence intensities by the coefficient matrix, **C** (Eqn. 5); the second-order total differentiation at the center of the window can be calculated by simple calculation using Eqn. (6).

2.2.2 Results and Discussions.

2.2.2.1 Excitation-emission matrices of ATP

The EEM of the ATP standard solution is shown in Figure 2.3. The ATP fluorescent peak is at Ex 284 nm and Em 388 nm (Fig. 2.3a), as confirmed by previous studies (Ex, 292 nm; Em, 388 nm) (Christensen et al., 2006); (Ex, 272 nm; Em, 390 nm) (Schwedt et al., 1987). For the ATP standard solution of 10^{-7}mol l^{-1}, the fluorescence peaks likely caused by ATP were observed at Ex 290 nm and Em 395 nm and 410 nm (Fig. 2.3b).

2.2.2.2 Excitation-emission matrices of *Pseudomonas fluorescens* culture

The EEM of *Pseudomonas fluorescens* culture (5.3 x 10^8 CFU ml^{-1}). The fluorescent peak at Ex 290 nm and Em 340 nm is assigned to tryptophan, an aromatic amino acid present in bacteria. In addition, a small peak observed at Ex 340 nm and Em 460 nm was assigned to NAD(P)H, a metabolic product of bacteria. The ATP fluorescent peak is seen at Ex 288 nm and Em 390 nm (Fig. 2.3); however, no corresponding fluorescent peak was observed in the EEM of *Pseudomonas fluorescens* culture (Fig. 2.4), as the ATP fluorescent peak is masked by the large fluorescent peak of tryptophan. Thus, it was aimed to separate the overlapping peaks of tryptophan and ATP to detect ATP fluorescence, as described in the following section.

2.2.2.3 Detection of ATP fluorescence from EEM of *Pseudomonas fluorescens* culture using two-dimensional Savitzky–Golay second-order differentiation

To detect ATP fluorescence in *Pseudomonas fluorescence* culture, two-dimensional Savitzky–Golay second-order differentiation was applied to EEMs of *Pseudomonas fluorescens* culture. We chose *Pseudomonas fluorescens* because *Pseudomonas* is a dominant species involved in the microbial spoilage of meat (Ercolini et al., 2006).

Figure 2.5 shows the second-derivative EEM of *Pseudomonas fluorescens* (3.8×10^8 CFU ml^{-1}) that was obtained using the two-dimensional Savitzky–Golay second-order differentiation procedure on EEM data. Because the fluorescence intensities around the tryptophan peak (Ex, 290 nm; Em, 330 nm) exceeded the maximum measurable fluorescence intensity of 10 000 (Fig. 2.1), the second derivatives cannot be calculated in this wavelength area (Fig. 2.5). In general, the negative peak of the second-derivative corresponds to the raw spectral peak (figure in Kitamura, 2007). Negative values of the second-derivative fluorescence intensity near Ex 290 nm and Em 340 nm (around the deleted area in Fig. 2.5) were observed, corresponding to the tryptophan peak. The aim was then to detect the fluorescent peak from ATP, which is located at Ex 288 nm and Em 388 nm, using this two-dimensional Savitzky–Golay second-order differentiation. However, no negative peak was observed at the wavelength pair above (red dashed circle, Fig. 2.5). To investigate the second-derivative fluorescence intensities, the second-

derivative emission spectra at the excitation wavelength of 284 nm were obtained (Fig. 2.7b). No fluorescence peak was observed in the raw spectra (Fig. 2.7a). Slight fluctuations in second-derivative fluorescence intensities were observed around Em = 386 nm; however, no obvious peak was observed in the second-derivative emission spectra. Therefore, ATP fluorescence was not detected using the second-derivative procedure. We then carried out another second-derivative procedure on the second-derivative EEMs, yielding a fourth-derivative procedure (Fig. 2.6). Figure 2.6 shows the fourth-derivative EEMs of *Pseudomonas fluorescens* (Fig. 2.6a) and that with an enlarged scale and limited wavelength (Fig. 2.6b). In the fourth-derivative EEM, the region around Ex 290 mm and Em 340 mm (the wavelength pair where tryptophan fluorescence peak is located) was deleted because fourth derivatives cannot be calculated correctly because of the saturation of fluorescence intensity from tryptophan. Large, positive fourth-derivative fluorescence intensities around Ex 290 nm and Em 330 nm were observed, corresponding to the tryptophan peak. Negative fourth-derivative fluorescence intensities adjacent to positive fourth-derivative fluorescence intensities occurred because the negative values accompany the direct positive peak. Notably, small positive peaks at Ex 284 nm and Em 388 nm, 396nm, and 410 nm were observed (enclosed in red dashed circle, Fig. 2.6b), likely representing ATP fluorescence because ATP fluorescent peaks occur at Ex 288 nm and Em 388 nm (Fig. 2.3). In addition, fluorescence peaks of the ATP standard solution of 10^{-7} mol l^{-1} were observed at Ex 290 nm and Em 395 nm, 410 nm. To investigate these positive ATP fluorescence peaks, the fourth-derivative fluorescence intensity at the

excitation wavelength of 284 nm was determined (Fig. 2.7c). Note that the spectra in Figs. 2.7b and 2.7c differ from that obtained by applying one-dimensional derivative procedures to the raw fluorescence spectra data at the excitation wavelength of 284 nm (Fig, 2.7a). For raw and second-derivative spectra, no peaks were observed apart from that of tryptophan (Fig. 2.7a, b), although fluctuations in second-derivative fluorescence intensities around Em = 388 nm were observed. In contrast, positive peaks were observed at 388 nm, 394 nm, and 412 nm in fourth-derivative fluorescence intensities (Fig. 2.7c). These positive peaks were considered to represent ATP because the ATP fluorescent peaks occur at Ex 284 nm and Em 386 nm and 410 nm, as described above. Therefore, the ATP fluorescence of *Pseudomonas fluorescens* culture was successfully detected using fourth-derivative EEM.

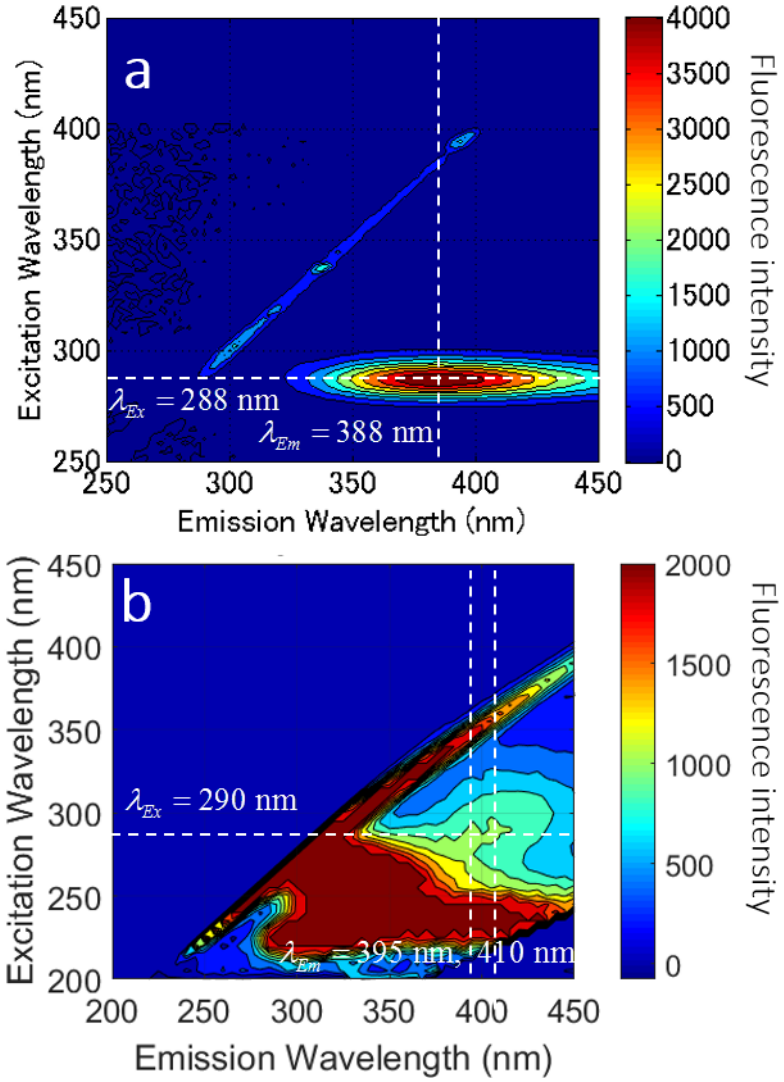

Figure 2.3. Excitation-emission matrix of ATP 2-sodium hydrate solution (10^{-3} mol l^{-1}) (a) and ATP standard solution (10^{-7} mol l^{-1}) (b). ATP has a fluorescent peak at Ex 288 nm and Em 390 nm (a), and at Ex 290 nm and Em 395 nm, 410 nm (b). The strong fluorescence intensities around Ex 250 nm and Em 325 nm was probably caused by other components of the ATP standard solution.

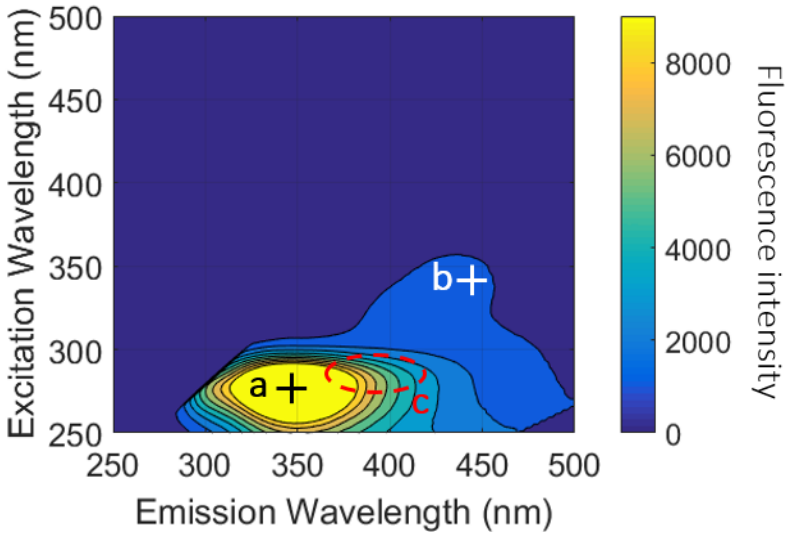

Figure 2.4. Excitation-emission matrix of *Pseudomonas fluorescens* culture (1.0 x 10^8 CFU ml^{-1}). The large peak around Ex 290 nm and Em 346 nm is caused by tryptophan (a), and the small peak at Ex 340 nm and Em 460 nm is caused by NAD(P)H. The area enclosed by the red dashed line indicates the location of the ATP fluorescence peak that is masked by tryptophan fluorescence.

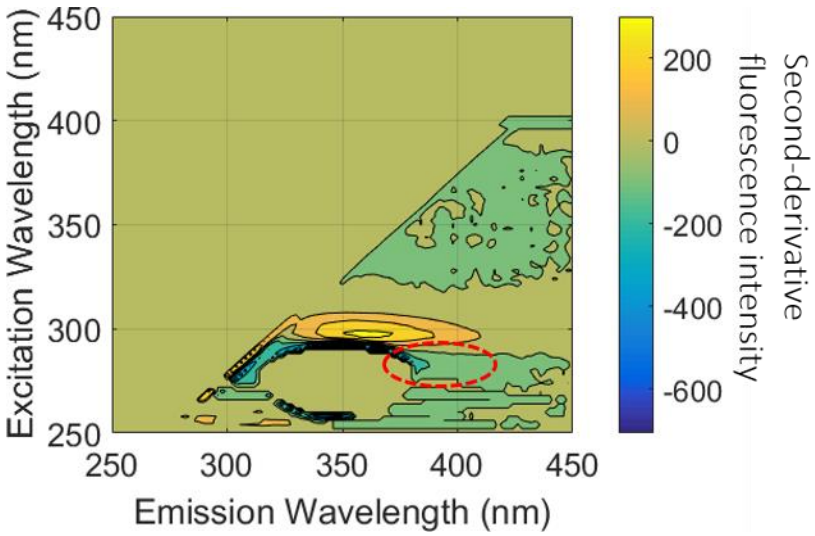

Figure 2.5. Second-derivative EEM of *Pseudomonas fluorescens* culture. The areas around Ex 290 nm and Em 346 nm was deleted because the second-derivative fluorescence intensities cannot be calculated correctly owing to the saturation of fluorescence intensities. The red dashed circle indicates the region of ATP fluorescence, which is masked by tryptophan in this case.

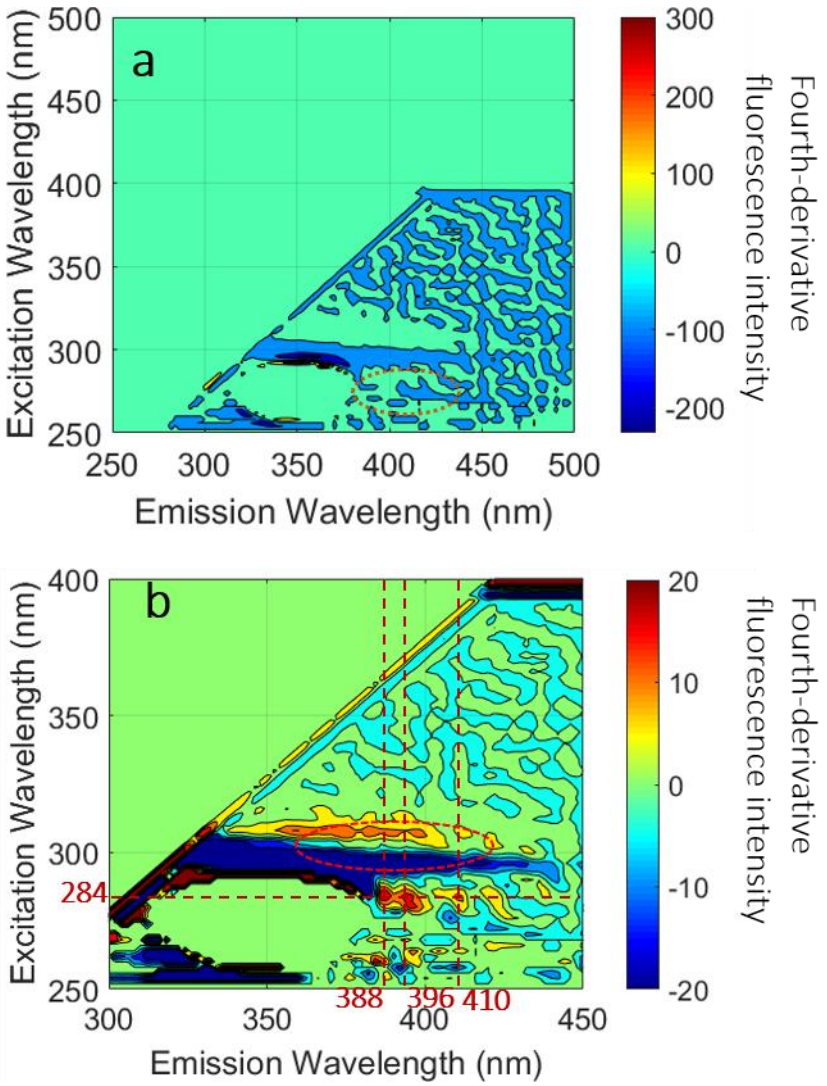

Figure 2.6. Fourth-derivative EEM of *Pseudomonas fluorescens*culture (a) and that with limited excitation wavelength to 300–450 nm and emission wavelength to 250–350 nm with enlarged scale (b). Small positive peaks around Ex 286 nm, and Em 286 nm and 412 nm were observed in the fourth-derivative EEM (b); therefore, ATP fluorescence was successfully detected from *Pseudomonas fluorescens* culture.The area around Ex 290 nm

and Em 330 nm was deleted where fourth-derivatives cannot be calculated correctly caused by saturation of fluorescence intensities by tryptophan.

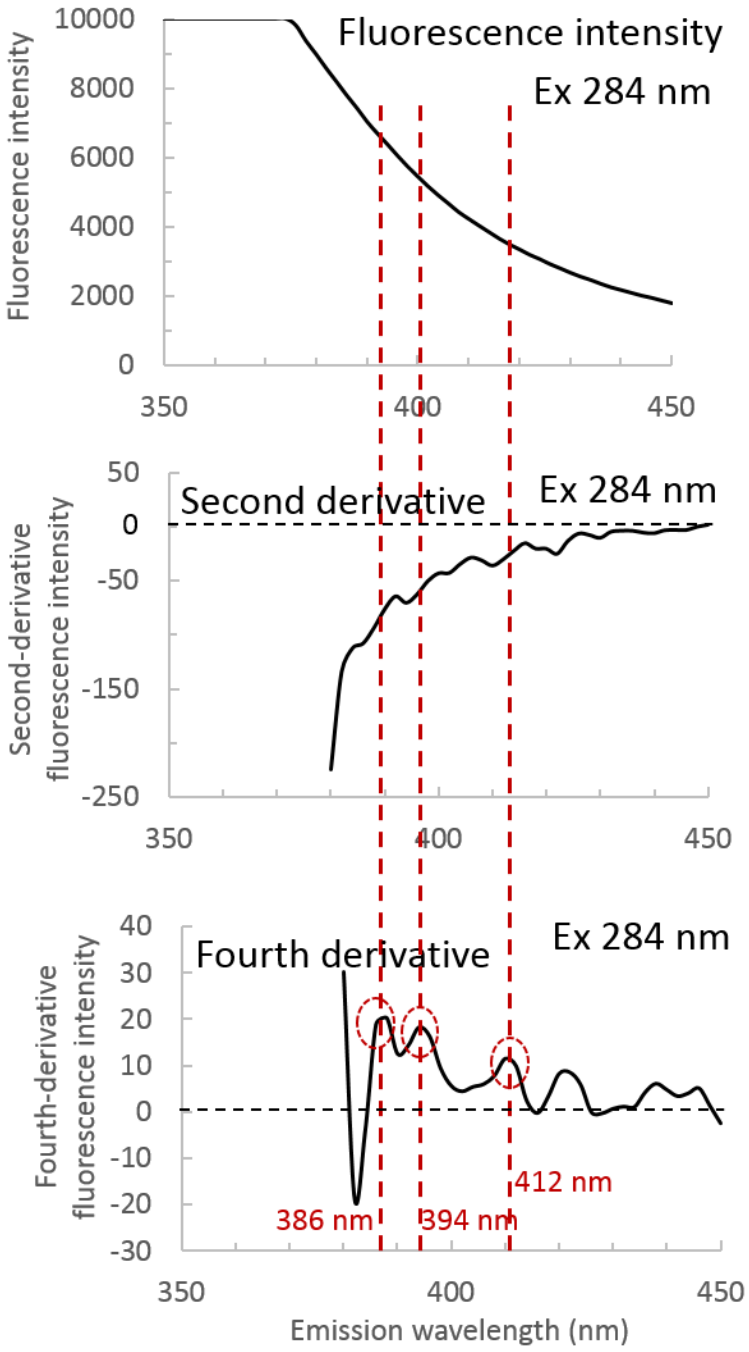

Figure 2.7. Fluorescence raw spectra (a), second-derivative fluorescence spectra (b), and fourth-derivative fluorescence spectra (c) of *Pseudomonas fluorescens* at the excitation wavelength of 284 nm. No peaks were observed in the raw spectra or second-derivative

spectra (a, b), but positive peaks apart from tryptophan were observed at 386 nm, 394 nm, and 412 nm using the fourth-derivative procedure. Note that second-derivative fluorescence spectra (b) and fourth-derivative fluorescence spectra (c) differed from those obtained by the application of only one-dimensional second-derivative or fourth-derivative procedure on the raw fluorescence spectra (a).

2.3 Quantitative evaluation of aerobic plate count and ATP content of pork surface with EEMs coupled with two-dimensional Savitzky–Golay second-order differentiation

2.3.1 Materials and Methods

Sample preparations

Pork loin meat was used as the study material. Pork meat was chosen because of its ease of handling and relatively uniform surface. The pork loin meat was purchased from a retailer and sliced to a thickness of 5 mm. The pork meat slices were then cut into 4.5 x 4.5 cm pieces. This size was selected for the convenience of fluorescence intensity measurement. The samples (n = 28) were stored at 15°C for up to 72 h. Four pork samples were used to determine EEMs, aerobic plate count, and ATP content every 12 h from 0 h to 72 h (28 samples in total). Excitation-emission matrices were measured at four locations for each pork sample by rotating the sample for each measurement as described in Sec. 2.2.3.3.

Measurement of the ATP content and plate count

Aerobic plate counts were performed by first swabbing a 4 × 4 cm area of the pork surface using a cotton-tipped swab, as described by Bautista et al. (1998). To ensure adequate sampling, the area was swabbed in horizontal and vertical directions. In addition, the swab was rotated between the index finger and thumb in a back and forth motion. The quartz

glass that was placed on the pork surface (for the convenience of measuring fluorescence intensities) was also swabbed in the same manner to collect the microorganisms on its surface. The tips of both swabs were then cut off and immersed in 9 ml phosphate buffer solution and mixed with vigorous agitation. The solution was diluted to an appropriate concentration such that the number of colonies on Petrifilm would be 25–250, (standard technique for measurement of aerobic plate count). The diluted sample (1 ml) was dripped onto Petrifilm and incubated at 35°C for 48 h. The number of red colonies was counted, and the aerobic plate count per swabbed area (16 cm^2) was calculated.

The ATP content was measured with a luminosensor (AB-2200, Atto Corp., Japan). First, a standard curve was constructed by measuring the relative light units (RLUs) of a standard ATP solution (LL-101-1, Toyo-B-Net Co) by adding 100 µl luciferin–luciferase complex (LL-101-1, Toyo-B-Net Co.) in the range of 10^{-7}–10^{-12} mol l^{-1}. The dilution prepared for the aerobic plate count was used to measure pork sample RLUs. Diluted samples (100 µl) were measured after the addition of extractant (LL-100-2, Toyo-B-Net Co.) and luciferin–luciferase complex (LL-101-1, Toyo-B-Net Co.). After 10 s, the RLU was measured. The RLUs were determined twice in two test tubes, and the mean value was calculated for the ATP content of the pork surface.

Measurement of fluorescence intensities

Fluorescence intensities of pork surface was measured with the same manner as Sec. 2.2.1.2 and EEMs of pork surface were obtained. For the measurement condition, the photomultiplier voltage was set at 540 V and slit width of excitation and emission light was 5 nm and 10 nm, respectively.

In order to investigate the wavelength location of ATP fluorescence on pork surface, the EEMs of pork surface on which 1 ml ATP solution of 1.0×10^{-1} mol ml^{-1} was inoculated was measured and compared with EEM of control sample. The value of positive peak of fourth-derivative fluorescence intensity probably due to ATP fluorescence was compared.

The fluorescence intensities from tryptophan reached the maximum measurable fluorescence intensity (9999) because of the device condition; therefore, the second derivatives could not be calculated correctly because of this saturation of the fluorescence intensity. Thus, region of the EEM from Ex ≤ 310 nm and Em ≤ 402 nm was excluded.

The fluorescence intensities from tryptophan reached the maximum measurable fluorescence intensity (10 000) because of the device condition; therefore, the second derivatives could not be calculated correctly because of this saturation of the fluorescence intensity. Thus, region of the EEM from Ex ≤ 310 nm and Em ≤ 402 nm was excluded.

Partial least squares regression

Partial least squares regression (PLSR), one of the most popular chemometric analyses, has been used recently for the quantitative evaluation of spectroscopic data. PLSR is based on principle component analysis (PCA). Figure 2.8 shows a schematic of PCA and PLSR. PCA is described in singular value decomposition, and the fluorescence information is decomposed into score (T) and loading (P^T). New axes are constructed to retrieve the maximum possible information from the fluorescence data. Loading shows the weight of each wavelength toward the constructed axes. In PLSR analysis, PCA is conducted on both fluorescence information and response variables (aerobic plate count or ATP content); thus, in most cases, the latent variable 1 (LV 1) shows the changes in the response variable (in some cases, this is not true; thus, the meaning of LV 1 or LV 2 should be carefully identified by grouping data in the score plot). The total 112 data sets were divided into a training set of 84 samples and a test set of 28 samples. The ATP content and pork surface plate count were calibrated using raw EEMs, the second-derivatives EEMs, or fourth-derivative EEMs of pork surface with 80 training samples by PLSR. The optimum latent variable (LV) was determined by random cross-validation (n = 3). The ATP content and plate count then were validated using the test data. Data analysis was performed using UnscramblerX 10.3 (Camo software, Japan).

Principle component analysis (PCA)

$$\mathbf{X} = \mathbf{TP}^{\mathbf{T}} \qquad \mathbf{XP} = \mathbf{T}$$

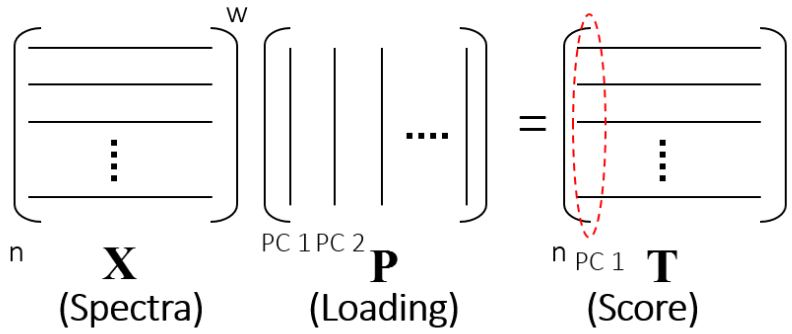

w: wavelength

n: sample numbver

$$t_1 = f_1 p_1 + f_2 p_2 + f_3 p_3 +$$

t_1, t_2, t_3,… are determined to maximize the information of the matrix

Partial least squares regression (PLSR)

$$\mathbf{Xb} = \mathbf{Y} \quad \Rightarrow \quad (\mathbf{TP}^{\mathbf{T}})\mathbf{b} = \mathbf{UQ}^{\mathbf{T}}$$

t_1, t_2, t_3,… are orthogonal; therefore, regression model can be constructed without multicollinearity

Figure 2.8. A schematic of principle component analysis of spectroscopic data and partial least squares regression (PLSR) analysis. In PCA, the spectroscopic data is decomposed into score (T) and loading (P^T). In PLSR analysis, PCA is implemented on the matrix of fluorescence intensities, X, and response variable (aerobic plate count or ATP content), Y, respectively; then, the regression coefficient (b) is determined.

2.3.2 Results and Discussion

2.3.2.1 Aerobic plate count and ATP content of pork surface

Figure 2.9a shows the relationship between aerobic plate count and ATP content. The aerobic plate count of the pork surface ranged from 10^3–10^8 CFU cm^{-2}, and the ATP content of the pork surface ranged from 10^{-13}–10^{-9} mol cm^{-2}. A good correlation between them was observed (determination coefficient, 0.94), which confirms the previous report by Bautista et al. (1998) that ATP content can be used as an indicator of microbial contamination of meat.

Changes in ATP content per cell is shown in Fig. 2.9b. The ATP content per cell was 10^{-15} mol CFU^{-1} at the initial stage of storage, but decreased with time. After 24 h, it reached approximately 10^{-18} to 10^{-17} mol CFU $^{-1}$ (Fig. 2.9b). Given that ATP of the ATP content of gram negative bacteria is on the order of 10^{-18} mol CFU $^{-1}$ (Monji, 2000) at the initial storage time, the detected ATP is not in bacteria but in the pork itself.

2.3.2.2 Excitation-emission matrices of pork surface

Figure 2.10 shows the EEMs of pork meat surface at 0 h (Fig. 10a) and 72 h (Fig. 10b, c). Figure 10c is the EEM with the scale enlarged to cover fluorescence intensity at 0–2000.

In all of the EEMs shown in Fig. 2.10a–c, we observed strong fluorescence intensities around Ex = 290 nm and Em = 330 nm, caused by tryptophan. Since the setting of the fluorescence spectrophotometer was set relatively higher to focus on ATP fluorescence, which emits relatively weak fluorescence, the fluorescence intensities in the surrounding areas were saturated to the maximum measurable value of the device (10 000). A fluorescence peak at Ex 340 nm and Em = 460 nm was also observed at 72 h (**B** in Fig. 2.10b, c), assigned to NAD(P)H (in this study we describe both NADH and NADPH as NAD(P)H). A relatively small fluorescence peak also was observed at Ex = 420 nm and Em = 596 nm, which is likely caused by porphyrins. Schneider et al. (2008) investigated porphyrin fluorescence (zinc protoporphyrin, proporphyrin IX and magnesium protoporphyrin) and demonstrated that the zinc protoporphyrin fluorescence peak occurs at Ex = 420 nm and Em = 594 nm.

2.3.2.3 Detection of ATP fluorescence from EEM of pork meat surface

To detect the ATP fluorescence information of pork surface from EEM, two-dimensional Savitzky–Golay second-order differentiation was applied to pork surface EEMs. Figure 11 shows the second-derivative EEM of pork surface at 72 h. Here the window size extracted for Savitzky–Golay differentiation was 5 x 5 points (8 x 8 nm; m = 2 in Eqn. 1). In general, negative peaks in second-derivative fluorescence intensity correspond to the fluorescence intensity peaks. The negative peak **a** in Fig. 2.11 is from tryptophan, **b** is from NAD(P)H, **c** is

from protoporphyrin, and these negative peaks correspond to the fluorescence intensity peak (Fig. 10c). Note that a positive peak was also observed adjacent to the negative second-derivative peak of tryptophan, enclosed with a dashed line **a** in Fig. 2.11. This positive peak accompanied the negative peak of tryptophan in the second-derivative procedure. The second-derivative procedure produces not only the direct negative peak that directly corresponds to the fluorescence peak but also produces the positive peak that accompanies the negative peak. Therefore, this positive peak is caused by tryptophan fluorescence. A small negative peak at Ex 326 nm and Em 404 nm is assigned to vitamin B_6 (pyridoxine) on the pork surface, because the Vitamin B_6 fluorescence peak occurs at Ex 328nm and Em = 393 nm (Christensen et al., 2006).

The ATP fluorescence peak is located in the region enclosed within the dashed line **e** in Fig. 2.11; however, it is not clear in this figure whether the ATP fluorescence information is completely separated from the other peak. The second-derivative information at one excitation wavelength (284 nm at 72 h) was investigated because ATP is known to have a fluorescent excitation peak at 284 nm. Figure 12a-c show the raw fluorescence spectra, the second-derivative fluorescence spectra, and the fourth-derivative fluorescence spectra at the excitation wavelength of 284 nm, respectively. Notice that the spectra shown in Fig. 2.12b and c differ from those obtained by applying only a second-derivative procedure or a fourth-derivative procedure to the fluorescence spectra shown in Fig.

2.12a. Small negative peaks at 386 nm and 412 nm were observed in second-derivative fluorescence intensities (Fig. 2.12a), and these peaks were separated from the negative peak of tryptophan (a large negative peak around 370 nm). Therefore, the application of two-dimensional Savitzky–Golay second-order differentiation was partly successful in detecting ATP fluorescence.

However, when we looked into the changes in second-derivative fluorescence spectra at Ex = 284 nm, we found that the second-derivative fluorescence intensity around 388 nm has large differences in baseline movement between samples (Fig. 2.12b). This difference was likely caused by tryptophan fluorescence. In particular, the value of fourth-derivative fluorescence intensity at Ex = 284 nm and Em = 412 nm was positive, although a small convex area was observed at 412 nm in all samples (Fig. 2.12b). Thus, not all tryptophan fluorescence information was eliminated in second-derivative fluorescence spectra.

To completely eliminate the effect of tryptophan, two-dimensional Savitzky–Golay second-order differentiation was again implemented on the second derivative EEMs of pork surface; that is, fourth-derivative analysis of EEM data was implemented. Figure 2.13 shows the fourth-derivative EEM of pork surface at 72 h, with an enlarged scale to limit the wavelengths to 250—400 nm for excitation and 300–450 nm for emission (Fig. 2.13). In fourth-derivative EEMs, the positive peaks of fourth-derivative fluorescence intensity

correspond to fluorescence peaks. Large positive fourth-derivative fluorescence intensities around Ex 290 nm and Em 330 nm is caused by tryptophan fluorescence (area enclosed by red dashed line, (Fig. 2.13**a**). A small positive peak was observed at Ex = 302 nm and Em = 402 nm (area enclosed by red dashed line, Fig. 2.13**b**).

In order to justify that this positive peak of fourth-derivative fluorescence intensity comes from ATP, EEM of meat surface that ATP solution was inoculated were compared with EEM of control sample (Fig. 2.14a, b). Significantly higher value in fourth-derivative fluorescence intensity at Ex 300 nm and Em 410 nm was observed (Fig. 2.14a, b, c); therefore, the positive peak at Ex 300 nm and Em 412 nm can be concluded to be due to ATP fluorescence.

To investigate the spectral differences in detail, the raw fluorescence spectra, second-derivative, and fourth-derivative spectra at the excitation wavelength of 302 nm are shown in Fig. 2.15. Note that Fig. 2.15b and Fig. 2.15c differ from the derivative spectra obtained by applying only the one-dimensional derivative procedure to the raw fluorescence emission spectra shown in Fig. 2.15a. Compared to the raw fluorescence spectra, the fluorescence intensity decreased over the range of 380–440 nm, indicating a decrease in the contribution by tryptophan. Apart from the tryptophan fluorescence peak, no fluorescence signal was detected (Fig. 2.15a). In the second-derivative fluorescence spectra, a large negative value less than 400 nm was observed, which corresponds to the tryptophan fluorescence peak. A very small convex region toward the negative direction

of the y-axis was observed around 410 nm, but the peak from ATP itself was not detected separately. In fourth-derivative fluorescence spectra, the baseline movement was absent over the range of 390–420 nm. Moreover, a small positive peak was observed around 410 nm (Fig. 2.15c). The positive and negative peaks at 400 nm and 406 nm are caused by tryptophan. To observe this small peak in detail, we investigated the fourth-derivative fluorescence spectra at the excitation wavelength of 302 nm, limiting the emission wavelengths to 390–440 nm and the range of fourth-derivative fluorescence intensity of– 10 through 30, as shown in Fig. 2.16. The ATP fluorescence peak is clearly separated from the tryptophan peak. Therefore, ATP fluorescence was successfully detected on pork surface using the fourth-derivative procedure. When we looked the tendency of the peak value at 410 nm, a decrease in fourth-derivative fluorescence intensity at Em 410 nm was observed during 0–24 h, which likely corresponds to the degradation of pork surface tryptophan (this relationship will be elaborated in the following section). After 24 h, the positive peak at Em = 410 nm increased with time. Taking into consideration that ATP fluorescence peaks were observed at Ex = 284 nm and Em = 388, 396, and 410 nm in *Pseudomonas florescens* cultures (Fig. 2.8c), this positive peak is likely caused by ATP fluorescence. The peak excitation wavelength differed between the standard solution (288 nm) and *Pseudomonas fluorescens* culture (284 nm), but this wavelength shift likely results from environmental differences. Fluorescence peaks are known to shift in response to the surrounding environment, such as pH; thus, the excitation peak of ATP fluorescence probably shifted from 284 nm to 302 nm on pork meat surface.

2.3.2.4 Relationship between aerobic plate count and fourth-derivative fluorescence intensity

Figures 2.17–2.19 show the relationship between aerobic plate count and fourth-derivative fluorescence intensity from tryptophan (Ex = 300 nm and Em = 400 nm), NAD(P)H (Ex = 340 nm and Em = 456 nm), and ATP (Ex = 302 nm and Em = 410 nm). The tryptophan wavelength pair was selected because the fluorescence intensities were saturated caused by the high sensitivity of the device. Note that the positive peak of this wavelength pair accompanied the direct positive peak of tryptophan. In the early stage of microbial spoilage (up to 10^6 CFU cm^{-2}), the fourth-derivative fluorescence intensity differed slightly. This small change was probably because the increase in tryptophan within microorganisms offset the degradation of tryptophan on the pork surface by microorganisms. Above 10^6 CFU cm^{-2}, the fourth-derivative fluorescence intensity from tryptophan dramatically decreased (Fig. 2.17). This decrease in tryptophan fluorescence occurred because the degradation of tryptophan by microorganisms outweighed the increase in tryptophan in microorganisms.

The fourth-derivative fluorescence intensity at Ex = 340 nm and Em = 456 nm, assigned to NAD(P)H, increased with aerobic plate count (Fig. 2.18). This relationship is consistent with NADPH and NADH production. NADPH is produced by the HMP pathway (during the degradation of glucose), and NADH is produced in the glycolytic pathway, TCA cycle, and fatty acid oxidation.

Figure 2.19a, b shows the relationship between fourth-derivative fluorescence intensity at Ex = 284 nm and Em = 410 nm, is the peak assigned to ATP, and aerobic plate count (Fig. 2.19a) or ATP content (Fig. 2.19b) of pork surface. A correlation was observed between aerobic plate count and fourth-derivative fluorescence intensity at Ex = 302 nm and Em = 410 nm (correlation coefficient, 0.50), and this correlation is consistent with ATP production of microorganisms. As microbial spoilage progresses, ATP also increased because ATP content of microorganisms remains relatively constant. For Gram-negative bacteria, the amount of ATP per cell is approximately 10^{-18} mol cell^{-1} (*E. coli*) (3.6 x 10^{-18} mol cell^{-1} for *Pseudomonas spp.*) (Monji, 2000). We should pay attention here to three factors: one is that the fourth-derivative fluorescence intensity with aerobic plate count decreased from 10^3 to 10^5 CFU/cm^2 (Fig. 2.19a), likely caused by the degradation of ATP from pork surface. ATP is present not only in microorganisms but also in pork meat itself. At the initial stage of microbial spoilage, ATP from the pork surface outweighs that of the microorganisms. This higher ATP content in the pork probably leads to the higher ATP fluorescence signal. A higher ATP fluorescence signal was observed even in the lower range of ATP content of 10^{-13} to 10^{-12} mol cm^{-2} (Fig. 2.19b). Here, the fluorescence intensity of the meat was measured non-destructively by lighting the excitation light on the meat surface. In contrast, ATP content measured by the swabbing technique also includes ATP from pork itself. However, the ATP content measured by the fluorescence technique was probably higher than that measured by the swabbing technique, and this difference leads to the higher ATP fluorescence signal relative to ATP content. The second

factor is that the aerobic plate count was transformed into logarithm, while the fourth-derivative fluorescence intensity was not. The relationship between the logarithm of the fourth-derivative fluorescence intensity at Ex = 302 nm and Em = 410 nm and the aerobic plate count or ATP content of pork surface is shown in Fig. 2.19c and Fig.2.19d, respectively. A smaller correlation was observed (determination coefficient, 0.47), possibly caused by the variation in the fourth-derivative fluorescence intensity in the range of low aerobic plate count. Finally, there was great variation in fourth-derivative fluorescence intensity at Ex 302 nm and Em 410 nm between samples with the same aerobic plate count (or ATP content). The fluorescence intensities of pork surface were measured in four locations for each sample, while the aerobic plate count and ATP content were measured only once for each 4 × 4 cm sample. Thus, the fluorescence intensities varied between tested locations in each sample. To consider the variation in fluorescence intensities within a same sample, the mean value of the fourth-derivative fluorescence intensity was calculated for each pork sample and compared to the aerobic plate count (Fig. 2.19e) or ATP content (Fig. 2.19f). The mean value of the fourth-derivative fluorescence intensity had a higher correlation to aerobic plate count (determination coefficient, 0.65) or ATP content (determination coefficient, 0.81) than that of raw fourth-derivative fluorescence intensity (Fig. 2.19c, d). In this case, the fourth-derivative fluorescence intensity was higher at the initial stage of microbial spoilage, probably because of the contribution of ATP from the pork itself, but good linearity was observed over 10^5 CFU cm^{-2} (where the data from 0 h were excluded; determination

coefficient, 0.84 vs. aerobic plate count). This observation supports the successful detection of the ATP fluorescence signal from fourth-derivative EEMs.

2.3.2.4 Development of prediction models for aerobic plate count and ATP content of pork surface by PLSR using 2-dimensional Savitzky–Golay second-order differentiation

The prediction models of aerobic plate count and ATP content of pork surface were developed from EEMs, second-derivative EEMs, and fourth-derivative EEMs by PLSR. First, the prediction models were developed using raw EEMs. Of 112 total datasets, 84 were used for developing the model (calibration) and the other 28 were used for validation. The prediction with the raw EEMs of pork surface showed reasonably good accuracies (correlation coefficient, 0.91; root mean squared error of prediction (RMSEP), 0.74 $\log_{10}$ CFU cm^{-2}) (Table 1). Figure 20 shows the score plot of principle component (PC) 1 and PC 2. The PC 1 score increased with aerobic plate count (Fig. 2.20), indicating that PC 1 reflects the changes in microbial spoilage. A small tendency toward decrease in the PC 2 score was observed in the early stage of microbial spoilage; however, this tendency was not observed in the higher aerobic plate count group (shown in green triangles in Fig. 2.20). Thus, it is unclear what the PC 2 score means. Figure 21 shows the LV 1 loading plot for the prediction of aerobic plate count from fluorescence intensities. LV 1 loading indicates the weight of each wavelength on the LV 1 score. Taking into consideration that

LV 1 reflected the increase in aerobic plate count, the wavelength area with the higher absolute value of LV 1 loading reflected the contribution of the fluorescence intensity of that wavelength to the prediction model. The absolute values of LV 1 loading around λ_{Ex} = 300 nm and λ_{Em} = 400 nm are high and negative in value (**a** in Fig. 2.21). Note that the fluorescence intensities around Ex 290 nm and Em 330 nm were saturated to the maximum measurable value of the device; thus, these saturated areas were eliminated for calculation of the prediction model. The wavelength pair of Ex = 300 nm and Em = 400 was caused by tryptophan fluorescence. This high absolute value with a negative sign indicates that the fluorescence intensities at Ex = 300 nm and Em = 400 nm decreased with aerobic plate count. This decrease in tryptophan fluorescence with microbial spoilage corresponds to the degradation of tryptophan on the pork surface by microorganisms, as shown in Figure 2.17. In addition, higher positive, absolute values of LV 1 loading were observed at Ex 340 nm and Em 460 nm (**b** in Fig. 2.21), which are consistent with the increase in fluorescence intensity from NAD(P)H with aerobic plate count of pork surface. This relationship matches the production of NADH and NADPH by microorganisms. Therefore, the model developed here reflects changes in fluorescence intensities from tryptophan and NAD(P)H, as reported by Oto et al. (2013).

Prediction models were also developed using the second-derivative fluorescence intensities to allow for inclusion of ATP fluorescence information (Table 2). The second-derivative (or fourth-derivative, or sixth-derivative) EEMs areas of Ex ≤ 402 nm and Em ≤ 310 nm were deleted in the region of the second-derivative EEMs because the fluorescence intensities of the area around the tryptophan peak were maximally saturated. The aerobic plate count and ATP content calibrated and predicted from the second-derivative fluorescence intensities had higher prediction accuracy (correlation coefficient, 0.94) than that developed from raw fluorescence intensities. The score and loading plot was then investigated to determine which wavelengths contributed to the prediction model. The score plot showed that the PC 1 score increased with aerobic plate count, indicating that PC 1 reflects microbial spoilage (Fig. 2.22). LV 1 loading indicated a high absolute value at Ex = 300 nm and Em = 400 nm with a negative value, reflecting the increase in second-derivative fluorescence intensity at Ex 300 nm and Em = 400 nm with microbial spoilage (**A** in Fig. 2.23). We should note that the second-derivative fluorescence intensity at this wavelength pair of Ex = 300 nm and Em = 400 nm was positive, and this positive peak accompanied the direct negative peak corresponding to the fluorescence peak from tryptophan. The decrease in the accompanying positive peak of second-derivative fluorescence intensity reflects the decrease in fluorescence intensity; thus, this high absolute value with a negative sign reflects the decrease in tryptophan fluorescence. As described before, this relationship is consistent with the degradation of tryptophan of pork surface by microorganisms. In addition, high absolute values at Ex 340 nm and Em

460 nm and at Ex 420 nm and Em 594 nm were observed with a negative sign, shown in **B** and **C** in Fig. 2.23, respectively, corresponding to the production of NAD(P)H and porphyrins by microorganisms. However, no contribution of ATP fluorescence was observed in the prediction of aerobic plate count from second-derivative EEMs. The absolute value at Ex = 284 nm and Em = 410 nm was high, with a negative sign (**D** in Fig. 2.23); however, taking into consideration that the excitation wavelength peak of ATP fluorescence shifted from 284 nm to 302 nm on pork surface and that the negative peak of second-derivative fluorescence intensity from ATP was not observed apart from 72 h, this model did not reflect the changes in ATP fluorescence of pork surface. The ATP fluorescence signal was successfully detected from fourth-derivative EEMs; therefore, prediction models using fourth-derivative EEMs were developed to include the ATP fluorescence signal.

The prediction accuracies for aerobic plate count (correlation coefficient, 0.95; RMSEP of $\log_{10}$, 0.68, CFU cm^{-2}) were higher than those predicted from raw fluorescence intensities or second-derivative fluorescence intensities (Table 1, 2, 3). The contribution of wavelength to the prediction models was investigated. The LV 1 score increased with aerobic plate count (Fig. 2.24). Also, as a rule, the LV 2 score increased with aerobic plate count, although some LV 2 scores were low (Fig. 2.24). Figure 2.25 shows the LV 1 loading

with fourth-derivative fluorescence intensities for the prediction of aerobic plate count. The high absolute value of LV 1 loading with a negative sign around Ex 290 nm and Em 346 nm indicates that the fourth-derivative fluorescence intensity at this wavelength pair decreased with aerobic plate count. This relationship is consistent with the degradation of tryptophan as described above (Fig. 2.25a). It was difficult to understand what contributed to LV 2 loading around Ex 290 nm and Em 346 nm and whether these high absolute value with a negative sign reflected a decrease in tryptophan or another aromatic amino acid such as tyrosine. However, a relatively high absolute value with a positive sign is clear at Ex 302 nm and Em 410 nm, which corresponds to ATP production by microorganisms (Fig. 2.25b). That is, as microbial spoilage progresses, ATP from microorganisms also increases. Therefore, we can conclude that the models developed here reflect changes in not only tryptophan and NAD(P)H but also ATP. This additional inclusion of the ATP fluorescence signal makes the prediction accuracies higher when predicted using fourth-derivative procedure EEMs.

The benefit of using the fourth-derivative procedure on EEMs was confirmed by using the dataset of EEMs of pork surface, aerobic plate count, and ATP content by Oto (unpublished data). Fluorescence intensities, aerobic plate count, and ATP content were measured in the same manner as in this study except that the fluorescence

spectrophotometer parameters differed as follows: photomultiplier voltage, 400 V; slit width, 5 nm (for both excitation and emission); excitation wavelength, 250–300 nm; and emission wavelength, 250–400 nm. The prediction models for aerobic plate count and ATP content were developed by PLSR from EEMs, second-derivative EEMs, and fourth-derivative EEMs. In the dataset obtained by Oto, the prediction accuracies showed improvement (Table 4). In their data, it was difficult to understand what factor contributed to the improved prediction model because in this case the emission wavelength used was below 300 nm and the ATP fluorescence signal, which was located at Ex 302 nm and Em 410 nm, could not be detected. But the results of the improved model with the data by Oto demonstrated the efficacy of fourth-derivative procedure on EEMs. It can be concluded that fourth-derivative procedure was a beneficial technique for the data not only obtained in this study but other data.

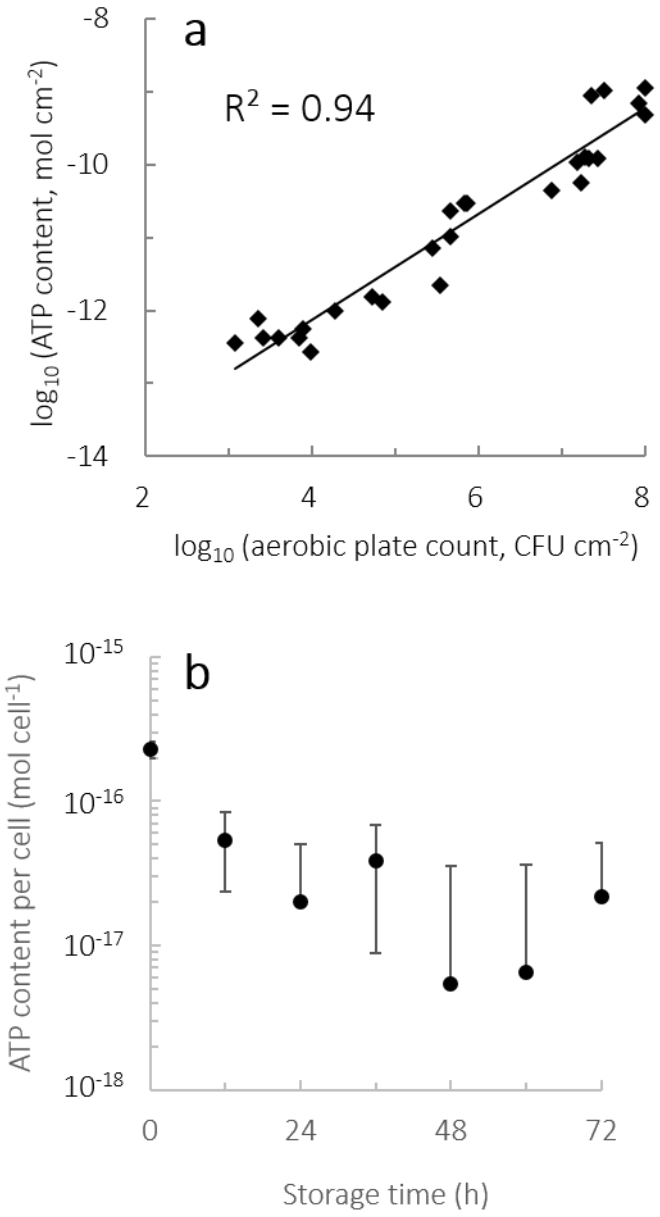

Figure 2.9. The relationship between aerobic plate count and ATP content (a) and changes in ATP content per cell (b). A good correlation (determination coefficient, 0.94) indicates that ATP content can be used as an indicator of the microbial contamination of meat (a). The ATP content per cell was approximately 10^{-16} mol $cell^{-1}$ and declined with time,

reaching approximately 10^{-18} to 10^{-17}, which is the amount of ATP reported in gram-negative bacteria (Monji, 2000).

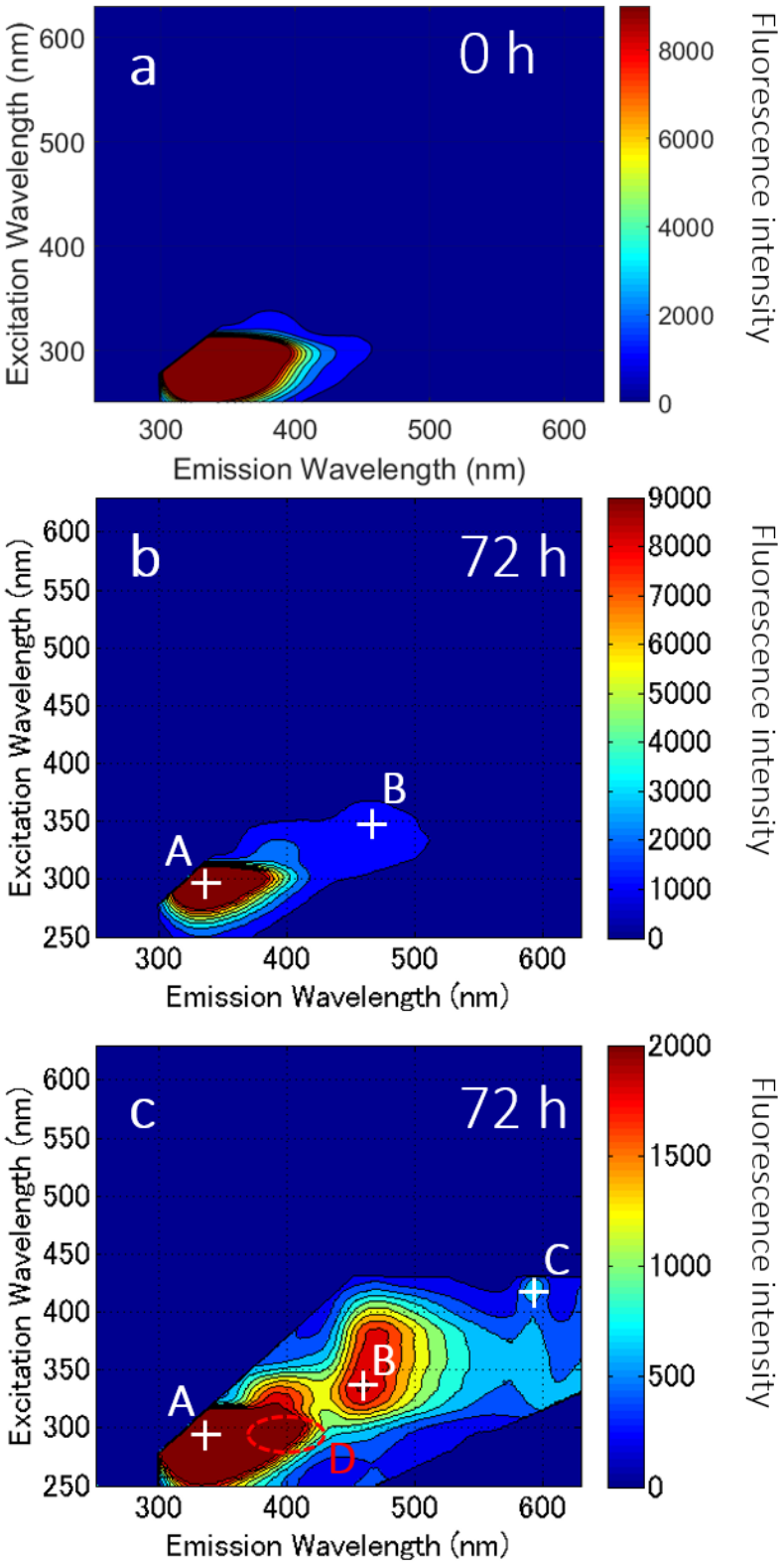
a
0 h
Excitation Wavelength (nm)
Emission Wavelength (nm)
Fluorescence intensity
b
72 h
A
B
c
72 h
A
B
C
D

Figure 2.10. Excitation-emission matrices of pork surface at 0 h (a) and 72 h (b, c). Fig. 9c is an enlargement of the EEM of pork surface at 72 h, with a smaller range of fluorescence intensity (0–2000). Fluorescent peaks are attributed to the following components: Ex 290 nm and Em 330 nm, tryptophan (**A** in **b** and **c**); Ex 340 nm and Em 460 nm, NAD(P)H (**B** in **b** and **c**); and Ex 420 nm and Em 594 nm, zinc protoporphyrin (**C** in **c**). ATP fluorescence was masked by the fluorescence of tryptophan (region enclosed by red dashed line in **D** in **c**).

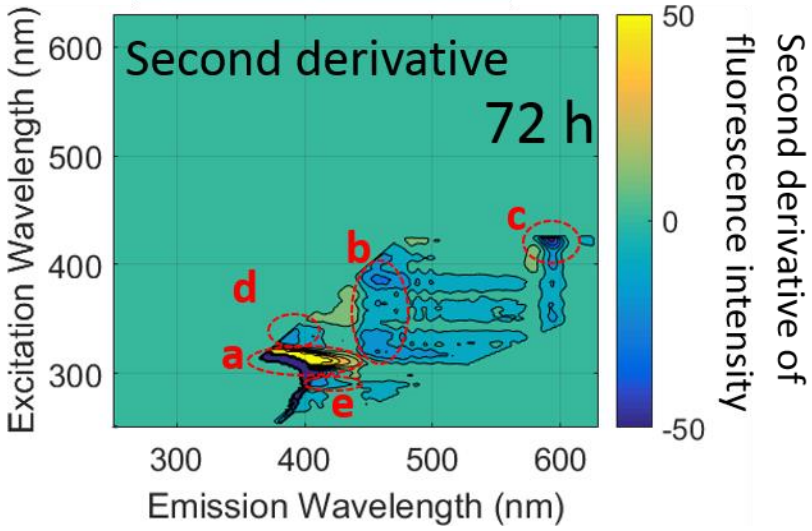

Figure 2.11. Second-derivative EEM of pork surface at 72 h. The negative peak at the wavelength pair enclosed by the dashed line corresponds to tryptophan (**a**); NAD(P)H (**b**); zinc protoporphyrin (**c**), and Vitamin B_6 (**d**). The negative value of the second-derivative fluorescence intensity at **e** is possibly caused by ATP.

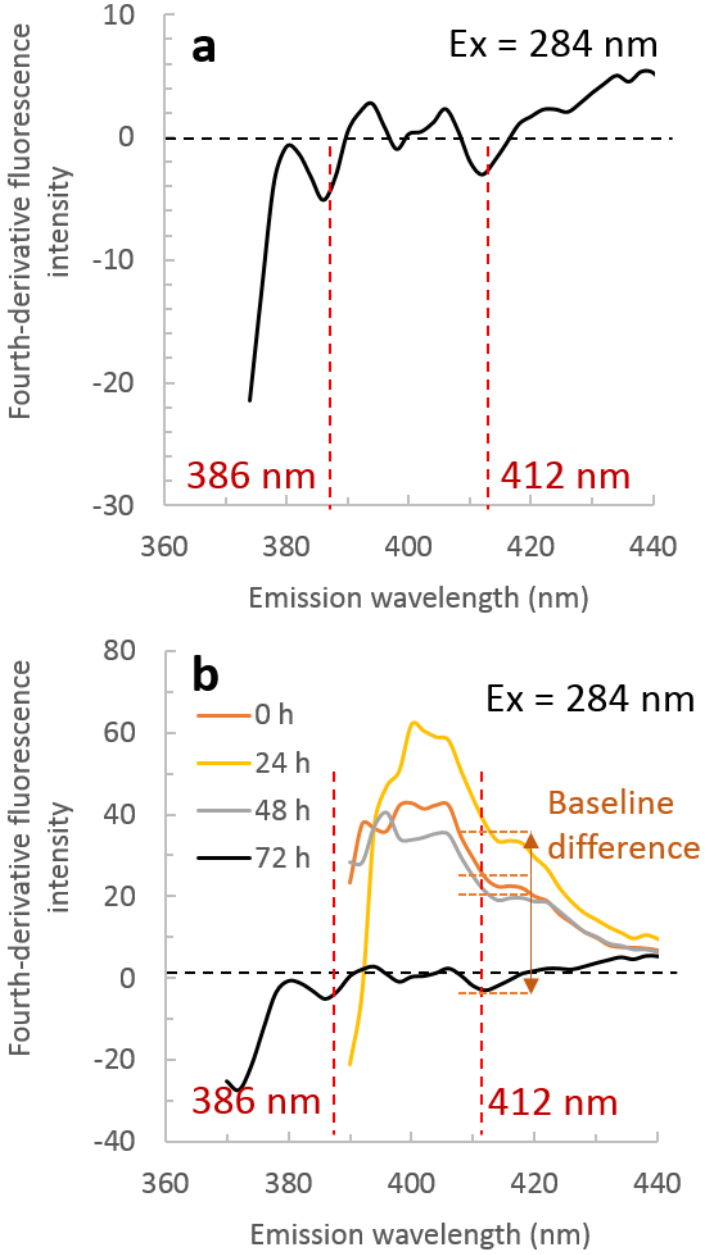

Figure 2.12. Second-derivative fluorescence spectra at the excitation wavelength of 284 nm for different samples at 0–72 h (figure with different samples in Fig. 2.11b). Although negative peaks were observed around 386 nm and 412 nm at 72 h (**a**, **b**), possibly from ATP, the baselines in the region of 390–420 nm differed between samples (**b**). Therefore,

it was difficult to conclude that the ATP fluorescence signal was detected with second-derivative fluorescence intensities from pork surface.

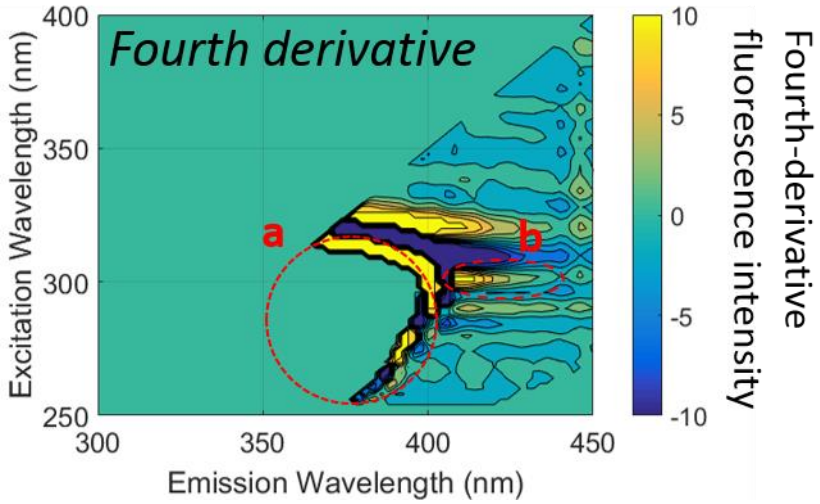

Figure 2.13. Fourth-derivative EEM of pork surface at 72 h. The area around Ex = 290 nm and Em = 330 nm was deleted because the fluorescence intensities were saturated to the maximum measurable value; therefore, fourth-derivatives cannot be calculated correctly. Positive values around Ex 290 nm and Em 360 nm (enclosed by dashed line **a**) was caused by tryptophan fluorescence. A small positive peak at Ex = 302 nm and Em = 402 nm was caused by ATP fluorescence, indicating that ATP fluorescence was successfully detected using fourth-derivative EEM of pork surface.

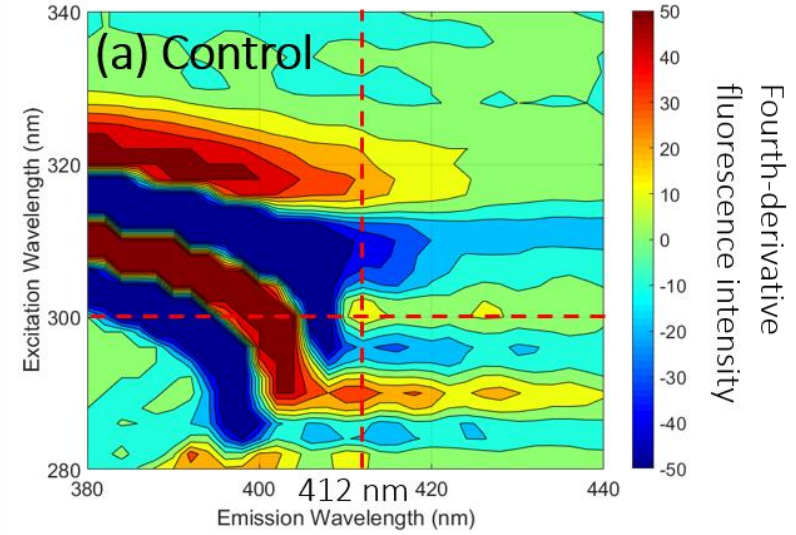

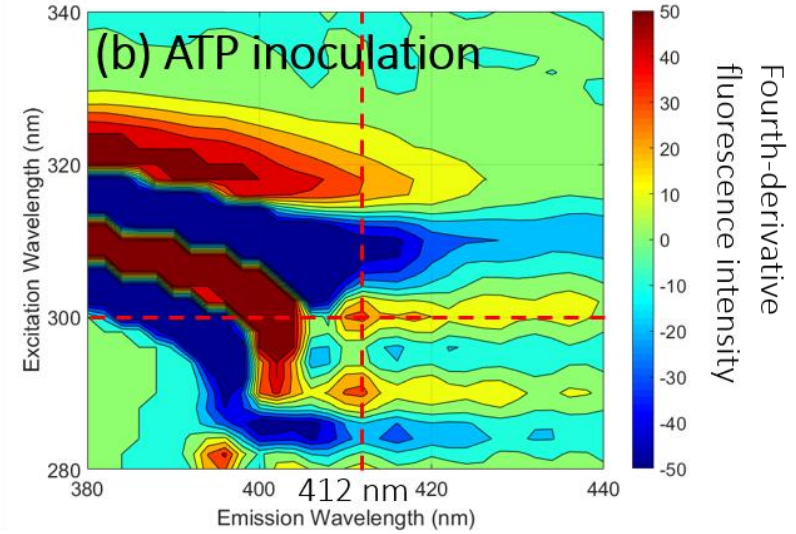

(c) A comparison at Ex 300 nm and Em 412 nm

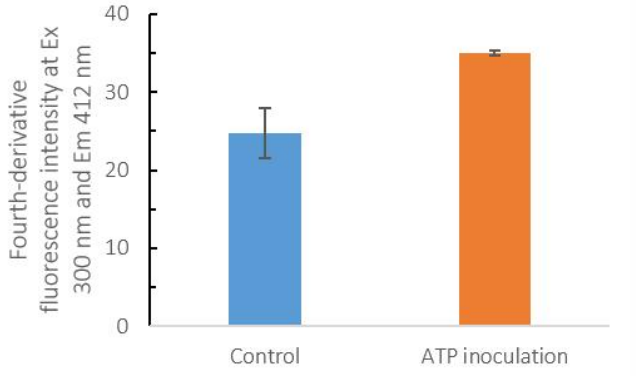

Figure 2.14. Fourth-derivative EEM of control meat surface (a) and that of meat surface on which ATP solution of 1 ml of 1.0 x 10^{-1} mol l^{-1} was inoculated. Significantly higher value in fourth-derivative fluorescence intensity at Ex 300 nm and Em 410 nm was observed, which justified that the positive peak of fourth-derivative fluorescence intensity at Ex 302 nm and Em 410 nm on pork surface was due to ATP fluorescence.

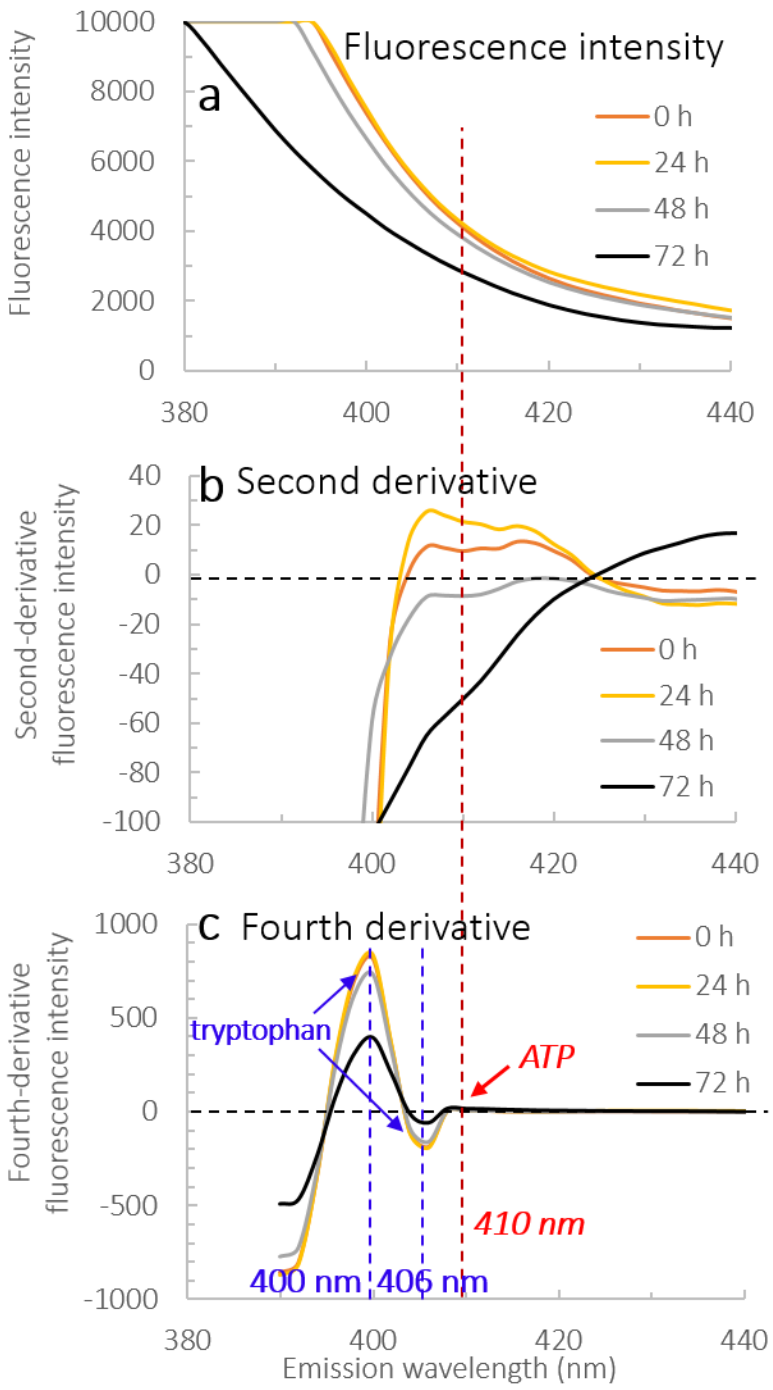

Figure 2.15. Fluorescence raw spectra (a), second-derivative fluorescence spectra (b), and fourth-derivative fluorescence spectra (c) of pork surface at the excitation wavelength of

302 nm. Second-derivative and fourth-derivative fluorescence intensities at wavelengths below 390 nm could not be calculated correctly, so they are not included. The largest peak of fluorescence intensity (**a**) and negative values of second-derivative fluorescence intensity (**b**) is caused by tryptophan. The baseline difference was removed using the fourth-derivative procedure (**c**). Fourth-derivative fluorescence intensities also revealed a positive peak at 400 nm and a negative peak at 406 nm caused by tryptophan and a very small positive peak at 410 nm (enlarged in Figure 15). Therefore, the ATP fluorescence peak was separated from that of tryptophan and was successfully detected in fourth-derivative fluorescence intensities.

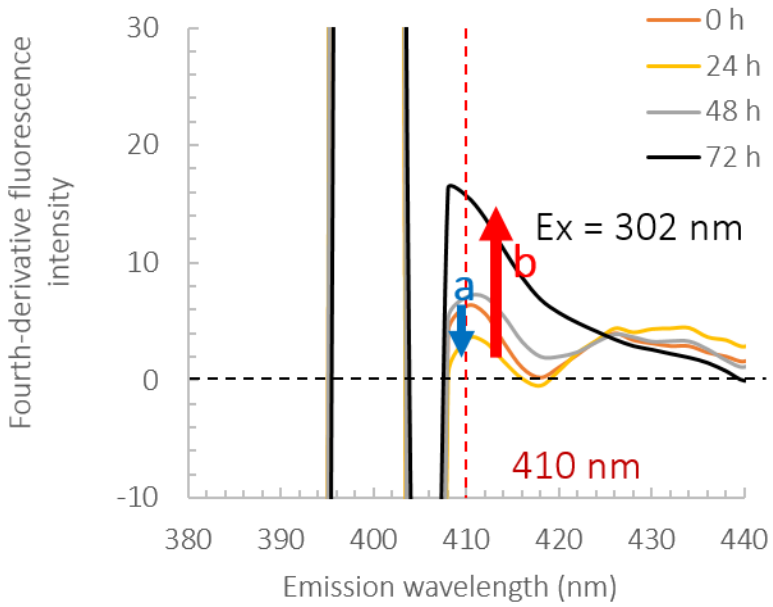

Figure 2.16. Fourth-derivative fluorescence spectra at the excitation wavelength of 302 nm from different samples (0–72 h) with a fourth-derivative fluorescence intensity range of–10 through 30. The positive peak at 400 nm occurred because it accompanied the tryptophan peak. The positive peak of fourth-derivative fluorescence intensity at 410 nm, which is separate from the tryptophan peak, is caused by ATP. The fourth-derivative fluorescence intensity increased with time apart from 0–24 h, which correlates with the increase in ATP accompanying microbial growth (b). The initial decrease in fourth-derivative fluorescence intensity at Ex 302 nm and Em 410 nm (a) probably occurred because ATP from pork itself outweighed the ATP from microorganisms during the initial stage of microbial spoilage but was degraded over time.

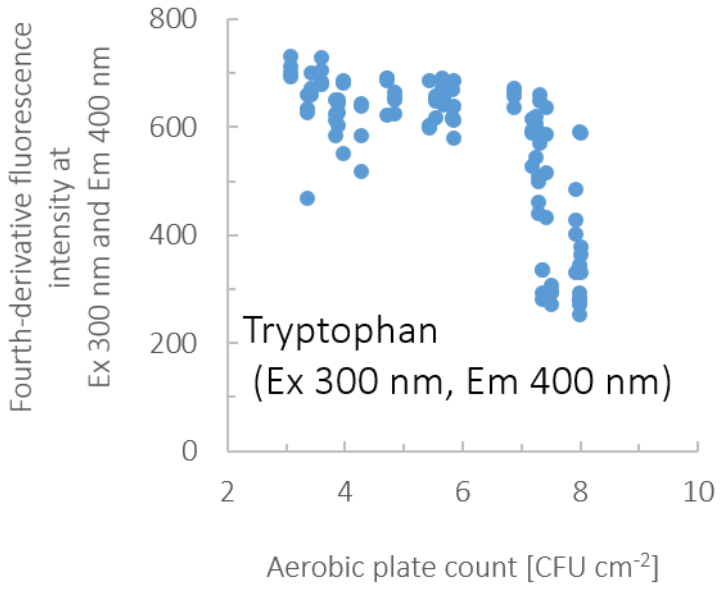

Figure 2.17. Fourth-derivative of fluorescence intensity at Ex = 290 nm and Em = 390 nm, which is caused by tryptophan, decreased with aerobic plate count. Decrease in fourth derivative of fluorescence intensity is consistent with the degradation of tryptophan by microorganisms as microbial spoilage progressed.

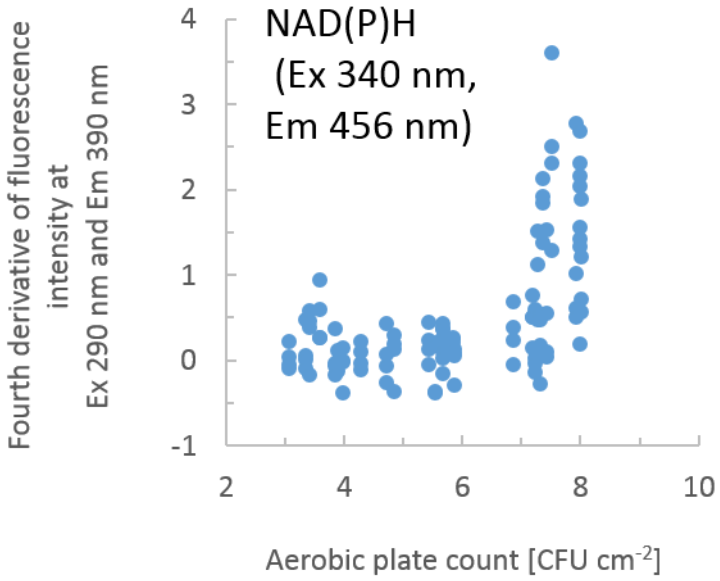

Figure 2.18. Fourth-derivative fluorescence intensity at Ex 340 nm and Em 456 nm, caused by NAD(P)H, increased with aerobic plate count, consistent with NADPH and NADH production by the HMP pathway during glucose degradation metabolism and glycolysis, respectively.

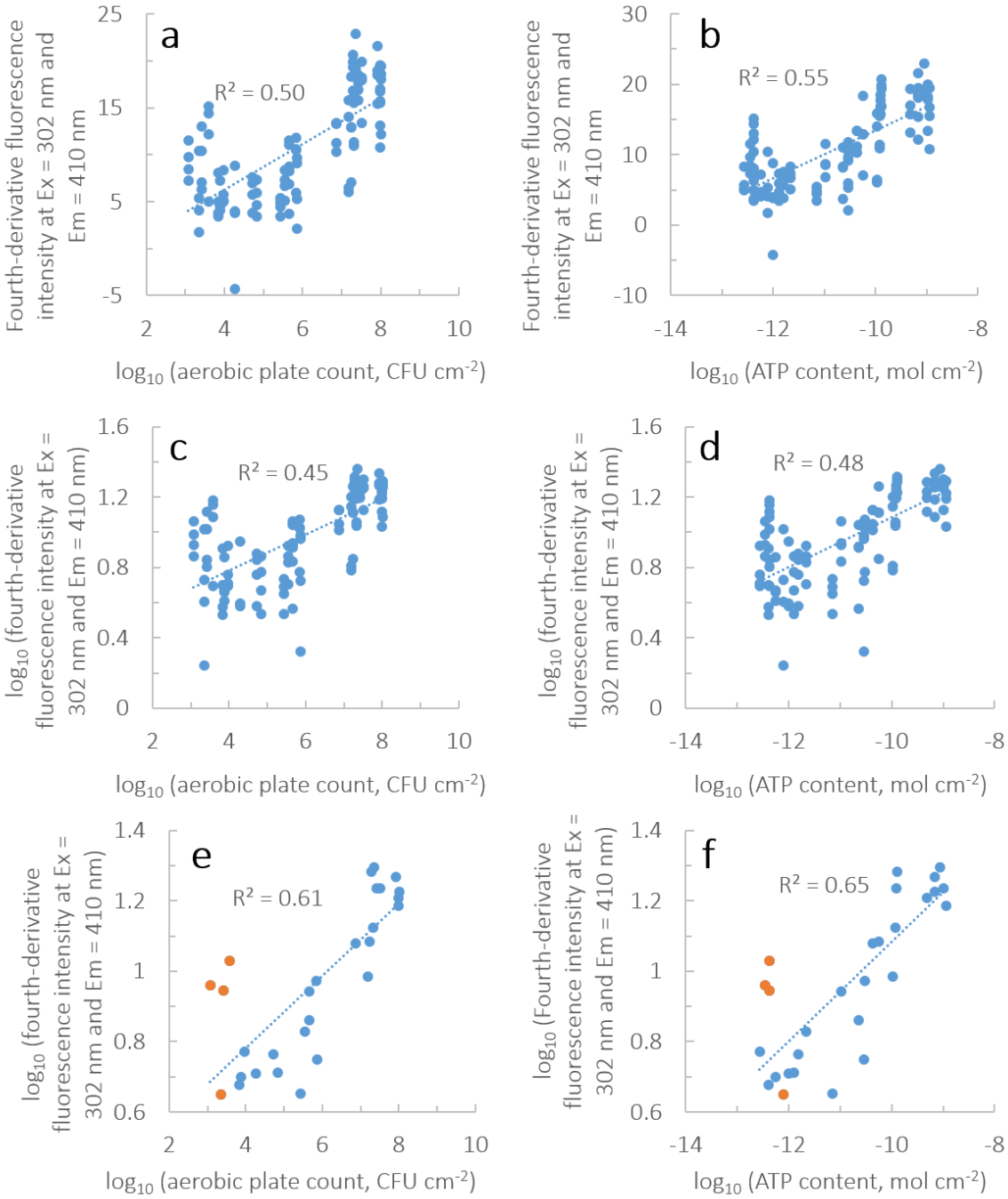

Figure 2.19. The fourth-derivative fluorescence intensity at Ex 302 nm and Em 410 nm increased with aerobic plate count (**a**, **c**, **e**) and ATP content (**b**, **d**, **f**) because

microorganisms contain ATP. Fourth-derivative fluorescence intensity at Ex 302 nm and Em 410 nm was transformed into logarithms in **c** and **d** because aerobic plate count or ATP content was transformed into logarithm. Also, the fourth-derivative fluorescence intensity was measured at four sites in each pork sample, but the aerobic plate count and ATP content were measured from one area of each 4 × 4 cm^2 sample. The mean of the fourth-derivative fluorescence intensity was calculated and plotted against aerobic plate count or ATP content (**e** and **f**). A good linearity with exclusion of the 0 h data (shown in orange circle) shows the relationship between aerobic plate count (or ATP content) and ATP fluorescence signal from the microorganisms and not the pork itself. The fluorescence signal at 0 h indicated the ATP fluorescence from the pork alone. The higher ATP fluorescence signal at 0 h even against ATP content (f) was probably because the ATP content measured was that picked up by the swabbing technique; therefore, the ATP content did not include all the ATP from the pork surface, which is measured in fluorescence information.

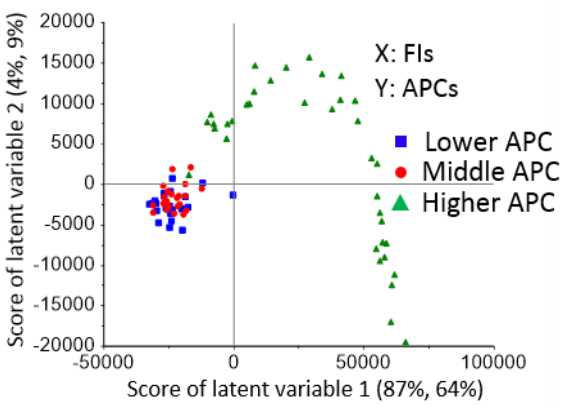

Figure 2.20. Score plots of LV 1 and LV 2 with the explanatory variable of fluorescence intensity and response variable of aerobic plate count. The LV 1 score increases with aerobic plate count, indicating that LV 1 reflects microbial spoilage.

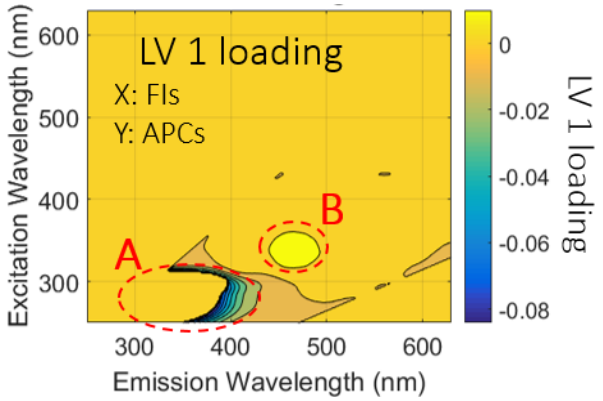

Figure 2.21. LV 1 loading contour for the prediction of aerobic plate count with fluorescence intensity. High absolute values with negative signs around the tryptophan peak (Ex 290 nm and Em 330 nm) shown in **A** reflects the decrease in tryptophan fluorescence with microbial spoilage, which is consistent with the degradation of tryptophan of pork surface by microorganisms. High absolute values around Ex 340 nm and Em 460 nm (**B**) indicated the increase in NAD(P)H fluorescence, which is consistent with NAD(P)H production by microorganisms.

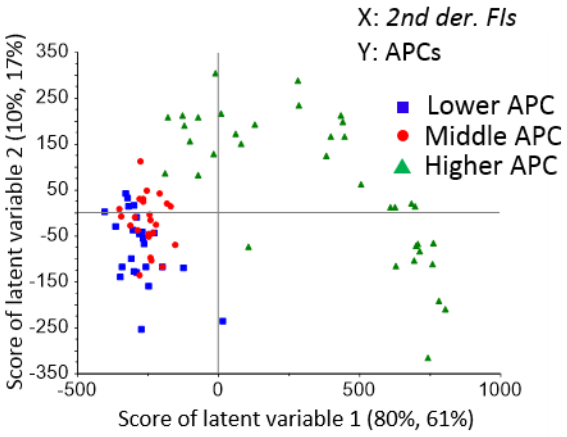

Figure 2.22. Score plots of LV 1 and LV 2 with the explanatory variables of *second-derivative* fluorescence intensity and response variable of aerobic plate count. The LV 1 score increases with aerobic plate count, indicating that LV 1 reflects progressive microbial spoilage. Also, there was a small tendency of increased LV 2 loading with aerobic plate count, indicating that LV 2 reflects microbial spoilage.

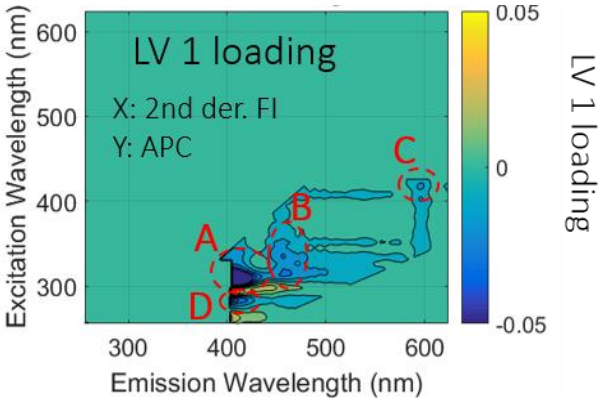

Figure 2.23. Enlarged plot of LV 1 loading for the prediction of aerobic plate count from *second-derivative* fluorescence intensities. The high absolute value with negative sign at Ex 304 nm and Em 404 nm (**A**) reflects the decrease in second-derivative fluorescence intensity, consistent with the degradation of pork surface tryptophan with microbial spoilage. Note that the second-derivative fluorescence intensities of these wavelength areas were positive and these second-derivative fluorescence intensities accompanied the tryptophan fluorescence peak (**A**). The high absolute value with negative sign at Ex 340 nm and Em 460 nm reflects the decrease in second-derivative fluorescence intensity from NAD(P)H, which is consistent with NAD(P)H production by microorganisms (**B**). The higher absolute value at Ex 420 nm and Em 592 nm with negative sign reflects the decrease in second-derivative fluorescence intensity from zinc protoporphyrin, consistent with porphyrin production by microorganisms (**C**). Higher absolute values with a negative sign at Ex 280 nm and Em 406 nm were caused by tyrosine degradation (**D**). The second-derivative fluorescence intensities at these regions were also positive because of tryptophan, as described above.

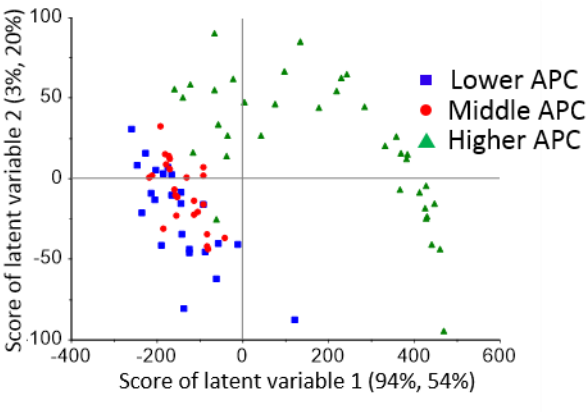

Figure 2.24. Plot of LV 1 and LV 2 scores with the explanatory variable of *fourth-derivative* fluorescence intensity and response variable of aerobic plate count. LV 1 score increased with aerobic plate count, indicating that LV 1 reflects the progression of microbial spoilage. LV 2 loading also increased with aerobic plate count, indicating that LV 2 also reflects microbial spoilage progression.

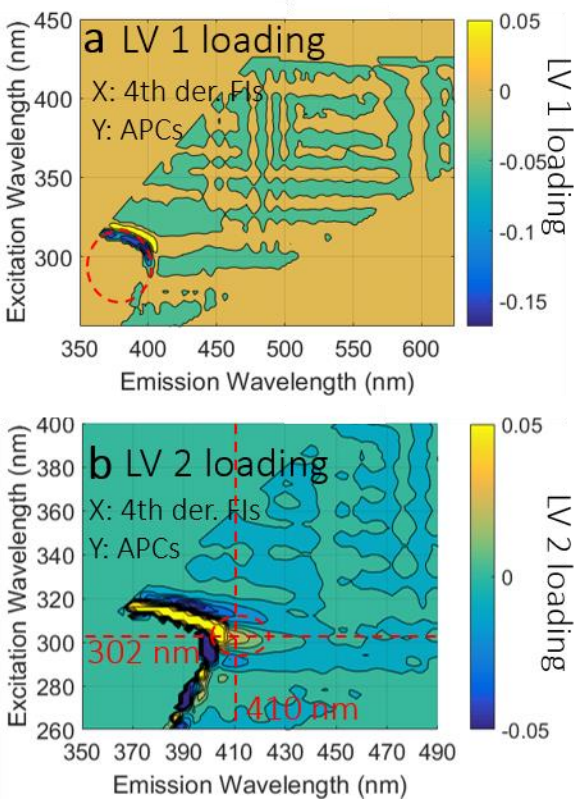

Figure 2.25. LV 1 loading (a) and LV 2 loading (b) for the prediction of aerobic plate count of pork surface using *fourth-derivative* fluorescence intensities. The high absolute value of LV 1 loading at Ex 300 nm and Em = 400 nm with a negative sign reflects the decrease in fourth-derivative fluorescence intensities from tryptophan, consistent with the degradation of tryptophan by microorganism. High LV 2 loading at Ex 274 nm and Em 390 nm reflects the decrease in fourth-derivative fluorescence intensity from tyrosine, consistent with the degradation of tyrosine by microorganisms. Finally, the relatively large absolute value of LV 2 loading at Ex = 302 nm and Em = 410 nm indicates that the fourth-derivative fluorescence intensity from ATP increases with aerobic plate count, which is consistent with ATP production by microorganisms during microbial spoilage.

Table 1. Prediction of aerobic plate count and ATP content of pork surface using EEMs by PLSR

		r_p	RMSEP
Fluorescence intensity	$\log_{10}$ (aerobic plate count, CFU cm^2)	0.91	0.75
Fluorescence intensity	$\log_{10}$ (ATP content, mol cm^2)	0.91	0.58

Table 2. Prediction of aerobic plate count and ATP content of pork surface from second-derivative EEMs by PLSR

Explanatory variable	Objective variable	r_p	RMSEP
Second derivative of fluorescence intensity	$\log_{10}$ (aerobic plate count, CFU cm^2)	0.94	0.74
Second derivative of fluorescence intensity	$\log_{10}$ (ATP content, mol cm^2)	0.92	0.62

The unit of RMSEP is $\log_{10}$ (CFU/cm^2) or $\log_{10}$ (molcm^2)

Table 3. Prediction of aerobic plate count and ATP content of pork surface from second-derivative EEMs by PLSR

Explanatory variables	Objective variables	r_p	RMSEP
Fourth derivatives of fluorescence intensities	$\log_{10}$ (aerobic plate count, CFU/cm^2)	0.95	0.68
Fourth derivatives of fluorescence intensities	$\log_{10}$ (ATP content, mol cm^2)	0.94	0.56

Table 4. Prediction of aerobic plate count and ATP content of pork surface from second-derivative EEMs by PLSR

Explanatory variable	Objective variable	r_p	RMSEP
Fluorescence intensity	$\log_{10}$ (aerobic plate count, CFU/cm^2)	0.86	1.0
Fluorescence intensity	$\log_{10}$ (ATP content, molcm^2)	0.92	0.83
Fourth derivative of fluorescence intensity	$\log_{10}$ (aerobic plate count, CFU cm^2)	0.87	1.0
Fourth derivative of fluorescence intensity	$\log_{10}$ (ATP content, mol cm^2)	0.90	0.95

3. Mathematical modeling of penetration of aerobic bacteria into meat

Nondestructive and rapid quantitative evaluation technique of aerobic plate count and ATP content of meat surface has been developed with fluorescence spectroscopy. However, bacteria have been known to penetrate into meat (Gill & Penney, 1977). Understanding of bacterial penetration makes it easy to grasp the non-contaminated safe region, which leads to safer provision of meat to consumers. The main pathogenic strain of bacteria for meat spoilage is *Pseudomonas,* which is highly aerobic. However, the mechanisms of penetration of aerobic bacteria into meat is unclear. Therefore, first, the mechanistic understanding of penetration of aerobic bacteria into meat was aimed using mathematical modeling. With this mechanistic understanding, the quantitative evaluation of microbial contamination of interior of meat with mathematical modeling was aimed. It is demonstrated that mathematical modeling of penetration of aerobic bacteria is mainly explained by oxygen diffusion, and mathematical modeling allows us to quantitatively evaluate the microbial contamination level of interior of meat using the surface bacterial concentration, which has been shown to be able to be predicted with fluorescence spectroscopy. Also, the mechanistic understanding of involvement of oxygen diffusion in penetration of aerobic bacteria shows that penetration depth is irrelevant of when bacteria attached on meat surface, and it can be evaluated from surface bacterial concentration.

3.1 Penetration of aerobic bacteria into meat: mechanistic understanding

3.1.1 Background

When inspecting meat for bacteriological safety, the degree of contamination is checked using, e.g., the swab method, which removes bacteria from the surface using a sterile swab. Such methods assume primarily that bacterial contamination exists only at the surface and not in the interior of the meat. However, bacteria have been known to penetrate into meat (Elmossalami & Wassef, 1971; Gill & Penney, 1977) and can result in food spoilage and food poisoning of consumers. Examples of bacterial species of concern in regard to their penetration into meat are *Pseudomonas*, *Salmonella*, *Enterobacter, and Campylobacter.* Mechanistic understanding of bacterial penetration into meat can make it easier to develop improved mitigation strategies (better prevention of contamination and improved inspection) for microbial safety of meat. Also, the mechanics understanding allows the quantitative evaluation of microbial contamination of interior of meat, which allows to locate the safe region of interior of meat, leading to safer provision of meat to consumers.

How do bacteria penetrate into meat?

Bacteria migrate into meat via gaps between muscle fibers and endomysia (Gill et al., 1984). The formation of these gaps is explained in the following section. Electron

micrographs of penetrated tissue clearly show that bacteria invade along the gap areas that develop with rigor mortis between contractile elements of muscle cells and the surrounding endomysia (Gill et al., 1984). Thomas et al. (1987) also showed that invasive isolates of *Serratia* and *Pseudomonas* were found in the spaces between perimysia and muscle fiber bundles and endomysia and muscle fiber. Noriega et al. (2009) also detected depressions and tissue perforations of chicken flesh around bacterial colonies.

How do the gaps form?

Figure 3.1 summarizes the current understanding of the formation of gaps through which bacteria can migrate. The earliest change is the partial detachment at the interface between a perimysial sheet and the endomysium of the outermost fibers in a bundle in which it contacts. After rigor mortis onset, pH falls due to the formation of lactic acid, and then actomyosin is formed by combining actin with myosin, which forms a cross-bridge. This cross-bridge produces the lateral force and then this physical force causes the shrinkage of muscle fiber (Matsubara & Got, 1984). When the perimysial–endomysial junction ruptures and the fiber bundles begin to shrink in a way that is largely unconstrained by residual attachments to the perimysium, hydrostatic pressure is generated within the fiber bundle opposing shrinkage. When the muscle fiber shrinks, gaps are formed between the muscle fiber bundle and the perimysium (Offer & Cousins, 1992). Gaps between fibers do not appear until about 24–48 h *post mortem*, by which

time, rigor mortis has presumably developed. During rigor mortis development, a further type of structural change occurs: there is at least partial rupture of the interface between muscle fibers and the endomysial network. At rigor mortis onset, the tension within the transverse structural elements of the fiber bundles may be substantially higher than that which occurs when the fiber bundles detach from the perimysial network, and this may now be sufficient to rupture the fiber–endomysial interface. Ruptures between muscle fibers and the endomysium could conceivably occur either at the interface between the fiber contents and the cell membrane, or at the interface between the cell membrane and the basement membrane. The subsequent gaps between muscle fiber and the endomysium are formed because of separation between muscle fibers and the endomysial network. The breakage of cell membranes at this time allows the sarcoplasmic proteins of the muscle fibers to diffuse freely into the extracellular space between the fibers and the endomysial network. Offer and Cousins (1992) proposed that the sarcoplasmic proteins are also able to cross the endomysial sheets and appear in the space between the fiber bundles and the perimysial network and hence appear in drippings from meat. The investigations by Offer and Cousins (1992) were made on only the *sternomandibularis* beef muscle; however, the same structural changes were observed in poultry regarding the formation of gaps between endomysia and muscle fibers or perimysia and fiber bundles (Liu et al., 1994). This study is, therefore, relevant at least to the safety of both beef and poultry.

Role of proteolysis in bacterial penetration

Proteolysis is the breakdown of proteins into smaller molecules catalyzed by cellular enzymes called proteases. Proteolysis has been considered required for (Gill & Penney, 1977), not required for (Sikes & Maxcy, 1980), and irrelevant to (Gill et al., 1984) bacterial invasion, since solutions of sarcoplasmic proteins at neutral pH have low viscosity (Amberson et al., 1964) and provide little additional resistance to penetration. Instead, reduced bacterial penetration was attributed to increased sarcoplasmic protein viscosity during rigor mortis (Gill et al., 1984). Thus, there is controversy as to why *proteolytic* bacteria penetrate more rapidly than *non-proteolytic* bacteria even though sarcoplasmic protein offers little barrier to bacterial migration.

Modeling of bacterial penetration

Modeling of bacterial penetration could not be located in the literature. Grijspeerdt (2001) developed a model for the penetration of bacteria into eggs. In related experimental work, Segel et al. (1977) stated that the average motility (random motion of bacteria using their flagella) of bacterial populations should be identified with a diffusivity parameter and developed a simple capillary assay for quantifying this parameter with sufficient accuracy to make it a valuable tool in assessing motility. Ford et al. (1991) designed the stopped-flow diffusion chamber (SFDC), which provides a well-characterized chemical gradient and reliable method for measuring bacterial migration behavior.

Capillary assay and SFDC are also used to measure chemotactic sensitivity coefficients (Ford & Lauffenburger, 1991; Lewus & Ford, 2001; Ford et al., 1991; Ford & Lauffenburger, 1992).

Missing mechanistic understanding

In spite of the abovementioned advances, a mechanistic understanding of bacterial penetration into meat has not been achieved. In particular, why does proteolysis make a significant difference in penetration rates between *proteolytic* and *non-proteolytic* bacteria even though sarcoplasmic protein offers little barrier to bacterial invasion due to its low viscosity? What makes proteolytic bacteria migrate more rapidly? What are the main factors regulating bacterial migration? Comprehensive knowledge of bacteria–environment interactions that answers these questions could be critically important for food safety.

Objectives of this study

This study hypothesizes that bacterial penetration can be explained by considering several important factors simultaneously: motility, chemotaxis, growth, and proteolysis. The possible effects of each factor in bacterial penetration into meat—motility, chemotaxis, growth, oxygen starvation, and proteolysis—are summarized in Table 3.1. Of the bacterial

species described above, *Pseudomonas* spp.*,* which is highly aerobic, is targeted for mathematical modeling because *Pseudomonas* is one of the most dominant bacterial species in microbial contamination of meat. This study is designed to develop a mathematical model of bacterial penetration into meat to provide a mechanistic understanding of the process. The model will include motility, chemotaxis toward oxygen, growth, and proteolysis. Using model results and sensitivity analysis, the goal is to understand how each mechanism or factor (and in combination) contributes to bacterial penetration.

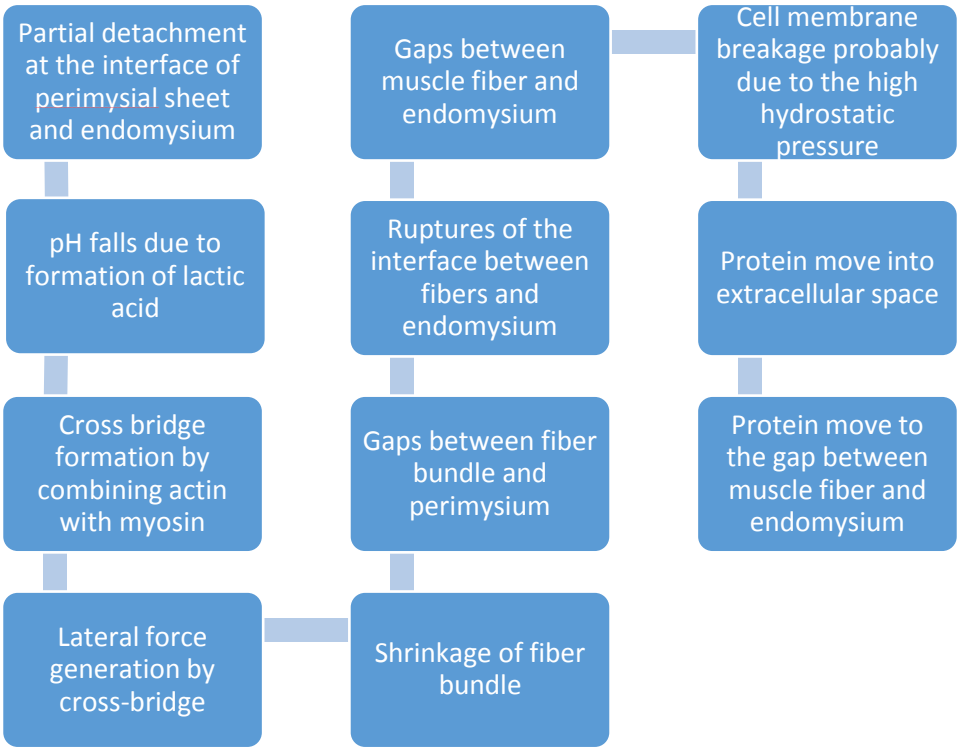

Figure 3.1. A schematic of the gap formation process.

Table 3.1 Factors affecting penetration rates

Motility	Spontaneous, diffusion-like movement of bacteria from higher to lower concentration; increases penetration.
Chemotaxis	Movement toward higher concentration of stimulus, i.e., toward the surface of the gap where oxygen concentration is higher; reduces penetration
Growth	Increases driving forces by increasing the concentration gradient of bacteria
Oxygen starvation	Reduces motility under very low oxygen concentration; reduces penetration
Proteolysis	Decreases resistance to transport by reducing viscosity within the gap; increases penetration

3.1.2 Modeling

The mathematical model consists of three parts: (1) oxygen diffusion into meat before bacterial inoculation; (2) bacterial migration following inoculation; and (3) following this migration, bacterial migration into a swab, as used in experimental studies. Oxygen diffusion prior to bacterial inoculation and bacterial migration into a swab is included to match model conditions against experimental procedures reported in the literature. Bacterial migration is simulated using this oxygen concentration profile. In the experiment conducted by Thomas et al. (1987), both top and bottom surfaces were likely exposed to air for a short time after removing a 1.5 x 1.5 x 1.5 cm^3 cube, so oxygen diffused into the gap before bacterial migration. The strain of bacteria chosen to study its penetration was *Pseudomonas* spp., based on its being highly aerobic. Following bacterial migration into the meat, bacterial migration into the swab is simulated for comparison with experimental results that involve swabbing.

3.1.2.1 Geometry

Figure 3.2 shows the model geometry used in this study—a two-dimensional rectangle of 10 µm width and 1.5 cm depth. The gap between fiber bundles and perimysia or between muscle fiber and endomysia can vary by 10–100 µm (Tornberg, 2013) and a 10 µm size was considered reasonable because the gap size in our photomicrographs of beef was 10 µm (Fig. 3.3). The depth of 1.5 cm was chosen because a 1.5 cm–wide cube of poultry was

used in the experimental work by Thomas et al. (1987), which was used to validate the model. The swabbing technique from the experiments was approximated as a 2 mm swab attached to the bottom surface after the simulation of bacterial migration, on the assumption that the amount of bacteria migrating into the swab over a given time will be what would have been picked up by a swabbing process.

3.1.2.2 Governing equation

3.2.2.1 Bacterial transport

Bacterial transport is described using a one-dimensional diffusion equation with appropriate reactions (Segel et al., 1977)

$$\frac{\partial c}{\partial t} = \underbrace{\overbrace{\mu'}^{\text{motility coefficient}} \frac{\partial^2 c}{\partial z^2}}_{\text{Motility or random motion}} - \underbrace{\frac{\partial}{\partial z}\left(\overbrace{\chi_0'}^{\text{chemotactic coefficient}} \overbrace{r(a)}^{\text{oxygen starvation}} \overbrace{\frac{\partial a}{\partial z}}^{\text{oxygen gradient}} c \right)}_{\text{Chemotactic transport}} + \underbrace{\overbrace{r(a)}^{\text{oxygen starvation}} \overbrace{\left(\frac{q}{1+q} \right)}^{\text{adjustment function}} \overbrace{u_{\max}\left(1 - \frac{c}{c_{\max}} \right)}^{\text{inhibition function}} c}_{\text{Growth}} \qquad (3.1)$$

where c [CFU ml^{-1}] is the bacterial concentration and a [mmol ml^{-1}] is the oxygen (chemoattractant) concentration. The terms in Eqn. 3.1 are due to motility, chemotactic transport, and growth, respectively.

3.2.2.1.1 Motility

Motility is treated as a function of viscosity of sarcoplasmic protein and oxygen starvation.

Dependence on viscosity of sarcoplasmic protein

For the random motility coefficient, a value of 3.5 x 10^{-9} m^2 s^{-1} is used from the work of Barton and Ford (1995) on *Pseudomonas viscous* at room temperature (25°C). This is measured by a Stopped-Flow Diffusion Chamber (SFDC). An SFDC provides a well-characterized chemical gradient and a reliable method for measuring bacterial migration behavior (Ford & Lauffenburger, 1991).

The dependence of viscosity on random motility coefficient can be expressed in two possible ways

$$\mu = \frac{F_d{}^2 \tau_c}{108\pi^2 R^2 \eta^2} \tag{3.2}$$

$$\mu = \frac{F_d \lambda}{18\pi R \eta} \tag{3.3}$$

where η is the viscosity of sarcoplasmic protein solution within the gap. The random motility coefficient is related to its swimming speed as (Lovely & Dalquist, 1975)

$$\mu = \frac{v^2 \tau_c}{3} \tag{3.4}$$

where v [μm s^{-1}] is the velocity of bacteria and τ_c [s] is the correlation time. The swimming speed is related to the viscosity by the Stokes equation

$$v = \frac{F_d}{6\pi R\eta} \tag{3.5}$$

where F_d is the frictional force. The tendency toward inverse linearity between swimming speed and viscosity was observed by Ping et al. (2013). If τ_c is essentially independent of viscosity (which seems likely for bacteria such as *E. coli* or *Salmonella* that perform a distinct tumble), then, by substituting for v from Eqn. 3.5 into Eqn. 3.4, Eqn. 3.2 is derived. On the other hand, the random motility coefficient can also be described as

$$\mu = \frac{v\lambda}{3} \tag{3.6}$$

where λ [μm] is the free path of bacteria. If the free path is independent of viscosity, Eqn. 3.3 can be derived by substituting Eqn. 3.5 into Eqn. 3.6. Therefore, the random motility coefficient can be expressed in two ways: as inversely proportional to square viscosity (Eqn. 3.2) and as inversely proportional to viscosity (Eqn. 3.3). This discussion of the relationship between viscosity and the random motility coefficient is concerned solely with the fluid mechanical effects of viscosity changes on motility, assuming no change in

the swimming mechanism (Segel et al., 1977). However, swimming speed is apparently affected by the viscosity from Eqn. 3.5. The free path can be expressed as

$$\lambda_p = \frac{v}{p_t} \tag{3.7}$$

where p_t [s^{-1}] is tumbling frequency. If tumbling frequency is independent of viscosity (that is, bacteria show a distinct tumble), λ_p is not independent of the viscosity from Eqns. 3.5 and 3.7. Therefore, Eqn. 3.2 is more agreeable. In this study, the dependence of the random motility coefficient on the viscosity of sarcoplasmic protein is described by Eqn. 3.2 and is expressed as (assuming F_d and τ_c to be constant):

$$\mu' = \frac{\mu_0 \eta_{\text{water}}^{\ 2}}{\eta^2} \tag{3.8}$$

where μ_0 is the random motility coefficient in water, η_{water} is viscosity in water, and η is viscosity of sarcoplasmic protein solution.

The determination of sarcoplasmic protein viscosity within the gap, which depends on sarcoplasmic protein concentration, is described below. The gap is filled with sarcoplasmic protein that comes from sarcoplasm created by the disruption of endomysia (Offer & Cousins, 1992). The sarcoplasmic proteins, which make up the cytoplasm, have a concentration of approximately 260 mg ml^{-1} (Pearson & Young, 1989). A gap in meat through which bacteria migrate is known as a drip channel. Drip is formed by draining

caused by the gravity of water through the gaps between muscle fiber bundles and perimysia or between muscle fibers and endomysia (Offer & Cousins, 1992). Therefore, in our modeling, protein concentration of drip from meat is used for the sarcoplasmic protein concentration of the gap. For the protein concentration of drip from poultry, the protein concentration of drip from broiler breast muscle is 192.1 mg ml^{-1} for dark meat and 152.2 mg ml^{-1} for light meat (Bowker & Zhuang, 2013). Chicken breast muscle was used in experimental work by Thomas et al. (1987).

Viscosity dependence on sarcoplasmic protein concentration was taken from Russel et al. (1983):

$$\frac{\eta}{\eta_{\text{water}}} = 1 + 2.5\varphi + \underbrace{\left(2.5 + \frac{3}{40}\left(\frac{d_{eff}}{r} \right)^5 \right)}_{s} \varphi^2 + O(\varphi^3) \tag{3.9}$$

$$= 1 + 2.5\varphi + s\varphi^2 + O(\varphi^3) \tag{3.10}$$

where d_{eff} is the effective interparticle distance and r is the radius of a particle. The magnitude of *s* (i.e., the coefficient of the quadratic), or the value of d_{eff}, is dictated by considering the hydrodynamic contributions and interaction potential for specific dispersion (a higher charge implies a larger d_{eff} and large *s*, for example) (Sharma et al.,

2011). The s value for the sarcoplasmic protein was determined using Eqn. 3.10 with the known viscosity value of drip from beef and the φ value calculated as described below.

The viscosity of drip from beef with a protein concentration of 81.6 mg ml^{-1} is 2.7 mPa·s at 25°C (Hertog-Meischke et al., 1998). The volume fraction of solute (φ) may be expressed in terms of the volume (v_h [cm^3]) of an individual hydrodynamic particle and the number of such particles per ml of solution (NS/M) (Richards, 1993):

$$\varphi = \frac{NSv_h}{M} \tag{3.11}$$

where S [mg ml^{-1}] is the solute concentration, N [mol^{-1}] is Avogadro's number, and M [g mol^{-1}] is the solute molecular mass. The coefficient of sarcoplasmic protein, NV_h/M, is determined as follows. For sarcoplasmic protein, most of the truly soluble protein in the extract consists of glycolytic enzymes. Sarcoplasmic protein is 40% glycolytic enzyme, 5% creatine kinase, 0.2-2% myoglobin, and other substances. Glycolytic enzymes contain phosphoglycerate kinase, lactate dehydrogenae, and phosphofructo kinase (Scopes, 1970). The molecular mass (M) for each protein is shown in Table 2. For hydrodynamic volume, assuming it is perfectly spherical (because the sarcoplasmic protein is a globular protein), v_h is calculated from

$$v_h = \frac{4\pi r_h^{\,3}}{3} \tag{3.12}$$

where r_h [nm] is the hydrodynamic radius. Hydrodynamic radii and calculated hydrodynamic volume of the proteins are shown in Table 2. The coefficient N_{Vh}/M for each protein was calculated, with a mean of 1.6 (Table 2), which is taken as the representative value for the sarcoplasmic protein. Using the N_{Vh}/M value of 1.6 and a protein concentration of S = 81.6 mg ml^{-1}, the φ value is calculated as 0.13. Using η = 2.7 mPa·s for the sarcoplasmic protein, for a concentration of 81.6 mg ml^{-1} (Hertog–Meischke et al., 1998), for φ = 0.13, from Eqn. 3.10, the value of s is calculated to be 64. The protein concentration of drip from chicken breast muscle, which was assumed to be the same as that in the gap, is 152.2 mg ml^{-1} (Bowker & Zhuang, 2013). The value of φ, which corresponds to a protein concentration of 152.2 mg ml^{-1}, is 0.24. Therefore, the viscosity of sarcoplasmic protein in the gap (η_{spp}) for chicken breast muscle can be estimated from Eqn. 10 to be 6.2 mPa·s. A value of 6.2 mPa·s was used in the simulation as the initial sarcoplasmic protein viscosity within the gap. From Eqn. 3.9, with a value of s of 64, d_{eff}/r= 3.8 can be obtained. In general, the value of s depends upon specific interactions (and the model used) and on a system in which only hard sphere repulsion applies, i.e., $d_{eff}/r = 2$ (Sharma et al, 2011). Surface charges of sarcoplasmic protein may contribute to the higher s value. However, electric charge is small in sarcoplasmic protein and large in myofibrillar protein. Other factors involved in interactions between protein and protein probably affect the high s value. The viscosity of water at 25°C was determined based on Kestin et al. (1978).

Dependence on oxygen starvation

Motility is correlated with oxygen concentration. Bacteria lose motility when the ambient oxygen concentration falls below some critical value (Tuval et al., 2005). Thus, the random motility coefficient was changed into a value for immotility below this level of critical oxygen concentration (Eq. 13). The top surface of the gap is exposed to air, keeping this surface in equilibrium with air. However, until oxygen diffuses into the deep bottom of the gap, the oxygen concentration there is very low. Transition from sharp and fast motility to immotility occurs when bacteria exhaust oxygen (Douarche et al., 2009). Oxygen starvation of bacteria was introduced into modeling as

$$\mu' = \begin{cases} \mu_{motile} (a > a_c) \\ \mu_{immotile} (a \le a_c) \end{cases} \tag{3.13}$$

where a_c is a critical oxygen concentration below which bacteria lose motility, μ_{motile} is the random motility coefficient of motile bacteria, and $\mu_{immotile}$ is the random motility coefficient of immotile bacteria. The random motility coefficient of immotile bacteria (5 x 10^{-11} m^2 s^{-1}) (Nossal & Chen, 1972) is close to the diffusivity calculated from the Einstein–Stokes Equation (about 1 μm diameter sphere), which is the approximate diameter of *Pseudomonas*.

Critical oxygen concentration was determined by the equation

$$a_c = a_e a_s \tag{3.14}$$

where a_s is the equilibrium oxygen concentration and a_e is the oxygen starvation coefficient. An oxygen starvation coefficient of a_e = 0.3, from experimental data on a *Bacillus subtilis* strain reported by Tuval et al. (2005), was used in this study. This strain has also been considered highly aerobic, like *Pseudomonas* spp.

3.1.2.2.1.2 Chemotaxis

Bacteria show chemotaxis toward oxygen, i.e., oxygen works as a chemoattractant (Adler, 1973). The simplest form of chemotactic response suggested by Keller and Segel (1973) was used for the chemotactic term. Chemotactic motion is phenomenologically described by a convection-like transport coefficient (Chen et al., 1998; Keller & Segel, 1971; Rivero et al., 1989; Lewus & Ford, 2001). The chemotactic sensitivity coefficient represents the fractional change in cell-dispersal capability per unit of fractional change in receptor occupancy (Lewus & Ford, 2001). Adler et al. (2012) investigated aerotaxis of *E.coli* with a microfluidic device.

Dependence on the viscosity of sarcoplasmic protein

The chemotactic coefficient is assumed to be inversely proportional to viscosity,

$$\chi_0' = \frac{\chi_0 \eta_{water}}{\eta} \tag{3.15}$$

because the swimming speed of bacteria is inversely proportional to the viscosity (Eqn. 3.5) and the chemotactic velocity is proportional to the swimming speed. The chemotaxis coefficient in water was determined from the typical chemotactic velocity of 10 μm s^{-1} (Tuval et al., 2005). From the equation

$$\frac{\chi_0 a_s}{l} = 10 \ \mu\text{m s}^{-1} \tag{3.16}$$

with l = 1 mm and a_s = 0.264 mmol l^{-1}, χ_0 was determined as 3.79 x 10^{-8} m^2 s^{-1}.

Dependence on oxygen concentration

The *r(a)* factor was introduced because the chemotactic response also vanishes under the critical oxygen concentration (Tuval et al., 2005). Chemotactic behavior can be observed only in motile bacteria.

$$r(a) = \begin{cases} 1 & (a > a_c) \\ 0 & (a \le a_c) \end{cases} \tag{3.17}$$

3.1.2.2.1.3 Growth

Bacterial growth is expressed as (Barayni & Roberts, 1994):

$$\frac{\partial c}{\partial t} = r(a)\alpha(t)u(c)c \tag{3.18}$$

The $r(a)$ factor, defined by Eqn. 3.17, ensures that, due to oxygen starvation, bacterial growth does not occur below critical oxygen concentrations. Here the adjustment function, *α(t),* depends on *q(t)*, which represents the physiological state of the cells (Baranyi et al., 1993)

$$\alpha(t) = \frac{q(t)}{1+q(t)} \tag{3.19}$$

The physiological state can be expressed as

$$\frac{\partial q}{\partial t} = \begin{cases} u_{\max} q(t) & \left(c \geq 10 \text{ CFU ml}^{-1}\right) \\ 0 & \left(c < 10 \text{ CFU ml}^{-1}\right) \end{cases} \tag{3.20}$$

The adjustment function, as given in Eqn. 3.19, can be considered a transformation of quantity *q(t)* and expressed as the same 'readiness' of the cells for the actual environment. SEM micrographs have revealed tissue perforations around colonies, which suggest incipient growth at depth (Noriega et al., 2010). To include the incipient growth at a depth where bacterial concentration is almost zero (that is, at a depth bacteria hardly reached), it was assumed that the physiological state of the cells is a constant value (initial value, q_0) as expressed in Eqn. 3.20.

The $u(c)$ function is called the 'inhibition' function because it ensures the transition of the growth curve to the stationary phase:

$$u = u_{\max}\left(1-\left(\frac{c}{c_{\max}}\right)^{m}\right) \tag{3.21}$$

A value of m = 1 was used here, corresponding to the logistic, or Pearl–Verhurst, growth model. The initial value of a physiological state can be calculated as a product of the lag parameter and maximum specific growth rate.

$$q(0) = \frac{1}{e^{h_0}-1} \tag{3.22}$$

$$h_0 = \lambda u_{\max} \tag{3.23}$$

The maximum specific growth rate and the lag phase values were obtained from parameters of growth of *Pseudomonas spp.* in poultry (Li et al., 2014).

3.1.2.2.2 Oxygen transport

Oxygen transport was considered as

$$\frac{\partial a}{\partial t} = D_{O2}{}' \frac{\partial^2 a}{\partial z^2} - \kappa_C \tag{3.24}$$

where $D_{O2}{}'$ [m^2 s^{-1}] is the diffusivity of oxygen in a sarcoplasmic protein solution and κ [mol s^{-1} cell^{-1}] is the coefficient of the bacterial oxygen consumption rate. Following the Einstein–Stokes law, the diffusivity of oxygen is made inversely proportional to the viscosity of fluid in the gap

$$D_{O2}{}' = \frac{D_{O2}\eta_{water}}{\eta} \tag{3.25}$$

3.1.2.2.3 Proteolytic kinetics

Bacterial proteolysis on sarcoplasmic protein within the gap is expressed in terms of the Michaelis–Menten equation:

$$-\frac{\partial S}{\partial t} = \frac{V_{max} S}{K_m + S} \tag{3.26}$$

where S [mg ml^{-1}] is the sarcoplasmic protein concentration, V_{max} [mg h^{-1} ml^{-1}] is the maximum reaction rate, and K_m [mg ml^{-1}] is the Michaelis constant. Kinetic parameters of *Pseudomonas* spp. on sarcoplasmic protein from chicken breast muscle were measured, as described in Sec. 3.2. The maximum reaction rate hardly varied in the bacterial

concentration range of 10^5–10^7 CFU ml^{-1} (results not shown). In addition, microbial proteolysis occurred at a very late stage of spoilage (Dainity et al., 1975), that is, when the bacterial concentration reached close to the maximum concentration rate. Therefore, for simplicity, the reaction rate was considered constant over a bacterial concentration of 10^5 CFU ml^{-1} and, below this bacterial concentration, the reaction rate was considered zero.

3.1.2.3 Boundary and initial conditions

3.1.2.3.1 Oxygen diffusion before bacterial inoculation

The boundary condition for oxygen diffusion at both the top and bottom surfaces of the gap is $a\ (z = 0, z_0) = a_s$. This boundary condition means that both surfaces are exposed to air.

3.1.2.3.2 Bacterial migration following inoculation

For the boundary condition at the top surface, $c\ (z = 0, t) = 3.3 \times 10^{10}$ CFU ml^{-1} was used. The volumetric bacterial concentration, which is equivalent to 10^7 CFU cm^{-2}, was estimated. The initial bacterial concentration on the top surface (the inoculated surface) is given in CFU cm^{-2}. Gill and Penney (1977) noted, for example, that “bacteria were

inoculated on the upper surface of the meat to give an initial cell density in excess of 10^7 CFU cm^{-2}.'' As discussed below, the surface bacterial concentration from the experimental data in this study also justifies the surface bacterial concentration, which is equivalent to 1 x 10^7 CFU cm^{-2}.

The thickness of the bacterial colony was estimated to be approximately 3 μm for *Pseudomonas* (Su et al., 2012). Using this thickness, the volumetric bacterial concentration is calculated as follows:

$$\frac{10^7\left[\text{CFU cm}^{-2}\right]\times 1\left[\text{cm}^2\right]}{3\times 10^{-4}\left[\text{cm}\right]\times 1\left[\text{cm}\right]\times 1\left[\text{cm}\right]} = 3.3\times 10^{10}\left[\text{CFU ml}^{-1}\right] \tag{3.27}$$

This value is justified by this study's experimental data as follows: the measured surface bacterial concentration was 1.0 x 10^4 CFU cm^{-2} while the volumetric concentration of the whole chunk was 9.0 x 10^4 CFU ml^{-1} (see Sec. 3.1 for the experimental method). Thus, the total bacterial count in the meat sample, calculated from surface bacterial concentration with meat size of 4 cm x 4 cm x 0.3 cm, is calculated as

$$\text{(4 x 4 x 2 [top and bottom surfaces] + 4 x 0.3 x 4 [other 4 surfaces]) [cm}^2\text{]} \quad \text{x 1.0 x } 10^4 \text{ [CFU cm}^{-2}\text{]} = 3.68 \text{ x } 10^5 \text{ [CFU]}. \tag{3.28}$$

On the other hand, using the volumetric bacterial concentration, the total bacterial count is calculated as (3.29)

$$5\ [g] \times 9.0 \times 10^4\ [CFU\ ml^{-1}] = 4.5 \times 10^5\ [CFU],$$

with a meat density of 1 g ml^{-1}. Assuming that bacteria sufficiently penetrated the surface into the meat, the surface bacterial concentration of 1.0×10^4 CFU cm^{-2} is equivalent to the volumetric concentration of 9.0×10^4 CFU ml^{-1}. In addition, bacteria exist only in the gaps, which occupy only approximately 8.7% of the whole chunk of meat (Iwamoto et al., 2001); thus, the bacterial concentration in the gap should be 1 / 0.087 = 11.5 times larger than that of the whole chunk of meat. Therefore, the volumetric bacterial concentration in the gaps, which is equivalent to 10^4 CFU cm^{-2}, is estimated at 9.0×10^4 [CFU ml^{-1}] x 11.5 = 1.0×10^6 CFU ml^{-1}. The volumetric concentration, which is equivalent to 1.0×10^7 CFU cm^{-2}, is 1.0×10^9 CFU ml^{-1}.

One order of difference was observed between the volumetric concentration calculated from a bacterial thickness of 3 μm and concentration from the experimental data. This difference might be explained by the deviation from the assumption that the bacteria had penetrated deeply enough. If this assumption is not true (that is, bacteria penetrate more deeply over time), the volumetric concentration becomes higher than 1.0×10^9 CFU ml^{-1}. The experimental data justify the bacteria concentration of 3.3×10^{10} CFU ml^{-1}, which is equivalent to 1×10^7 CFU cm^{-2}.

Thus, a value of 3.3 x 10^{10} CFU ml^{-1} was used as the initial concentration for the modeling, which is likely equivalent to the surface bacterial concentration of 1.0 x 10^{7} CFU cm^{-2}. Finally, to observe the extent to which the boundary condition affects the process, sensitivity analysis, with respect to bacterial concentration at the boundary, was also conducted.

Boundary condition of oxygen transport

The oxygen concentration at the top of the gap is in equilibrium with air because the gap is exposed to it; therefore, at the top, $a\,(0, t) = a_s$ is used as the boundary condition. At the bottom, flux equals zero was used as a boundary condition because it rests on a solid surface.

$$\frac{\partial a}{\partial z} = 0\left(z = z_0\right) \tag{3.30}$$

For the initial oxygen concentration profile, oxygen concentration profile at the end of oxygen diffusion simulation for 5 minutes was used. This initial concentration is needed to compare experimental data from the literature in which meat samples are exposed to air for a certain time interval before inoculating the meat surface with bacteria. The value of 5 min is an estimate of how long the meat sample was exposed to air in the experimental studies of Thomas et al. (1987). Sensitivity analysis was conducted for this parameter

(exposure duration) to understand better how it affects the penetration process—this is discussed in Sec. 4.2.2.

3.2.3.3 Bacterial transport into a swab

As shown in Fig. 3.2b, a swab was attached to the bottom of the gap and bacterial diffusion from the gap to the swab part was simulated. This simulation was needed to compare the procedure with procedures reported in the experimental literature, in which penetration was assessed by swabbing the bottom surface (Thomas et al., 1987; Gill & Penney, 1977). The initial bacterial concentration in the swab was assumed to be zero because the tip of the swab was wet with sterile water. Oxygen concentration in the tip of the swab was assumed to be in equilibrium with air because the swab was small (2 mm thick) and it was exposed to air for at least several minutes, which is long enough for the water in the 2 mm–thick swab to come into equilibrium with air. The calculation of the penetration rate is described in Sec. 2.4.

3.1.2.4 How should the penetration rate in modeling be defined?

To define penetration, Thomas et al. (1987) assessed it “by swabbing the lower surface of muscle cubes via sampling port, followed by plating on nutrient agar and incubation at 25°C.” In Gill and Penney (1977), “penetration was deemed to have commenced when a

strip was found to contain bacteria in a depth of at least 2 cm. The rate of advance was calculated from the depths to which bacteria had penetrated in the remaining strip after further incubation."

The penetration rate in the modeling work here needs to be defined so that it can be compared with experimental data. The simulation is performed first without the swab (Figure 3.2a) and, when a minimum concentration is reached at the bottom (as explained later), a 2 mm–thick swab (Figure 2b) is added at the bottom of the gap. The initial bacterial concentration in the swab was zero. No boundary condition was assumed at the bottom of the gap (the boundary between the gap and the swab). The distribution coefficient between the gap and the swab part was neglected (equal to one) because the tip of the swab, due to the swabbing technique, was wet with sterilized water.

The amount of bacteria that would be picked up by a swabbing technique at the bottom of the gap was estimated by computing the total flux at the bottom and integrating it over 2 s (the time during which the tip of a swab is typically in contact with a meat surface in a common swabbing technique). Thus, the amount picked up by the swab per unit surface area, $c^s(t^*)$ [CFU cm^{-2}], was computed as

$$c^s(t^*) = \int_{t^*}^{t^*+2} Flux(z_0, t)dt = \int_{t^*}^{t^*+2} \left(\underbrace{-\mu \frac{\partial c}{\partial z}}_{\text{Flux due to motility}} + \underbrace{\chi_0 r(a) \frac{\partial a}{\partial z} c}_{\text{Flux due to chemotaxis}} \right) dt \tag{3.31}$$

(3.32)

where t^* is the time when the number of bacteria migrating out of the bottom surface first becomes detectable and is given by

$$c^s\left(t^*\right) > \frac{c^s_{min}\ [\text{CFU}]}{A_g\ [\text{cm}^2]}$$

where c^s_{min} [CFU] is the minimum detectable number on the meat surface detected by the swabbing technique and A_g [cm^2] is the surface area of the meat gap. A minimum detectable bacterial number of $c^s_{\min} = 15$ CFU is used here, as this is typical in the most common technique for counting bacteria when swabbing (Hedin et al., 2010). The value of A_g is estimated, based on the SEM photograph of chicken muscle by Iwamoto et al. (2000), to be 8.7% of the total surface area. For the computations here, the total surface area is 1.5 [cm] x 1.5 [cm] = 2.25 [cm^2], which leads to A_g = 0.087x2.25 = 0.196 [cm^2]. Therefore, the right-hand side in Eqn. 3.30 was determined to be 15 [CFU] /0.196 [cm^2] = 76.6 CFU cm^{-2}. The value of t^*, the minimum time satisfying Eqn. 3.32, was found by trial and error, i.e., running the simulation for various values of t^* until Eqn. 3.32 was satisfied as an equality. The penetration rate, R_p, is calculated from

$$R_p = \frac{z_0}{t^*} \tag{3.33}$$

This penetration rate will be compared for *proteolytic* and *non-proteolytic* conditions as well as for various bacterial transport parameter combinations.

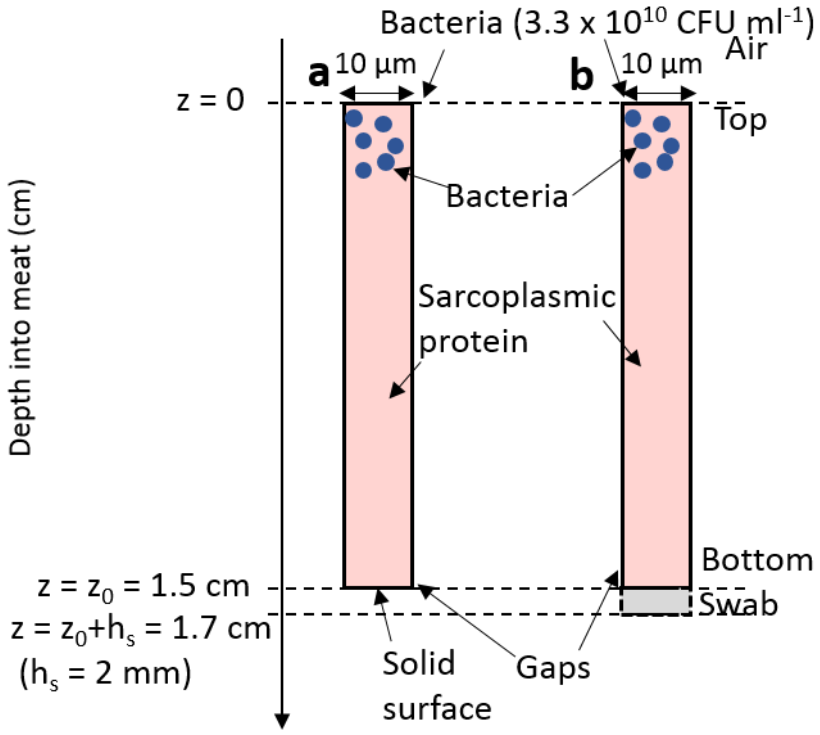

Figure 3.2. Schematic showing the geometry of the a) gap, the b) gap, and the swab used as the computational domain in modeling.

Table 3.2 Model parameters and values

Symbol	Parameters	Value	Bacterial species used and references
a	Oxygen concentration	Eqn. 3.24	
a_c	Critical oxygen concentration	0.0792 mmol l^{-1}; Eqn. 3.14	*Bacillus subtilis*; Tuval et al. (2005)
a_e	Oxygen starvation coefficient	0.3	*Bacillus subtilis*; Tuval et al. (2005)
a_s	Equilibrium oxygen concentration to air	0.264 mmol l^{-1}	
A_0	Total area of the meat	2.25 cm^2	
A_g	Area of gaps	0.20 cm^2	
c	Bacterial concentration	Eqn. 3.1	
c_{max}	Maximum bacterial concentration	3.3 x 10^{10} CFU ml^{-1}	
c^s_{min}	Minimum detectable bacterial number	15 CFU	*S. aureus* or *enterococci*; Hedin et al. (2010)
$c^s(t^*)$	Surface bacterial concentration at the bottom of the gap	Eqn. 3.29	
d_{eff}	Effective interparticle distance	Eqn. 3.9	Sharma et al. (2011)

D_{O2}	Diffusivity of oxygen	2.4×10^{-9} m^2 s^{-1}	Bennett (2007)
D_{O2}'	Diffusivity of oxygen in sarcoplasmic protein solution	Eqn. 3.25	
F_d	Drag force	Eqn. 3.2	
h_0	Potential growth	Eqn. 3.23	*Listeria, Salmonella, Yersinia, Escherichia coli*; Baranyi & Roberts (1994)
h_s	Width of the tip of swab	2 mm	
K_m	Michaelis constant	3.3 mg ml^{-1}	Our experimental result
M	Molecular mass	Table 3.2, Eqn. 3.11	
N	Avogadro's constant	6.02×10^{23} mol^{-1}	
p_t	Tumbling frequency	Eqn. 3.7	
$q(0)$	Initial physiological state	Eqn. 3.22	*Listeria, Salmonella, Yersinia, Escherichia coli*; Baranyi & Roberts (1994)
$q(t)$	Physiological state	Eqn. 3.20	*Listeria, Salmonella, Yersinia, Escherichia*

			coli; Baranyi & Roberts (1994)
r	Particle radius	Eqn. 3.9	
r_h	Hydrodynamics radius	Table 3.2	
R_p	Penetration rate	Eqn. 3.31	
s	Coefficient of the quadratic	Eqn. 3.10	Russel et al. (1983)
S	Sarcoplasmic protein concentration	Eqn. 3.11	
S_0	Initial sarcoplasmic protein concentration	152.2 mg ml^{-1}	Bowker & Zhuang (2013)
T	Time for the simulation of bacterial penetration	Eqn. 3.29	
t^*	Time when the number of bacteria migrating out of the bottom surface first becomes detectable	Eqn. 3.29, 3.30, 3.31	
u_{max}	Specific growth rate	0.68 h^{-1}	*Pseudomonas spp.*; Li et al. (2014)
$u(c)$	Inhibition function	Eqn. 3.21	*Listeria, Salmonella, Yersinia, Escherichia*

			coli; Baranyi & Roberts (1994)
v	Bacterial swimming speed	Eqn. 3.5	
v_h	Hydrodynamic volume	Table 3.2	
V_{max}	Maximum reaction rate	0.08 mg min^{-1} ml^{-1}	Our experimental result
z_0	Depth of meat	1.5 cm	
η	Viscosity of sarcoplasmic protein solution in the gap	Eqn. 3.10	
η_{water}	Viscosity of water	1.138×10^{-3} Pa·s	Kestin et al. (1978)
η_{SPP}	Viscosity of sarcoplasmic protein solution	6.2×10^{-3} Pa·s	Russel et al. (1989), Hertorg-Meischke (2012), and Bowker & Zhuang (2013)
κ	Oxygen consumption rate	5×10^{-12} mol s^{-1} $cell^{-1}$	*Escherichia coli*; Keller & Segel (1971)
λ	Lag phase	3.99 h	Li et al. (2014)
λ_p	Free path	Eqn. 3.7	

μ'	Random motility coefficient of bacteria in sarcoplasmic protein solution	Eqn. 3.8	
μ_{motile}	Random motility coefficient of motile bacteria in water	3.5×10^{-9} m^2 s^{-1}	*Pseudomonas viscous*; Barton & Ford (1995)
$\mu_{immotile}$	Random motility coefficient of immotile bacteria in water	5×10^{-13} m^2 s^{-1}	*Escherichia coli*; Nossal & Chen (1972)
τ_c	Correlation time	Eqn. 3.4	
φ	Volume fraction of solute	Eqn. 3.11	Richards (1993)
χ_0	Chemotactic sensitivity coefficient to oxygen in water	3.79×10^{-8} m^5 mol^{-1} s^{-1}	*Bacillus subtilis*; Tuval et al. (2005)
χ_0'	Chemotactic sensitivity coefficient to oxygen in sarcoplasmic protein solution	Eqn. 3.15	

Table 3.3 Hydrodynamic radius, molecular mass, and hydrodynamic volumes of typical proteins of sarcoplasmic protein. r_h: hydrodynamic radius; M: molecular mass; v_h: hydrodynamic volume; φ : volume fraction of the solution occupied by hydrodynamic solute particles.

Protein	r_h (nm)	M (kDa)	v_h (nm^3)	Nv_h/M	Literature
Phosphoglycerate kinase	3.0	45.0	113	1.5	Carlson et al. (2014)
Creatine kinase	4.0	81.0	268	2.0	Scopes (1970)
Lactate Dehydrogenase	5.0	142.0	524	2.2	Scopes (1970) and Jaenicke and Knof (1968)
Phosphofructo kinase	5.7	340.3	776	1.4	Carlson et al. (2014)
Phosphoglucose isomerase	4.0	125.2	268	1.3	Carlson et al. (2014)
Myoglobin	2.1	17.0	40	1.4	Wilkins et al. (1999)
Average		125.1		1.6	

3.1.3 Experimental method

3.1.3.1 Determination of surface and volumetric bacterial concentration of meat

Six pieces of a 5 g meat sample with dimensions of 4 cm x 4 cm x 0.3 cm were prepared. Three samples were used for determining surface bacterial concentration and the other three samples were used for determining volumetric bacterial concentration. The surface bacterial concentration was measured using the swabbing technique (details are described in Shirai et al., 2016), and then the volumetric bacterial concentration was measured by homogenizing the meat sample and counting the number of bacteria in the homogenized meat with an AC plate (AC plate, Nippon Bacterial Test Co., Ltd., Japan). Volumetric bacterial concentration was calculated by dividing by 5 ml (assuming 1 mg ml^{-1} of meat density).

3.1.3.2 Photomicrographs of cryosection of beef

Materials

Pieces of beef thigh from a local grocery store were obtained and used as samples. The meat sample was approximately 1 cm thick. Control and inoculated samples were prepared for obtaining photomicrographs of transverse sections. For the inoculated sample, *Pseudomonas fluorescens* was grown on LB agar medium (LB Daigo, Wako, Japan) at 30°C for 24 h (for bacterial preparation details, see Sec. 3.3.2) and then this

Pseudomonas culture was smeared onto the meat sample and incubated it at 15°C for approximately 24 h. The 15°C temperature was chosen to facilitate comparison with samples used in the experimental work of Thomas et al. (1987), which were incubated at that temperature.

Preparation of cryosections

Each sample was cut into a volume of approximately 1 cc and placed in a freezer (UT-2000F, Leica Microsystems, Japan). The sample was then placed on a ladle covered by aluminum foil and kept in a solvent consisting of polypeptone and acetone (1:1 in volume) at –90°C for about 1 min. After this first freezing procedure, the frozen sample was placed into a ladle and filled with the embedding medium. The sample was then placed into the freezing solvent again until the top surface was covered by frozen embedding medium. Over time, the embedding medium became frozen and white. A supporting material was then attached to the frozen sample. A cryofilm (Cryofilm type 2C(10), Section LAB Co, Japan) was placed on the frozen meat surface. The sample was sliced to a thickness of 50 µm using cryostat (CM1860, Leica Micorosystems, Japan). An approximately 5 mm cryosection depth from the surface was obtained because bacteria exist on the top surface even in a control sample.

Photomicrographs

Photomicrographs of cryosections of beef inoculated with *Pseudomonas* culture were obtained to confirm the pathway of bacterial penetration into meat. Specifically, there are two possible pathways: one is the gaps between muscle fibers and endomysia and the other is the gaps between muscle fiber bundle and perimysium, so the goal was to clarify which pathway is preferred for bacterial penetration into meat. Meat photomicrographs of the cryosections for both the control and inoculated samples were obtained using a light micrograph (DM LM 030 530 007, Leica Microsystem Wetzlar GmbH) taken with a digital camera (DXC-9150D, Leica Microsystems Ltd, Japan). The magnification of the object glass was x20 and that of the eyepiece was x10. Data were obtained using LAS 4.0 software (Leica Microsystems, Japan).

3.1.3.3 Measurement of proteolysis kinetic parameters of *Pseudomonas fluorescens* on sarcoplasmic protein from chicken breast muscle

Extraction of sarcoplasmic protein

Sarcoplasmic protein from chicken breast muscle was extracted following the procedure of Hay et al. (1973), with a slight modification. Approximately 5 g of excised muscle was minced and homogenized in 5 volumes of the extracting solution (0.25 M sucrose, 1 mM disodium (ethyl dinitrilo) tetraacetate (EDTA), 0.05 M Tris, pH 7.6) with a masher (BACcT

homogemasher, Nippon Bacterial Test Co., Ltd., Japan) in a masher bag (Masher Bag, Nippon Bacterial Test Co., Ltd., Japan). The extract was stirred gently for 1 h at 2°C and centrifuged at 2,500 g for 10 min (Hay et al., 1973). The supernatant was used as sarcoplasmic protein. Since the protein concentration of the extracted sample was low (approximately 20 mg ml^{-1}), the protein obtained using Amicon Ultra 15 mL Centrifugal Filters (Amicon Ultra-15 Centrifugal Filter Unit, Millipore, Japan) was concentrated to obtain a concentration of approximately 150 mg ml^{-1}.

Pseudomonas culture preparation

Pseudomonas fluorescens Migula ATCC 13525 was used for the proteolysis reaction. A glass ampule containing *Pseudomonas fluorescens Migula* (ATCC 13525) was purchased. It was broken carefully and 0.2 ml of LB liquid medium (LB Daigo, Nihon Pharmaceutical Co. Ltd.) was added for growth. The strain suspension was obtained by shaking the ampule. It was inoculated on an LB agar medium (LB Daigo, Nihon Pharmaceutical Co. Ltd.) with a disposal inoculating loop (TX2001, Eiken Chemical Co., Ltd., Japan) at 30°C for one day. The grown *Pseudomonas* was then inoculated into the LB liquid medium and this LB liquid medium containing *Pseudomonas* culture was incubated overnight in a shaking incubator (Shaker-VR, TAITEC, Japan) at approximately 160 rpm at 30°C. To prepare a higher concentration, the culture suspension was concentrated by centrifuging at 2,500 g for 30 min. The obtained concentrated *Pseudomonas* culture suspension was used for

proteolysis reaction. The bacterial concentration of *Pseudomonas* culture was measured using an AC plate (AC plate, Nippon Bacterial Test Co., Ltd., Japan).

Proteolysis reaction

To obtain the kinetic parameters, the method of Wrolstad et al. (2005) with modifications was followed. Concentrated sarcoplasmic protein and *Pseudomonas* culture were incubated at 25°C for approximately 1 h before proteolysis reaction to keep the temperature constant. Sarcoplasmic protein (0.1 ml) was prepared in each test tube except for the blank assay. *Pseudomonas* culture (0.01 ml) was added to each sarcoplasmic protein solution to initiate reaction. For the blank assay, only 0.01 ml *Pseudomonas* culture was added. After 60 min, 3 ml of 20% tetrachloroacetic acid (TCA) solution was added to each test tube to stop the reaction. The test tubes were then centrifuged for 5 min at 2,500 g and the supernatant was used for the protein concentration measurement to determine the TCA-soluble peptide protein content. Note that in the reaction solution, the *Pseudomonas* culture contained TCA-soluble peptides; thus, the test tube containing only the *Pseudomonas* culture for the blank assay was used, and the absorbance of the blank was subtracted from that of the supernatant. Protein concentration was measured by BCA assay (Wako Pure Chemical, Japan). The standard curve was constructed by bovine serum albumin (Sigma Aldrich, Japan). The quantities V_{max} and K_m were calculated by Lineweaver–Burk plot.

3.1.4 Experimental results and Discussions

3.1.4.1 Photomicrographs of bacterial penetration

Figure 3.3 shows the photomicrographs of transverse sections of inoculated beef thigh muscle. Sections with depths of approximately 5 mm depth were obtained. The myofibril (M), endomysium (E), and perimysium (P) are clearly seen in Fig. 3.3. In addition, there were gaps between muscle fiber and the endomysium and the muscle fiber bundle and the perimysium (shown as G in Fig. 3.3). In the control sample, no bacteria were observed in the meat sample. In the inoculated sample (Fig. 3.3), bacteria exist in the gap between the endomysium and muscle fiber (shown as B in Fig. 3.3). The observation therefore confirms the observation of Gill et al. (1984) that bacteria penetrate into meat through gaps between muscle fiber and endomysia. Also, this observation clarifies that bacteria preferentially migrate within the gaps between muscle fiber and endomysium to those between muscle fiber bundle and perimysium.

3.1.4.2 Proteolysis kinetics by *Pseudomonas* on sarcoplasmic protein

Proteolysis kinetics clearly shows the Michaelis–Menten type kinetics (Fig. 3.4). Using a Lineweaver-Burk plot, V_{max} of 4.8 mg h^{-1} ml^{-1} and K_m of 3.3 mg ml^{-1} for the proteolysis by *Pseudomonas* on sarcoplasmic protein from poultry were obtained. The bacterial concentration used for this determination was 3.7 x 10^7 CFU ml^{-1}. The V_{max} and K_m were

used for simulation of bacterial penetration. This maximum reaction rate is much smaller than that of proteolysis by Proteinase K, which is a commercial proteinase, on sarcoplasmic protein from fish. The maximum reaction rate of Proteinase K on sarcoplasmic protein from fish is approximately 38 $\mu mol\ min^{-1}\ ml^{-1}$ (Ghassem et al., 2014). The molecular mass of the sarcoplasmic protein was calculated to be approximately 100 kDa (Table 3.1); therefore, the maximum reaction rate of *Pseudomonas* on sarcoplasmic protein was three or four orders smaller than that of Proteinase K. Thus, the bacterial proteolysis reaction rate was much smaller than that of commercial proteinase.

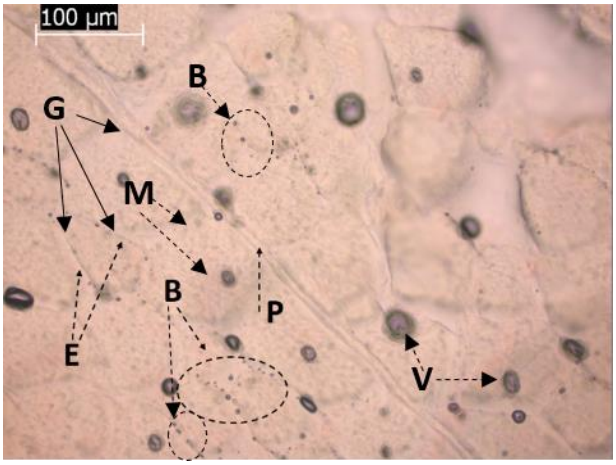

Figure 3.3. Photomicrograph of cryosection of transverse section of beef thigh muscle of a) control, and b) inoculated sample. E: endomysium; P: perimysium; B: bacteria; M: Myofibril; G: Gap; V: Vacuole. Sections to a depth of approximately 5 mm were obtained.

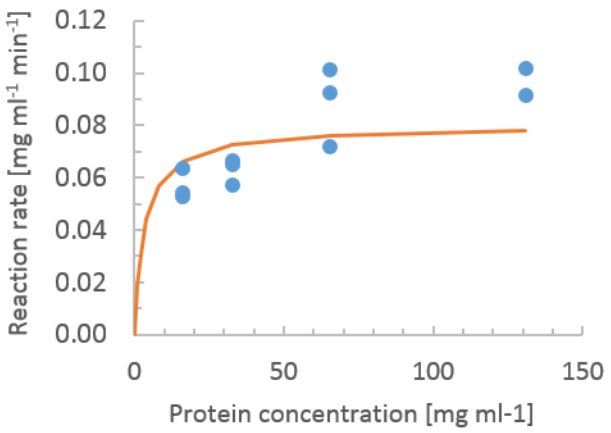

Figure 3.4. Experimentally obtained proteolysis kinetics of *Pseudomonas* on sarcoplasmic protein from poultry (bacterial concentration is 3.7 x 10^7 CFU ml^{-1}).

3.1.5 Simulation results and discussions

3.1.5.1 Effect of initial bacterial concentration on penetration rate

Few differences in bacterial penetration rates were observed when the initial bacterial concentration was in the range of 10^9 -- 10^{11} CFU ml^{-1} (Fig. 3.5a). A value of 1.0 x 10^{10} CFU ml^{-1} was used as the initial bacterial concentration for the simulation.

3.1.5.2 Sensitivity analysis for the exposure time to air

As the effect of oxygen was included in bacterial transport, the initial oxygen concentration profile had an effect on the bacterial penetration rate. In the experiment conducted by Thomas et al. (1987), a meat cube was exposed to air for a certain period of time in order for the gamma radiation to sterilize the interior of the meat; however, the duration of exposure to air is unknown. Therefore, sensitivity analysis for the exposure time to air was conducted. As the exposure time increased, the penetration rate of both *non-proteolytic* and *proteolytic* bacteria increased (Fig. 3.5b, c). This increase in penetration rate meant that the increase in the exposure time to air allowed oxygen to diffuse into the gap from the top and bottom surfaces, and higher oxygen concentrations within the gaps enabled bacteria to penetrate more rapidly because of the reduced effect of oxygen starvation. An estimate of 5 min of exposure to air was estimated as the exposure time in the work of Thomas et al. (1987) and was used here.

3.1.5.3 Penetration into chicken breast muscle at 25°C

Penetration of *non-proteolytic* and *proteolytic* bacteria into chicken breast muscle at 25°C was simulated for the strain *Pseudomonas fluorescens*.

Non-proteolytic bacteria

The simulated penetration rate of *non-proteolytic* bacteria into a 1.5 cm thick piece of meat was 0.039 cm h^{-1} while in the experimental work by Thomas et al. (1987) it was 0.038 cm h^{-1} (Fig. 3.6); therefore, a high level of agreement was observed between the simulation and the experimental results, validating the model. Figure 3.7 shows the detailed penetration results from the simulation. No proteolysis was considered for *non-proteolytic* bacteria; thus, the protein concentration within the gap remained constant (Fig. 3.7b). The bacterial concentration was high (Fig. 3.7a) to a depth of $a = a_c$, where a_c is the critical oxygen concentration under which bacteria lose motility (Fig. 3.7c). Below this depth, bacterial concentration decreased dramatically (Fig. 3.7c) due to oxygen starvation (Eqn. 3.13). The random motility coefficient of immotile bacteria was two or three orders of magnitude lower than that of motile bacteria (Nossal & Chen, 1972). At a depth where a is larger than a_c, bacteria were motile (Fig. 3.7c, d; Eqn. 3.13) and migrated quickly because of their large random motility coefficient (Fig. 3.7a). However, below that depth, bacteria lose motility (Fig. 3.7c, d) and thus hardly move. Generally, the bacterial migration of *non-proteolytic* bacteria is strongly regulated by oxygen starvation.

Proteolytic bacteria

The simulated penetration rate for *proteolytic* bacteria is 0.061 cm h^{-1}, which is lower than literature experimental data of *0.083* cm h^{-1} (Thomas et al., 1987), but the results are still close (Fig. 3.6). The reduced penetration rate predicted in this simulation probably can be attributed to the initial oxygen concentration profile. Whereas both the top and the bottom surfaces were exposed to air for five minutes in the simulation, the experimental samples (Thomas et al., 1987) may have been exposed to air for a longer time for the gamma irradiation process.

The bacterial concentration profile for *proteolytic* bacteria showed a similar shape with *non-proteolytic* bacteria; however, bacterial migration was more rapid than in the case of *non-proteolytic* bacteria (Fig. 3.6, Fig. 3.7a, e). This more rapid bacterial migration is obviously due to the degradation of sarcoplasmic protein by proteolysis (Fig. 3.7f). As bacteria migrate, *proteolytic* bacteria degrade sarcoplasmic protein (Fig. 3.7f), lowering the viscosity of the medium. This lower viscosity increases the random motility coefficient (Eqn. 3.8; Fig. 3.7h). In addition, the lower viscosity also leads to more rapid oxygen diffusion (Fig. 3.7g); thus, the effect of oxygen starvation becomes weaker because of oxygen diffusion deep in the gap (Fig. 3.7h). Below a depth of $a = a_c$, the random motility coefficient is a constant value of immotile bacteria (5×10^{-11} m^2 s^{-1}; Nossal & Chen, 1972) (Fig. 3.7g, h), which is much lower than that of motile bacteria (3.5×10^{-9} m^2 s^{-1}; Barton &

Ford, 1995). As described above, this means that bacteria lose motility under the critical oxygen concentration level (Fig. 3.7g, h). Therefore, the *proteolytic* bacteria penetration rate becomes higher than that of *non-proteolytic* bacteria (Fig. 3.7a, e). This process of penetration in *proteolytic* bacteria is summarized in Fig. 3.8. Proteolysis of sarcoplasmic protein reduces viscosity, leading motility increase directly (Fig. 3.8a) and indirectly through oxygen transport (Fig. 3.8b), and, therefore, bacterial penetration increases.

The effect of chemotaxis also increases with the degradation of sarcoplasmic protein (Eqn. 3.15). However, with the degradation of sarcoplasmic protein, motility is dominant over chemotaxis because viscosity has a greater effect on motility than on chemotaxis. Motility is inversely proportional to the square of viscosity, in contrast to chemotaxis, which is inversely proportional to viscosity (Eqns. 3.8 and 3.15). Therefore, chemotaxis is less influential in *proteolytic* bacterial migration than motility. Bacterial migration is regulated mainly by motility. The higher penetration rate of *proteolytic* bacteria relative to that of *non-proteolytic* bacteria confirms the observation of Thomas et al. (1987) that proteolysis speeds the process of penetration, presumably by hydrolyzing sarcoplasmic proteins within the gaps. This also validates the model against experimental data from the literature.

3.1.5.4 Combinations of factors that have effects on bacterial migration

To isolate the contribution of each factor to bacterial migration, simulations were performed for various combinations of motility, chemotaxis, and oxygen starvation.

As shown in Figure 3.9a, with only motility present (chemotaxis and starvation turned off) *non-proteolytic* bacteria penetrate very quickly (0.17 cm h^{-1}). By contrast, the penetration rate in experimental work is 0.038 cm h^{-1} (Thomas et al., 1987). This rapid penetration when only motility is present implies that some other factors slow the penetration rate. As oxygen starvation or chemotaxis is added, bacterial penetration is significantly reduced (Figs. 3.9b and 3.9c). Chemotaxis directly contributes to bacterial migration (Eqn. 3.1; Fig. 3.9b). In contrast, in oxygen starvation (Fig. 3.9c), the bacteria migrate normally until oxygen concentration reaches the critical value (Eqn. 3.13).

The penetration rate for *proteolytic* bacteria in all the conditions is more rapid than that for *non-proteolytic* bacteria. Proteolysis speeds bacterial migration by degrading sarcoplasmic protein (Fig. 3.9). In the presence of only motility and proteolysis (Fig. 3.9f), bacteria migrate too rapidly. The bacterial penetration rate is greatly reduced when only chemotaxis is added (Fig. 3.9g). Oxygen concentration at the top surface of the gap is in equilibrium with air; therefore, the driving force works on bacteria near the upper surface. Oxygen starvation considerably slows bacterial penetration (Fig. 3.9g). When combining both chemotaxis and oxygen starvation, little decrease was observed from motility and

starvation. Therefore, for *proteolytic* bacteria, oxygen starvation is the most influential factor in migration. To conclude, oxygen transport in the gap in the meat appears to be very influential in bacterial penetration. This conclusion suggests that storage under lower oxygen concentration perhaps reduces bacteria penetration into meat, contributing to food safety.

An anaerobic MAP packaging offers several advantages including decreased growth of spoilage organisms and pathogenic bacteria in MAP compared with polyvinyl chloride (PVC) due to the combined effects of anaerobic conditions and elevated CO_2 (Silliker et al., 1977). Prevention of microbial growth at the meat surface has already been achieved with MAP packaging (Hunt et al., 2004); however, microbial spoilage has been discussed only with regard to meat surfaces. The findings reported here show possible food safety improvement by preventing bacterial penetration into meat under low oxygen concentration.

These results may help resolve controversies over how proteolysis contributes to the mechanism of bacterial invasion. The simulation results demonstrate that the combination of chemotaxis and oxygen starvation perhaps explains why *non-proteolytic* bacteria penetrate more slowly, and that proteolysis makes a significant difference in the penetration rate (Fig. 3.6) even though the viscosity of sarcoplasmic protein is lower.

The absence of motility makes penetration unlikely. Immotile bacteria required more than 150 h to penetrate 1.5 cm into the meat (that is, the penetration rate was less than 0.01 cm h^{-1}) and this was true even when chemotaxis toward oxygen was not included for both *proteolytic* and *non-proteolytic* bacteria. The bacterial penetration into meat is a balance of motility and chemotaxis (Eqn. 3.1). In the early stage after inoculation of bacteria, the chemotactic term is dominant over motility for immotile bacteria because the random motility coefficient of immotile bacteria is three orders of magnitude lower than that of motile bacteria (Barton & Ford, 1995; Nossel & Chen, 1972). However, over time the chemotactic effect weakens because the oxygen concentration gradient decreases due to oxygen diffusion into the meat, and then the effect of motility becomes dominant over that of chemotaxis. Therefore, immotile bacteria can also penetrate into meat to a depth of 1.5 cm even though penetration is very slow.

3.1.5.5 Parametric sensitivity analysis

Parametric sensitivity analysis was performed to isolate the contributions from motility, chemotaxis, growth, proteolysis, and oxygen starvation. The results from this are shown in Fig. 3.10. The degree of proteolysis was varied by changing the maximum reaction rate, V_{max}. The degree of oxygen starvation was varied by changing the oxygen starvation coefficient, c_e. As can be seen from Fig. 3.10, oxygen starvation is the most sensitive

parameter determining the penetration rate. Critical oxygen concentration is described in $a_c = a_e\, a_s$. A 30% increase in the degree of oxygen starvation means $a_e = 0.39$ (a 30% increase from the normal value of 0.3) such that $a_c = 0.39\, a_s$. Therefore, bacteria lose motility more easily at reduced oxygen concentrations, slowing bacterial penetration. The next most sensitive parameter is proteolysis. As shown in Fig. 3.11, at higher proteolysis reaction rates bacteria migrate more rapidly. As described in the previous section, this faster migration is due not only to high motility coming from low viscosity but also to a reduced effect of oxygen starvation in the rapid oxygen diffusion that accompanies the decrease in viscosity as the sarcoplasmic protein degrades (Fig. 3.8). Therefore, proteolysis accelerates the penetration rate through rapid oxygen transport. Only a small difference in the penetration rate was observed due to motility or chemotaxis. Change in growth has little effect on the bacterial penetration rate (Fig. 3.10).

To improve the clarity and readability of this manuscript, conclusions from the parametric sensitivity analysis are assembled into a schematic in Fig. 3.11. Oxygen starvation and proteolysis are the primary factors affecting the bacterial penetration rate into meat. Motility, chemotaxis, and growth are secondary factors. Specifically, when oxygen starvation increases, bacteria are more likely to lose motility deeper in the gap, which reduces the penetration rate. A reduction in the proteolysis reaction rate also leads to slower protein degradation and slower viscosity decrease within the gap, thereby

reducing the penetration rate. Reductions in motility and growth directly reduce the bacterial penetration rate. An increase in chemotaxis reduces the penetration rate because the chemotactic driving force is toward the surface, where oxygen concentration is higher.

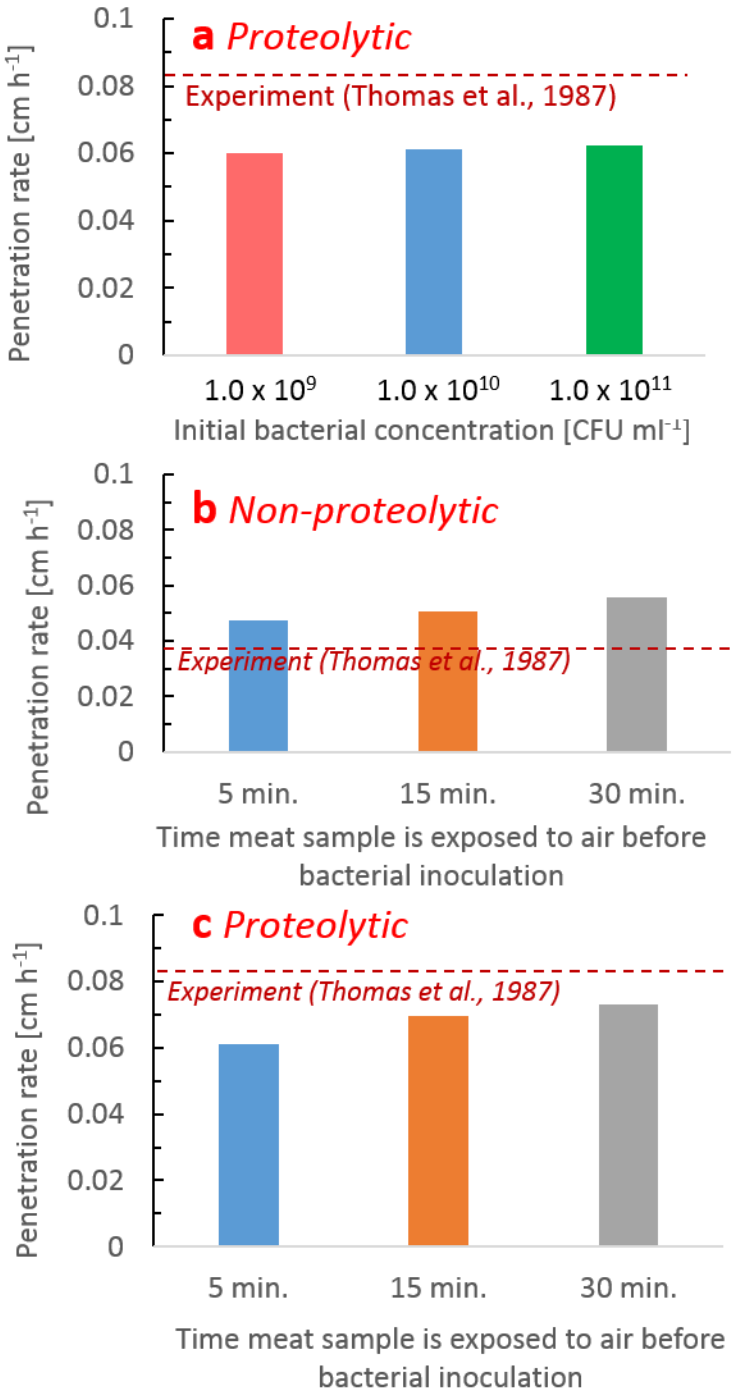

Figure 3.5. Sensitivity analysis of a) initial bacterial concentration of *proteolytic* bacteria, b) the exposure time to air of *non-proteolytic* bacteria, and c) the exposure time to air of *proteolytic*

bacteria. Red dashed lines indicate the penetration rate in experimental results reported in the literature (Thomas et al., 1987).

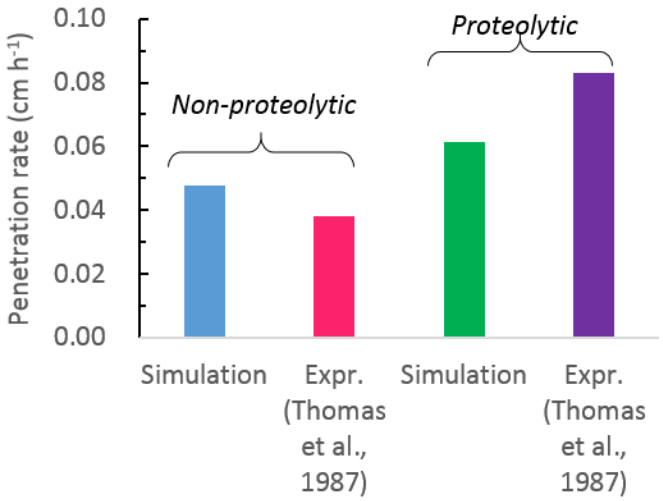

Figure 3.6. Predicted penetration rates of *proteolytic* and *non-proteolytic* bacteria from the simulation, compared with experimental results reported in the literature (Thomas et al., 1987).

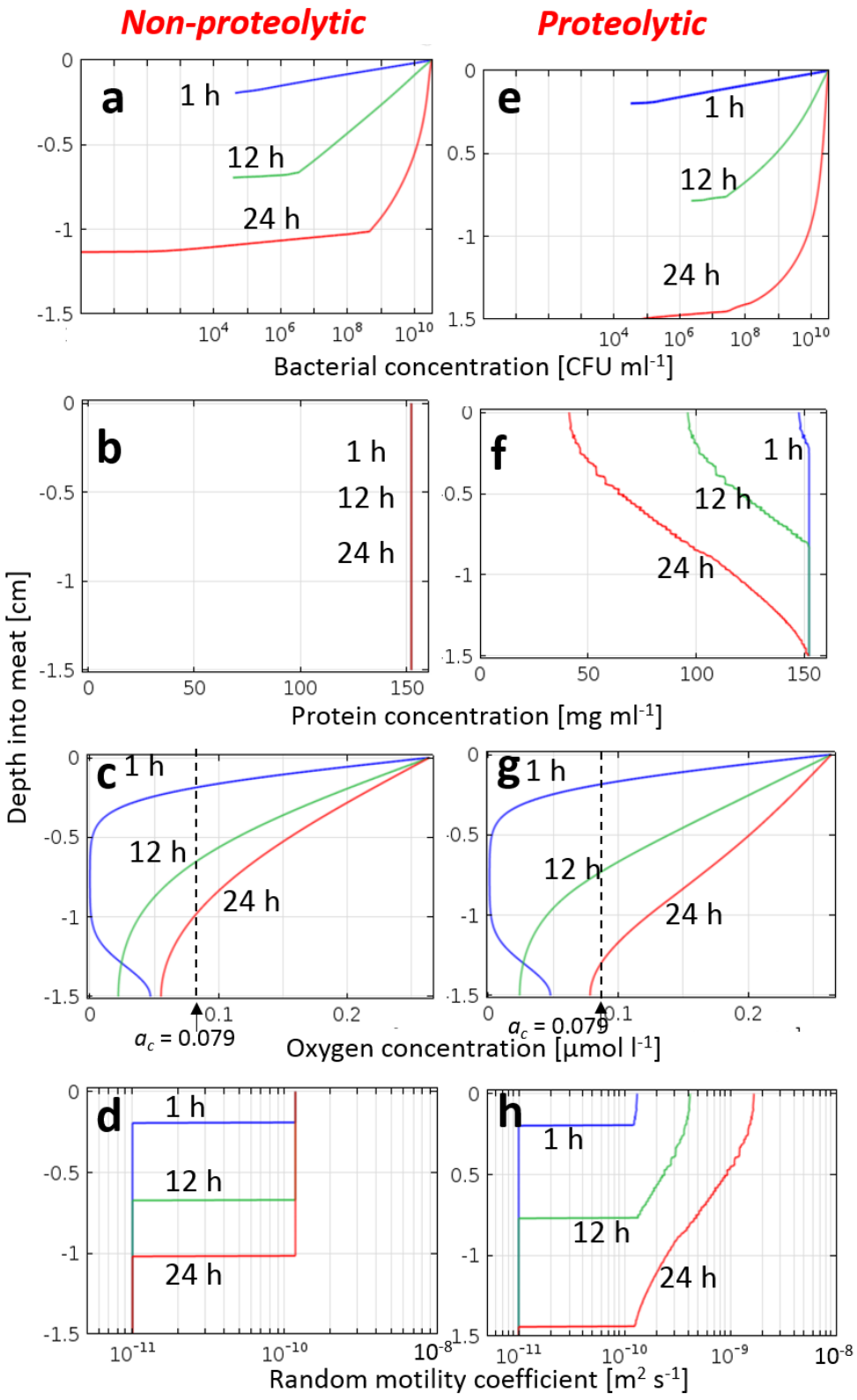
Non-proteolytic
Proteolytic
a
1 h
12 h
24 h
e
1 h
12 h
24 h
Bacterial concentration [CFU ml-1]
b
1 h
12 h
24 h
f
1 h
12 h
24 h
Protein concentration [mg ml-1]
Depth into meat [cm]
c
1 h
12 h
24 h
ac = 0.079
g
1 h
12 h
24 h
ac = 0.079
Oxygen concentration [µmol l-1]
d
1 h
12 h
24 h
h
1 h
12 h
24 h
Random motility coefficient [m2 s-1]

Figure 3.7. Simulation results showing how concentrations and motility vary with the position into the meat and the time of exposure for *non-proteolytic* and *proteolytic* bacteria. a) and e): bacterial concentration profile; b) and f): protein concentration profile; c) and g): oxygen concentration profile; d) and h): random motility coefficient profile.

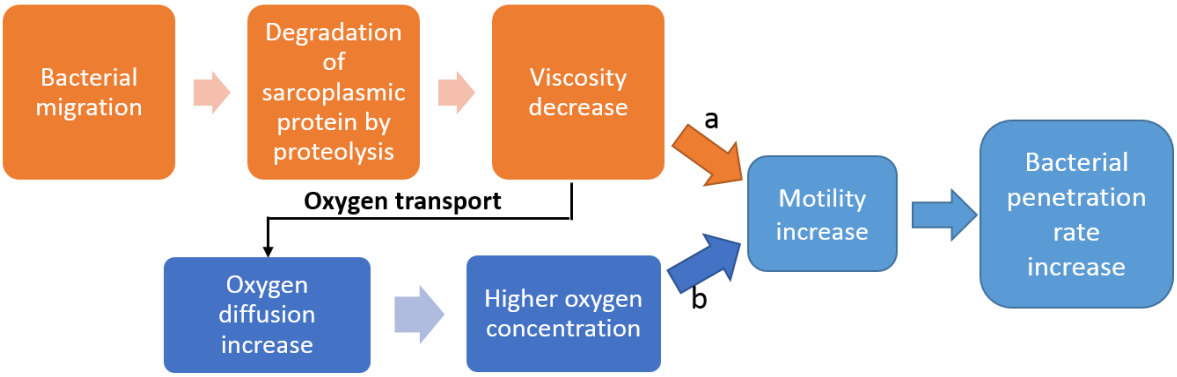

Figure 3.8. Proteolysis of sarcoplasmic protein lowers its viscosity, leading to motility increase a) directly, and b) indirectly through oxygen transport (oxygen starvation), thus increasing bacterial penetration for proteolytic bacteria.

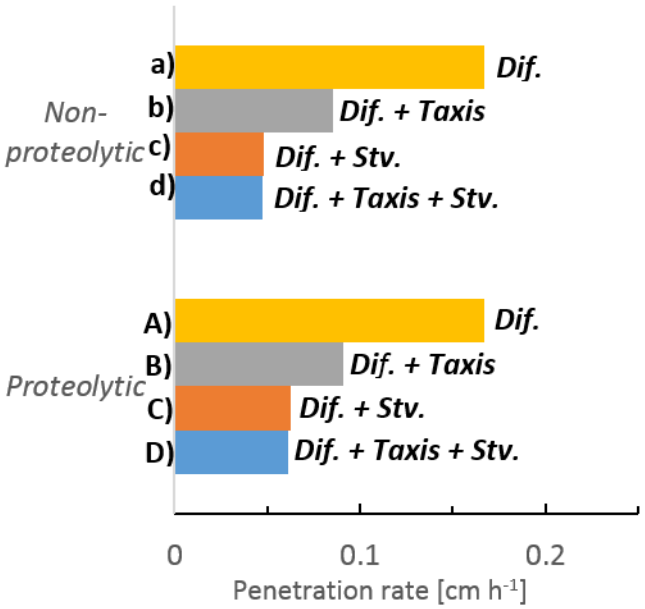

Figure 3.9. Computed penetration rates for various combinations of contributing factors—diffusion (Dif.), chemotaxis (Taxis), and starvation (Stv.)—showing the contributions from each combination.

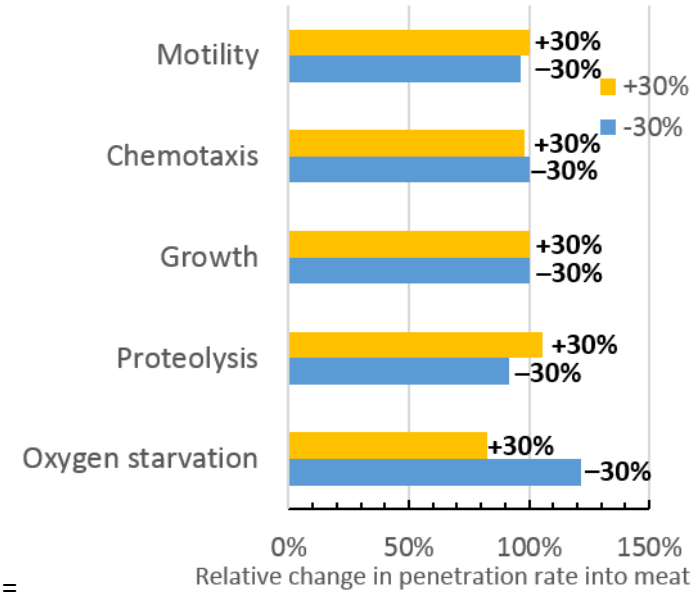

=

Figure 3.10. Parametric sensitivity analysis for determining the penetration rate of *proteolytic* bacteria

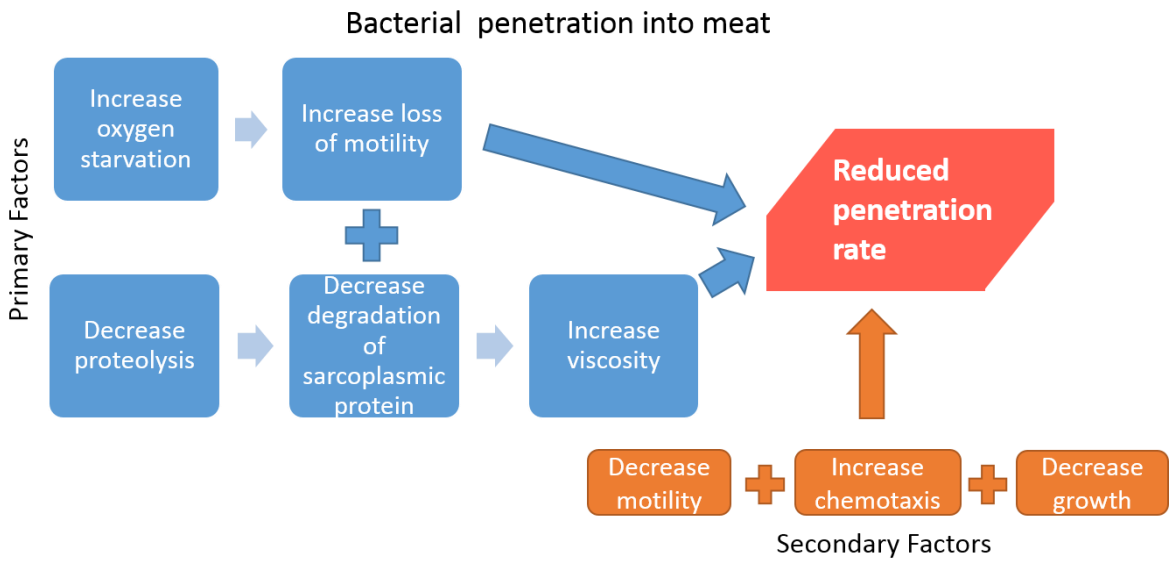

Figure 3.11. The primary factors for bacterial penetration were shown to be oxygen starvation and proteolysis, while motility, chemotaxis, and growth were secondary contributors.

3.2 Quantitative evaluation of microbial contamination of interior of meat using mathematical modeling coupled with the predicted surface bacteria concentration

3.2.1 The effect of the time of bacterial attachment after dissection on penetration depth

In order to quantitatively evaluate the microbial contamination of interior of meat coupled with surface contamination inspection, penetration of *Pseudomonas fluorescens* into meat was simulated and penetration depth into meat when inspecting the surface was determined. Penetration depth was determined here as the depth where bacterial concentration calculated in Eqn. 3.31 satisfied Eqn. 3.32 (that is, the surface bacterial concentration of meat reached over 15 CFU cm^{-2}). The duration of 24 h between the inspection of meat surface for bacterial concentration and dissection (threshold of being exposed to air) was assumed. However, the effect of the time when bacteria attached on meat surface on penetration depth is unclear. First, in order to investigate the effect of time of bacterial attachment on meat surface, simulation was implemented in different time before bacterial attachment. It was assumed that the microbial contamination of meat surface was checked 24 h after dissection of meat into blocks (this is the threshold of exposure of meat surface to air). In the simulation, oxygen diffusion (no bacterial migration) was conducted for t1 [h], and following this oxygen diffusion, bacterial migration into meat was simulated for t2 [h]. From the assumption above, $t_1 + t_2 = 24\ \mathrm{h}$. The effect of

time (t_1) from dissection to bacterial attachment on meat surface on penetration depth was investigated (Fig. 3.12). Up to 12 h of the duration before bacterial attachment (that is, the duration of penetration is from 12 h to 24 h), penetration depth stayed almost constant. Over 14 h of t_1 (that is, less than 10 h for penetration (t_2)), penetration depth slightly decreased (Fig. 3.12). As a whole, little change was observed in penetration depth in different timing of bacterial attachment. Therefore, it can be concluded that the timing of bacterial attachment has little effect on penetration depth. Importantly, from the viewpoint of safety, the penetration depth did not go beyond 1.0 cm if the duration for penetration (t_2) reached the maximum here, 24 h, Therefore, it is appropriate to use the timing of 12 h as an example, and from the viewpoint of safety, the penetration depth does not go further beyond the value of 12 h even though the duration for penetration increased. This little effect of duration of penetration on penetration depth comes from the mechanistic understanding of penetration of aerobic bacteria that bacterial migration is mainly regulated by oxygen transport.

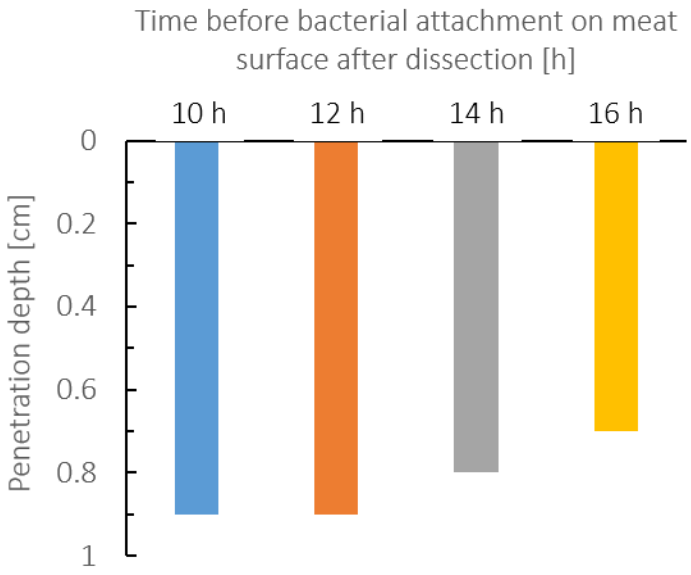

Figure 3.12. The effect of time before bacterial attachment after dissection on penetration depth into meat. Increase in duration before attachment after dissection meant the decrease in the duration for bacterial penetration (24 h in total). A small tendency of decreased penetration depth was observed as duration before bacterial attachment increased because of the less time for bacterial penetration.

3.2.2 Quantitative evaluation of the degree of penetration of aerobic bacteria into meat

Figure 3.13 showed the effect of surface bacterial concentration on penetration depth. In contrast to Fig. 3.12, the penetration depth changed largely among different surface concentration (boundary condition). Considering that the timing of bacterial attachment on meat has little effect on penetration depth, penetration depth can be quantitatively estimated from surface bacterial concentration even there is no knowing the timing when bacteria attached on meat surface. In section 2, the prediction models of aerobic plate count and ATP content of meat surface have been developed with fluorescence spectroscopy; thus, the surface concentration can be determined nondestructively and rapidly. Additionally, the mechanistic understanding of penetration of aerobic bacteria that penetration rate is mainly governed by oxygen diffusion allowed us to understand that the timing of bacterial attachment on meat surface has little effect on penetration depth. Also, the penetration depth is more dependent on surface bacterial concentration, and from this bacterial concentration, the penetration depth of aerobic bacteria into meat was quantitatively evaluated using mathematical modeling. Therefore, it can be concluded that the hygiene monitoring technique was developed which can evaluate the microbial contamination of meat surface and interior of meat simultaneously. Understanding of the degree of penetration is critical for food safety because it allows us the information about the location which is safe in the perspective of food safety of interior of meat.

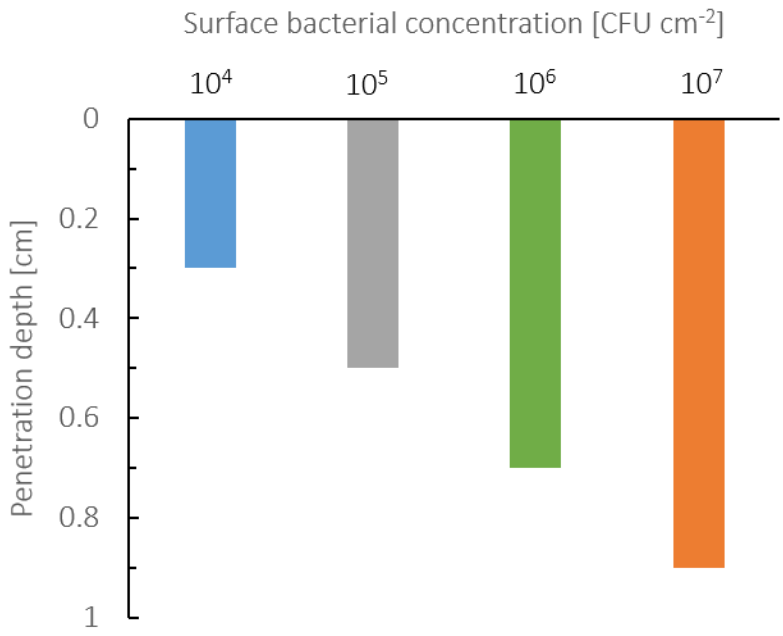

Figure 3.13. Penetration depth into meat increased with surface bacterial concentration. Surface bacterial concentration was assumed to be inspected 24 h after dissection (initial stage of exposure of meat surface to air). Considering that time when bacteria attached has little effect on penetration depth (Fig. 3.12), penetration depth can roughly evaluated from surface bacterial concentration.

4. Conclusions

A rapid, nondestructive system for hygiene monitoring of the meat surface was developed using EEMs. The ATP fluorescence peak was successfully separated from that of tryptophan, and the ATP fluorescence signal was detected from EEMs of *Pseudomonas fluorescens* culture using a fourth-derivative procedure at Ex = 284 nm and Em = 388 nm, 396 nm, and 410 nm. ATP fluorescence peak was also detected using pork surface EEMs coupled with a fourth-derivative procedure. Prediction models for aerobic plate count and ATP content of pork surface were developed using EEMs, second-derivative EEMs, and fourth-derivative EEMs. The highest prediction accuracies were obtained using fourth-derivative EEMs as explanatory variables (correlation coefficient, 0.95; RMSEP, 0.68 $\log_{10}$ CFU cm^{-2}). LV 1 loading for the prediction of aerobic plate counts from fourth-derivative EEMs revealed a decrease in the high contribution of tryptophan fluorescence, corresponding to the degradation of pork surface tryptophan by microorganism. LV 2 loading also revealed the contribution of the ATP fluorescence signal to the prediction model. Therefore, we can conclude that including the ATP fluorescence signal in the prediction models in addition to tryptophan and NAD(P)H offered higher prediction accuracies. These models are practical because they reflects changes in ATP production, tryptophan degradation, and NAD(P)H production by microorganisms.

Mechanistic understanding whereby aerobic bacteria penetrate into meat will allow for the provision of safer meat to consumers. The degree of microbial contamination of the meat interior will also be better understood is the mechanism of bacterial penetration is elucidated. Therefore, the penetration of aerobic bacteria into meat was mathematically modeled using diffusion-reaction type equations. Photomicrographs of transverse sections of beef show that bacteria penetrate within the gaps between muscle fibers and the endomysia. The domain for the transport model was the sarcoplasmic fluid in this gap. Proteolysis in the fluid changed its viscosity which, in turn, affected transport. The dependence of motility on viscosity and oxygen concentration was included in the modeling of bacterial transport.

Penetration of bacteria into meat appears to depend on a balance between motility, which encourages movement deeper into the meat, and chemotaxis toward the surface where there is higher oxygen concentration. The reduction in motility caused by oxygen starvation at deeper locations significantly affects the process. The predicted penetration rates compared reasonably well for both *non-proteolytic* and *proteolytic* bacteria. More rapid bacterial penetration during proteolysis is caused by both high motility and increased oxygen diffusion (reduced starvation and chemotaxis) in a reduced viscosity fluid caused by the degradation of sarcoplasmic protein. In both *proteolytic* and *non-proteolytic* bacteria, oxygen starvation has a greater effect than chemotaxis in reducing

the penetration rate. The mechanistic understanding revealed in this study inform potential techniques for reducing bacterial penetration by controlling environmental factors such as temperature and oxygen levels. Therefore, these insights into the mechanisms of bacterial penetration of meat are beneficial for reducing the risk of meat pathogen outbreaks. The penetration depth was quantitatively evaluated using mathematical modeling, indicating that the penetration depth is almost independent of the timing of bacterial attachment on the meat surface and solely dependent on the surface bacteria concentration and the time when meat surface is exposed to air. Therefore, the penetration depth can be quantitatively evaluated using mathematical modeling. This quantitative evaluation of penetration depth may lead to the provision of safer meat to consumers.

Finally, simultaneous quantitative evaluation technique of surface aerobic plate counts and penetration depth into meat was developed with fluorescence spectroscopy and mathematical modeling.

Acknowledgements

I would like to thank Prof. Seiichi Oshita, my major supervisor, for helpful discussions and personal communications. I also would like to thank to Prof. Yoshio Makino for his advice regarding details of my research through laboratory seminars. A part of this research was conducted under the supervision of Prof. Ashim Datta, Cornell University. I greatly appreciate his support of my research on the mathematical modeling of the penetration of aerobic bacteria. The help from Dr. Junichi Sugiyama and Dr. Masatoshi Yoshimura through discussions of fluorescence spectroscopy is greatly appreciated. I also greatly appreciate the discussions I had with Professor Eva Tornberg. The editorial corrections by Ms. Margaret Stevens are also greatly appreciated. I would like to express my gratitude to Ms. Oto for the discussions regarding fluorescence spectroscopy and data analysis using her data.

References

Adler, J. 1973. A Method for Measuring Chemotaxis and Use of the Method to Determine Optimum Conditions for Chemotaxis by Escherichia coli. *Journal of General Microbiology*, 74(1), 77–91.

Adler, M., Erickstad, M., Gutierrez, E., & Groisman, A. 2012. Studies of Bacterial Aerotaxis in A Microfluidic Device. Lab on a Chip, 12(22), 4835.

Ait-Kaddour, A., Boubellouta, T., & Chevallier, I. 2011. Development of a portable spectrofluorimeter for measuring the microbial spoilage of miced beef. *Meat Science*, *88,* 675–681.

Amberson, W. R., Bauer, A. C., & Philpott, D. E. 1964. Obtained by Ultracentrifugation of Red and Heart Muscles of the Rabbit. Journal of Cellular and Comparative Physiology, 63(1), 7‑24.

Anonymous. 2001. Commission decision of 8 June 2001 (2001/471/EC). *Official Journal of the European Communities L165*, 48–53.

Baranyi, J., Roberts, T. A., & Mcclure, P. 1993. A Non-Autonomous Differential Equation to Model Bacterial Growth. Food Microbiology, 10, 43‑59.

Baranyi, J. & Roberts, T. A. 1994. A Dynamic Approach to Predicting Bacterial Growth in Food. International Journal of Food Microbiology, 23, 3-4. 277-294.

Barton, J. W. & Ford, R. M., 1995. Determination of Effective Transport Coefficients for Bacterial Migration in Sand Columns Determination of Effective Transport Coefficients for Bacterial Migration in Sand Columns. Applied and Environmental Microbiology, 61(9), 3329–3335.

Bautista, D. A., Sprung, D. W., Barbut, S., & Gri, M. W. 1998. A Sampling regime based on an atp bioluminescence assay to assess the quality of poultry carcasses at critical control points during processing, *Food Research International, 30*, 803-809.

Bennett. 2007. Mass Transfer and Separation Processes: Principles and Applications, second ed. Edited by D. Basmadjian. CRC Press/Taylor & Francis Group, Boca Raton.

Bowker, B. C. & Zhuang, H. 2013. Relationship between Muscle Exudate Protein Composition and Broiler Breast Meat Quality. Poultry Science, 92(5), 1385–92.

Carlson, B. E., Vigoreaux, J. O., & Maughan, D. W. 2014. Diffusion Coefficients of Endogenous Cytosolic Proteins from Rabbit Skinned Muscle Fibers. Biophysical Journal, 106(4).

Chen, K. C., Ford, R. M., & Cummings, P. T. 1998. Perturbation Expansion of Alt’s Cell Balance Equations Reduces to Segel’s One-Dimensional Equations for Shallow Chemoattractant Gradients. SIAM Journal on Applied Mathematics, 59(1), 35–57.

Cheng, J., & Sun, D. 2015. Recent applications of spectroscopic and hyperspectral imaging techniques with chemometric analysis for rapid inspection of microbial spoilage in muscle foods. *Comprehensive Reviews in Food Science and Food Safety*, *14*.

Christensen, J., Norgaard, L., & Engelsen, S. B. 2006. Multivariate autofluorescence of intact food systems. *Chemical Reviews, 106*, 1979–1994.

Cornforth, D., & Hunt, M. 2008. Low-Oxygen Packaging of Fresh Meat with Carbon Monoxide: Meat Quality, Microbiology, and Safety. American Meat Science Association, (2), 1‑10.

Dainty, R. H., Shaw, B. G., De Boer, K. a, & Scheps, E. S. 1975. Protein Changes Caused by Bacterial Growth on Beef. The Journal of Applied Bacteriology, 39(1), 73‑81.

Douarche, C., Buguin, A., Salman, H., & Libchaber, A. 2009. E. Coli and Oxygen: A Motility Transition. Physical Review Letters, 102(19), 2‑5.

Dufour, É., Frencia, J. P., & Kane, E. 2003. Development of a rapid method based on front-face fluorescence spectroscopy for the monitoring of fish freshness. *Food Research International, 36*, 415–423.

Durek, J., Bolling, J. S., Knorr, D., Schwägele, F., & Schlüter, O. 2012. Effects of different storage conditions on quality related porphyrin fluorescence signatures of pork slices. *Meat science, 90,* 252–258.

Durek, J., Fröhling, A., Bolling, J., Thomasius, R., Durek, P., & Schlüter, O. K. 2016. Non-destructive mobile monitoring of microbial contaminations on meat surfaces using porphyrin fluorescence intensities. *Meat Science*, *115*, 1–8.

Egelandsdal, B., Kvaal, K., & Isaksson, T. 1996. Autofluorescence spectra as related to tensile properties for perimysium from bovine masseter. *Journal of food science 61*, 342–347.

Eisel, W. G., Linton, R. H., & Muriana, P. M. 1997. A Survey of Microbial Levels for incoming raw beef, environmental sources and ground beef in a red meat processing plant. *Food Microbiology, 14,* 273–282.

Ellis, D. I., Broadhurst, D., & Goodacre, R. 2004. Rapid and quantitative detection of microbial spoilage of beef by Fourier transform infrared spectroscopy and machine learning. *Analytica Chimica Acta, 514*, 193–201.

Ellis, D. I., Broadhurst, D., Kell, D. B., Rowland, J. J., & Goodacre, R. 2002. Rapid and quantitative detection of the microbial spoilage of meat by fourier transform infrared spectroscopy and machine learning. *Applied and Environmental Microbiology, 68*(, 2822–2828.

Elmossalami, E., & Wassef, N. 1971. Penetration of Some Microorganisms in Meat. Zentralblatt Fur Veterinarmedizin. Reihe B. Journal of Veterinary Medicine. Series B, 18, 329‐336.

Ercolini, D., Russo, F., Nasi, A., Ferranti, P., & Villani, F. 2009. Mesophilic and psychrotrophic bacteria from meat and their spoilage potential in vitro and in beef. *Applied and Environmental Microbiology*, *75*, 1990–2001.

FAO. 2014. FAO Stat. Production, Live animals. http://faostat3.fao.org/browse/Q/QA/E Accessed June 23, 2016.

Ford, R. M. & Lauffenburger, D. A. 1991. Measurement of Bacterial Random Motility and Chemotaxis Coefficients: II. Application of single-cell-based mathematical model. Biotechnology and Bioengineering, 37(7), 661‑672.

Ford, R. M. & Lauffenburger, D. A. 1992. A Simple Expression for Quantifying Bacterial Chemotaxis Using Capillary Assay Data: Application to the Analysis of Enhanced Chemotactic Responses from Growth-Limited Cultures. Mathematical Biosciences, 109(2), 127‑149.

Ford, R. M., Phillips, B. R., Quinn, J. A., & Douglas, A. 1991. Measurement of Bacterial Random Motility and Chemotaxis Coefficients: 1. Stopped-Flow Diffusion Chamber Assay. Biotechnology and Bioengineering, 37, 647-660.

Frank, J. F. 2001. Microbial attachment to food and food contact surfaces. *Advances in Food and Nutrition Research*, *43*, 319–370.

Ghassem, M., Fern, S. S., Said, M., Ali, Z. M., Ibrahim, S., & Babji, A. S., 2014. Kinetic Characterization of Channa Striatus Muscle Sarcoplasmic and Myofibrillar Protein Hydrolysates. Journal of Food Science and Technology, 51, 467‑475.

Gill, C. O., Leet, N. G., & Penney, N. 1984. Structural Changes Developing with Rigor That Facilitate Bacterial Invasion of Muscle Tissue. *Meat Science*, *10*, 265–274.

Gill, C. O. & Penney, N. 1977. Penetration of Bacteria into Meat. *Applied and Environmental Microbiology*. *33,* 1284–1285.

Grijspeerdt, K. 2001. Modeling the Penetration and Growth of Bacteria in Eggs. Food Control, 12(1), 7‑11.

Hamm, R. 1977. Postmortem Breakdown of ATP and Glycogen in Ground Muscle : A REVIEW, *Meat Science, 1*, 15-39.

Hay, J. D., Currie, R. W., Wolfe, F. H., & Sanders, E. J. 1973. Effect of Postmortem Aging on Chicken Muscle Fibrils. Journal of Food Science. 38(6), 981‑986.

Hedin G, Rynbäck J, Loré B. 2010. Reduction of Bacterial Surface Contamination in The Hospital Environment by Application of a New Product With Persistent Effect. Journal of Hospital Infection, 75(2), 112-115.

Hertog-Meischke, M. J. A., Smulderstand, I. F. J. M., & van Logtestijn, J. G. 1998. The Effect of Storage Temperature on Drip Loss from Fresh Beef. Journal of the Science of Food and Agriculture, 78, 522-526.

Hunt, M. C., Mancini, R. A., Hachmeister, K. A., Kropf, D. H., Merriman, M., Delduca, G., & Milliken, G. 2004. Carbon Monoxide in Modified Atmosphere Packaging Affects Color, Shelf Life, and Microorganisms of Beef Steaks and Ground Beef. Journal of Food Science, 69(1), FCT45‐FCT52.

Iwamoto, H., Tabata, S., K. Sakakibara, S. Nishimura , T. Gotoh, & Y. Koga. 2001. Scanning Electron Microscopic Observation of the Architecture of Collagen Fibres in Chicken M. Iliotibialis Lateralis. British Poultry Science, 42(3), 321-326.

Jaenicke, R. & Knof, S. 1968. Molecular Weight and Quaternary Structure of Lactic Dehydrogenase. 3. Comparative Determination by Sedimentation Analysis, Light Scattering and Osmosis. European Journal of Biochemistry, 4(2), 157‐163.

Karoui, R. & Blecker, C. 2011. Fluorescence spectroscopy measurement for quality assessment of food systems–a Review. *Food and Bioprocess Technology*, 4, 364–386.

Karoui, R., Martin, B., & Dufour, E. 2005. Potentiality of front-face fluorescence spectroscopy to determine the geographic origin of milks from the Haute-Loire department (France). *Le Lait*, 85, 223–236.

Keller, E. F. & Segel, L. A. 1971. Traveling Bands of Chemotactic Bacteria: A Theoretical Analysis. Journal of Theoretical Biology, 30(2), 235‐248.

Kestin, J., Sokolov, M., & Wakeham, W. A. 1978. Viscosity of Liquid Water in the Range −8 ° C to 150 ° C. Journal of Physical and Chemical Reference Data, 7, 3.

Krumm J. 2001. Savitzky-Golay Filters for 2D Images. http://research.microsoft.com/en-us/um/people/jckrumm/SavGol/SavGol.htm Accessed on October 18th, 2016.

Lewus, P. & Ford, R. M. 2001. Chemotaxis Bacterial Transport Population-Scale Assays. Biotechnology, 75, 3, 292-304.

Li, M., Li, Y., Huang, X., Zhao, G., & Tian, W. 2014. Evaluating Growth Models of Pseudomonas Spp. in Seasoned Prepared Chicken Stored at Different Temperatures by The Principal Component Analysis (PCA). Food Microbiology, 40, 41‐7.

Lin, M., Al-Holy, M., Mousavi-Hesary, M., Al-Qadiri, H., Cavinato, A.G., & Rasco, B.A. 2004. Rapid and quantitative detection of microbial spoilage in chicken meat by diffuse reflectance spectroscopy (600–1100 nm). *Letters in Applied Microbiology*, *39*, 148–155.

Liu, A., Nishimura, T., & Takahashi, K. 1994. Structural Changes in Endomysium and Perimysium during Post-Mortem Aging of Chicken Semitendinosus Muscle---Contribution of Structural Weakening of Intramuscular Connective Tissue to Meat Tenderization, Meat Science, 38, 315‐328.

Lovely, P. S. & Dahlquist, F. W. 1975. Statistical Measures of Bacterial Motility and Chemotaxis. Journal of Theoretical Biology, 50(2), 477‑496.

Matsubara, I. & Got, Y. E. 1984. Changes in the Lateral Filament Spacing of Skinned Muscle Fibres when Cross-bridges Attach. Journal of Molecular Biology, 173(1), 15‑33.

McEvoy, J. M., Sheridan, J. J., Blair, I. S., & McDowell, D. A. 2004. Microbial contamination on beef in relation to hygiene assessment based on criteria used in eu Decision 2001/471/EC. *International Journal of Food Microbiology*, *92*, 217–225.

Morita, Y., Komoda, E., Shiwaku, J., HoSOmi, T., Itagaki, M., Nakata, K., Nakai, H., Watanabe, S., Kozawa, K., Yamamoto, S., & Kimura, H. 2010. Contamination of Cattle and Pig Carcasses in Abattoir in Japan, *Japanese Journal of Food Microbiology*, *27*, 90–95.

Nicolai, B. M., Beullens, K., Bobelyn, E., Peirs, A., Saeys, W., Theron, K. I., & Lammertyn, J. 2007. Nondestructive measurement of fruit and vegetable quality by means of NIR spectroscopy : A review. *Postharvest Biology and Technology*, *46*, 99–118.

Nishino, K., Nakamura, K., Tsuta, M., Yoshimura, M., Sugiyama, J., & Nakauchi, S. 2013. Optmization of excitation-emission band-pass filter for visualization of viable bacteria distribution on the surface of pork meat. *Optics Express, 21*, 12579–12591.

Noriega, E., Laca, a, & Díaz, M. 2010. Decisive Role of Structure in Food Microbial Colonization and Implications for Predictive Microbiology. Journal of Food Protection, 73(5), 938‑951.

Nossal, R. Chen, S. 1972. Light Scattering from Motile Bacteria. Journal de Physique Colloques, 33 (C1), C1-171-C1-176.

Offer, G. & Cousins, T. 1992. The Mechanism of Drip Production: Formation of Two Compartments of Extracellular Space in Muscle Post Mortem. *Journal of the Science of Food and Agriculture, 58*, 107–96.

Oshita, S., Al-Haq, M. I., Kawagishi, S., Makino, Y., Kawagoe, Y., Ye, X., Shinozaki, S., & Hiruma, N. 2011. Monitoring of ATP and viable cells on meat surface by UV–Vis reflectance spectrum analysis. *Journal of Food Engineering, 107*, 262–267.

Oto, N., Oshita, S., Kawagishi, S., Makino, Y., Kawagoe, Y., Al-Haq, M. I., Shinozaki, S. & Hiruma, 2012. N. Non-destructive estimation of ATP contents and plate count on pork meat surface by UV-Vis reflectance spectrum analysis. *Journal of Food Engineering, 110*, 9–17.

Oto, N., Oshita, S., Makino, Y., Kawagoe, Y., Sugiyama, J. & Yoshimura, M. 2013. Quantitative evaluation of ATP content and plate count on pork meat surface by fluorescence spectroscopy. *Meat Science, 110*, 9–17.

Pearson, A. M. & Young, R. B. 1989. 9 – Sarcoplasmic Proteins. In: Muscle and meat biochemistry. Edited by Pearson, A. M. Academic Press, San Diego, USA.

Ping, L., Birkenbeil, J., & Monajembashi, S. 2013. Swimming Behavior of The Monotrichous Bacterium Pseudomonas Fluorescens SBW25. *FEMS Microbiology Ecology*, *86*(1), 36–44.

Pu, Y., Wang, W., & Alfano, R. R. 2013. Optical detection of meat spoilage using fluorescence spectroscopy with selective excitation wavelength. *Applied Spectroscopy, 67*, 210–213.

Richards, J. L. 1993. Viscosity And The Shapes of Macromolecules: A Physical Chemistry Experiment Using Molecular-Level Models in the Interpretation of Macroscopic Data Obtained from Simple Measurements. *Journal of Chemical Education*, *70*(8), 685.

Rivero, M. A., Tranquillo, R. T., Buettner, H. M., & Lauffenburger, D. A. 1989. Transport Models for Chemotactic Cell Populations Based on Individual Cell Behavior. *Chemical Engineering Science*, *44*(12), 2881–2897.

Russel, W. B., Saville, D. A., & Schowalter, W. R. 1989. Colloidal Dispersion. Cambridge University Press, Cambridge, New York, Post Chester, Melbourne, and Sydney.

Sádecká, J., & Tóthová, J. 2007. Fluorescence spectroscopy and chemometrics in the food classification: a Review. *Czech Journal of Food Sciences 25,* 159–173.

Sahar, A., Boubellouta, T., & Dufour E. 2011. Synchronous front-face fluorescence spectroscopy as a promising tool for the rapid determination of spoilage bacteria on chicken breast filet. *Food Research International*, 44, 471–480.

Schneider, J., Wulf, J., Surowsky B., Schmidt, H., Schwagele, F., & Schluter, O. 2008. Fluorimetric detection of protoporphyrins as an indicator for quality monitoring of fresh intact pork meat. *Meat Science, 80*, 1320–1325.

Scopes, R. K. 1964. The Influence of Post-Mortem Conditions on the Solubilities of Muscle Proteins. *Biochemical Journal,* 91 (1), 201-207.

Scopes, R. K. 1970. Characterization and Study of Sarcoplasmic proteins. In: The Physioloigy and Biochemistry of Muscle as a Food, 2. Edited by Briskey, E. J., Cassen, R. G., & Marsh, B. B. The University of Wisconsin Press, Madison, Milwaukee, and London.

Segel, L. A., Chet, I., & Henis, Y. 1977. Simple Quantitative Assay for Bacterial Motility. *Journal of General Microbiology*, 98, 329–337.

Sharma, V., Jaishankar, A., Wang, Y., & Mckinley, G. H. 2011. Rheology of Globular Proteins: Apparent Yield Stress, High Shear Rate Viscosity and Interfacial Viscoelasticity Of Bovine Serum Albumin Solutions. *Soft Matter*, *7*(9), 5150.

Schneider, J., Wulf, J., Surowsky B., Schmidt, H., Schwagele, F., & Schluter, O. 2008. Fluorimetric detection of protoporphyrins as an indicator for quality monitoring of fresh intact pork meat. *Meat Science, 80*, 1320–1325.

Schwedt, G., Ichinose, N., & Schnepel, F.M., 1987. Keiko Bunseki Kagaku. Baufu-kan, Tokyo, Japan (Japanese).

Sheridan, & Lynch. 1992. Influence of Processing and Refrigeration on The Bacterial Numbers of Beef And Sheep Offals. *Meat Science,* 24(2). 143–150.

Shimidzu, H., Hoshino, T., Ishioka, T., Morita, Y., Kuroda, A., and Hanasato, Y. 1998. Survey of bacterial contamination at poultry slaughter houses. *Journal of the Japan Veterinary Medical Association*, 51, 10 608–612.

Shirai, H., Oshita, S., & Makino, Y. 2016. Detection of Fluorescence Signals from ATP in The Second Derivative Excitation – Emission Matrix of A Pork Meat Surface for Cleanliness Evaluation. *Journal of Food Engineering*, *168*, 173–179.

Sikes, A. & Maxcy, R. B. 1980. Postmortem Invasion of Muscle Food by A Proteolytic Bacterium. Journal of Food Science, 45(2), 293‐296.

Silliker, J. H., Woodruff, R. E., Lugg, J. R., Wolfe, S. K., & Brown, W. D. 1977. Preservation of Refrigerated Meats with Controlled Atmospheres: Treatment and Post-Treatment Effects of Carbon Dioxide on Pork and Beef. Meat Science, 1(3), 195‐204.

SIragusa, G. R., & Cutter, C. N. 1995. Microbial ATP bioluminescence as a means to detect contamination on artificially contaminated beef carcass tissue. Journal of Food Protection, 58(7), 764–769.

Siragusa, G. R., Dorsa, W. J., Cutter, C. N., Perino, L. J., & Koohmaraie, M. 1996. use of a newly developed rapid microbial ATP bioluminscence assay to detect microbial contamination on poultry carcasses. *Journal of Bioluminscence and Chemiluminscence*.

Su, P.-T., Liao, C.-T., Roan, J.-R., Wang, S.-H., Chiou, A., & Syu, W.-J. 2012. Bacterial Colony from Two-Dimensional Division to Three-Dimensional Development. PLoS ONE, 7(9).

Sugiyama, J. & Tsuta, M. 2013. Discrimination and quantification technology for food using fluorescence fingerprint. in Japanese. *Nippon Shokuhin Kagaku Kogaku Kaishi, 60*(9), 457–465.

Swatland, H. J. 1987. Autofluorescence of adipose tissue measured with fiber optics. Meat Science, 19, 277–284.

Swatland, H. J., & Barbut, S. 1995. Optical prediction of processing characteristics of turkey meat using UV fluorescence and NIR birefringence, Food Research International. *28*(3), 227–232.

The Ministry of Heath, Labor and Welfare. 1993. A guide for sanitation monitoring at poultry processing plants by HACCP method (in Japanese).

Thomas, C. J., O'Rourkel, R. D., & Mcfwekin, T. A. 1987. Bacterial penetration of chicken breast muscle. *Food Microbiology,* 4, 87–95.

Tornberg, E. 2013. Engineering Processes in Meat Products and How They Influence their Biophysical Properties. Meat Science, 95, 871-878.Sahar, A., & Dufour, É. 2014. Use of Fourier transform-infrared spectroscopy to predict spoilage bacteria on aerobically stored chicken breast fillets. *LWT - Food Science and Technology*, *56*(2), 315–320.

Tokoro, M. M., Furuta, M., Miyazawa, K., Okumura, Y., Noda, K., & Maeda, S. 1995. Evaluation of the HACCP system processing for sanitary control in poultry (in Japanese). *Japanese Journal of Food Microbiology,* 11, 4, 227–232.

Tuval, I., Cisneros, L., Dombrowski, C., Wolgemuth, C.W., Kessler, J.O., & Goldstein, R.E., 2005. Bacterial Swimming and Oxygen Transport near Contact Lines. *Proceedings of the National Academy of Sciences*, 102, 2277–2282.

USDA. 1996. Pathogen Reduction: Hazard analysis and critical control point (HACCP) Systems; Final Rule. Federal Regulation 61, 38805–38855.

Wilkins, D. K., Grimshaw, S. B., Receveur, V., Dobson, C. M., Jones, J. a., & Smith, L. J. 1999. Hydrodynamic radii of native and denatured proteins measured by pulse field gradient NMR techniques. *Biochemistry*, *38*(50), 16424–16431.

Wold, J. P., Lundby, F., & Egelandsdal, B. 1999. Quantification of connective tissue (hydroxyprolin) in ground beef by autofuorescence spectroscopy. Journal of Food Science, 64(3), 377–383.

Wrolstad, R. E., Acree, T. E. Decker, E. A., Michael, H. P., David. S. R., Steven, J. S., , Charles F. S., Denise, S., & Sporns, P. 2005. Handbook of Food Analytical Chemistry. Wiley, New Jersey, USA.